

DETECTION AND ASSESSMENT OF FOOD, ENERGY, AND WATER IMPACTS OF SOLAR
PHOTOVOLTAIC CO-LOCATION IN THE CALIFORNIA'S CENTRAL VALLEY

By

Jacob Tyler Stid

A THESIS

Submitted to
Michigan State University
in partial fulfillment of the requirements
for the degree of

Geological Sciences—Master of Science

2021

ABSTRACT

DETECTION AND ASSESSMENT OF FOOD, ENERGY, AND WATER IMPACTS OF SOLAR PHOTOVOLTAIC CO-LOCATION IN THE CALIFORNIA'S CENTRAL VALLEY

By

Jacob Tyler Stid

Since Industrialization, the United States and many other countries around the world have realized the significant negative impacts of fossil fuel consumption and associated carbon emissions which are altering Earth's climate. To mitigate this change, there have been significant transitions from fossil fuels to renewable energy, with one viable option being mass deployment of solar arrays. Thus, large plots of land in regions such as California's Central Valley have begun to convert land, much of it agricultural, into solar arrays. Here, I work to understand the current solar installation practices and the impacts on food, energy, water, carbon, and the farmers who have decided to convert their land. I provide this information to encourage best installation practices and promote long term positive impact deployment.

In Chapter 1, I develop a comprehensive remotely-sensed dataset commercial-scale crystalline silicon solar installations in the Central Valley detailing precise panel locations, orientations, and time of installations. These attributes allowed for the assessment of current practices including frame technologies, panel packing, spatial field placement, and crop preferences. I then link those practices to federal and state policies and quantify sub-optimal installation practices. In Chapter 2, I deploy this new dataset in an Impact Analysis to project future food, energy, water, carbon, and economic implications of these installed arrays through a 25-year predicted lifespan. This new data leads to a better understanding of to-date solar installation practices and provides the information needed to improve future infrastructure as we move towards sustainability.

ACKNOWLEDGMENTS

Although this thesis embodies the work of the last two years, the capability to do such work was built out of being surrounded by phenomenal people, from birth to today. This Master's degree is yet another step on journey, and I intend to continue learning from, and being inspired by you all, so thank you.

I'll begin by thanking my advisors, Dr. David Hyndman and Dr. Anthony Kendall for their mentorship, passion in what they do, and for their kindheartedness, which is what drew me here in the first place. Dave was the only advisor I reached out to who genuinely wanted to get to know me and my prior research and worked to set up that meeting. In coming to the Student Symposium in 2019, I was immediately met with Anthony's positivity, optimism, and general elation for research and bettering the world. All followed by a wonderful two years of research, where they never failed to instill confidence and positive words in my work and life. In the same way, I would also like to thank Dr. Annick Anctil, for serving on this committee, and for her feedback and guidance as I delved into a new world of research in which I needed her guiding hand. Her student, Siddarth Shulka, was also instrumental in the completion of this work, and provided much insight and friendship throughout.

I would also like to thank my funding sources, without whom this work would not be possible. The USDA National Institute of Food and Agriculture, MSU Graduate School, MSU College of Natural Science, and MSU Department of Earth and Environmental Science have all paved the path for this work to be completed.

As for the Hydrolab, never in my life have I experienced an environment so supportive, trustworthy, and filled with leadership than the people I have had the privilege to work with here.

And bear in mind, I say this whilst only interacting with this group “in person” for roughly 9 months (due to COVID), so this kindness was immediate. Beginning from leadership, Dr. David Hyndman, Dr. Anthony Kendall, and Dr. Sherry Martin, have all proved to be just as great mentors in life as in work. At one point or another, every single member of the lab has answered a question, taken me to coffee, lunch, provided input, or has simply cared about my life both in and outside academia, enough to make a positive impact on my life. A special thanks to Brent Heerspink, who has provided countless instances of friendship and guidance throughout my time here, to Jeremy Rapp, not only for innumerable instances of technical guidance but also for some of the most intellectually stimulating and friendly conversations I have ever had, to Ally Brady, for being a guiding force and a caring soul from the moment she took on planning my visit for the Student Symposium in 2019, and to Quercus Hamlin, who’s morning office check-in visits have now been replaced with zoom visits, but their importance to me is all the same. I would also like to thank Chance Ford, Dr. Alex Kuhl, Behnaz Mizendehdel, Ben McCarthy, and Luwen Wan for their bountiful friendship and guidance throughout my time here. Additional department members I would like to thank are Ami McMurphy, Pam Robinson, Elizabeth McElroy, and Judi Smelser, who all make our lab, the department, and the world go round. I intend to continue to surround myself with these wonderful people by continuing into my PhD. in this lab.

External to the lab as well, several people have been forces of motivation in getting me to this point. I would like to thank my fellow NASA DEVELOP researchers, Elspeth Gates and Adriana LeCompte, along with the leadership of Sydney Neugebauer, Dr. Kenton Ross, and to Woods Hole Researchers Dr. Neil Ganju and Dr. Zafer Defne, you all made the DEVELOP term a massively fruitful one, challenged me to grow, and helped to pique my interest in new research areas all whilst battling through a pandemic. A special thanks to Dr. Jonathan Peterson, my

professor and an advisor at Hope College, who pushed me as an intellectual and who's passion and wisdom is still a guiding force today. I would also like to thank my long time best friend Christian Smith, from our endless discussions of the intricacies of the universe, to throwing a football around trying to catch it with one hand for six hours a day, you have challenged me to be the best man, friend, and researcher I can be. Thank you.

Finally, I would like to thank my wife, Karey Stid, for her never-ending unconditional love and guidance in every aspect of my life. You're an astoundingly amazing woman, who inspires me every day in both small and immense ways, and my excitement for the next 100 years of our life (advancements in medicine will get us there), is unbounded. I would also like to thank my parents, Wes and Lori Stid, and my sister Aly Stid. No acknowledgements section could ever hold all of the ways in which you have helped me get to this very place. I am who I am in every way because of you and could not be prouder of it. For you , both nature and nurture have done me well in life.

TABLE OF CONTENTS

LIST OF TABLES	viii
LIST OF FIGURES	ix
KEY TO ABBREVIATIONS.....	x
CHAPTER 1: Spatiotemporal identification and characterization of Agriculturally Co-Located Solar Photovoltaic Arrays in California’s Central Valley	1
Abstract.....	1
1. Introduction.....	2
2. Methods	7
2.1 Study area.....	7
2.2 Data.....	9
2.3 Integration of spatiotemporal segmentation to detect land cover change.....	11
2.4 New indices: NDPVI and NDB	12
2.5 Identifying geometrically linear and parallel panel systems.....	14
2.6 Identifying installation year	16
2.7 Determining to-date capacity, generation, and installation practices	19
3. Results and Discussion	23
3.1 Performance of the NDPVI and NBD indices in classification.....	23
3.2 Spatiotemporal identification of large-scale commercial PV arrays	24
3.3 Current commercial solar electricity production and observed policy responses.....	27
3.4 Packing factor and relative land productivity	31
3.5 Trends in installation practices	35
3.6 Total estimated crop loss and crop preferences	36
4. Conclusions.....	38
Acknowledgements.....	40
APPENDIX.....	41
CHAPTER 2: Implications of co-located solar PV installations on the FEW nexus in the Central Valley	56
Abstract.....	56
1. Introduction.....	57
2. Results.....	62
2.1 Resource and Economic Impact Result Description.....	62
2.2 Predicted impact on food production.....	63
2.3 Predicted impact on electricity production and forgone carbon emissions	65
2.4 Predicted impact on water use	66
2.5 Predicted lifetime financial impact from the cropland owner’s perspective	67
3. Discussion.....	68
3.1 Food, energy, water, and carbon emission resource impacts.....	68

3.2 Economic analysis and the need for preserving cropland.....	71
3.3 Limitations	72
4. Methods	73
4.1 Site description.....	73
4.2 Projected Resource Assumptions.....	73
4.3 Forgone food.....	74
4.4 Electricity production and carbon emissions	75
4.5 Change in water use	78
4.6 Simple economic budget from the cropland owner’s perspective	80
Acknowledgments	83
APPENDIX.....	84
REFERENCES	93

LIST OF TABLES

Table A1.1. LandTrendr GEE Parameters..... 44

Table 2.1. Cumulative Resource and Economic Impact Values..... 68

Table A2.1. Base, Low, and High Scenario Assumptions and Sources. 85

Table A2.1. (cont'd)..... 86

Table A2.2. Food Kcal Sources and Assumptions. 88

Table A2.2. (cont'd)..... 89

Table A2.2. (cont'd)..... 90

Table A2.2. (cont'd)..... 91

Table A2.3. Utility Service Provider Contribution to Co-Location..... 92

LIST OF FIGURES

Figure 1.1. Agriculture in the Central Valley, California.	9
Figure 1.2. PV Identification Framework.	12
Figure 1.3. Object-Based Panel Identification Workflow.	15
Figure 1.4. NDPVI Breakpoint Timeseries.	17
Figure 1.5. Solar PV Arrays in the Central Valley.	25
Figure 1.6. Installed Capacity and Annual Generation of Identified Arrays.	28
Figure 1.7. Packing Factor Deviation and Relative Land Productivity of frame technologies. ...	33
Figure 1.9. Installed Solar Crop Preferences.	37
Figure A1.1 PV Module Efficiency and Monocrystalline Share Through Time.	50
Figure A1.2 Identified PV Array Latitude and GHI Distributions.	51
Figure A1.3 Landsat NDPVI Timeseries Across Differing Landcovers.	54
Figure A1.4. Temporal Trends in Packing Factor Deviation and Relative Land Productivity. ...	55
Figure 2.1. Solar PV Lifespan Conceptual Diagram.	61
Figure 2.2. Cumulative Lifetime Food, Energy, Water, and Economic Impacts.	63
Figure 2.3. 2018 County Level Contribution to Forgone Kcal.	64
Figure 2.4. Cumulative Change in CO ₂ Emissions from Installed Solar PV.	66
Figure A2.1 Reported Temporal Module Efficiency and Extrapolated Monocrystalline and Polycrystalline Module Efficiencies.	87

KEY TO ABBREVIATIONS

PV	Photovoltaic
MW	Mega-Watts
GW	Giga-Watts
CONUS	Contiguous United States
ITC	Investment Tax Credit
NLCD	National Landcover Database
C-Si	Crystalline Silicon
NAIP	National Agriculture Imagery Program
USDA	United States Department of Agriculture
CDL	Cropland Data Layer
NDVI	Normalized Difference Vegetation Index
NDPVI	Normalized Difference Photovoltaic Index
NDB	Normalized Blue Difference
GEE	Google Earth Engine
PF	Packing Factor
RLP	Relative Land Productivity
Qsec	Quarter-Section (Public Lands Survey System)
GWh	Giga-Watt-hours
FEW	Food, Energy, and Water Nexus
LCA	Life Cycle Analysis
CO ₂	carbon dioxide

Mt	Mega Tonnes
O&M	Operation and Maintance
SGMA	Sustainable Groundwater Management Act
USGS	United States Geological Survey

CHAPTER 1:
SPATIOTEMPORAL IDENTIFICATION AND CHARACTERIZATION OF
AGRICULTURALLY CO-LOCATED SOLAR PHOTOVOLTAIC ARRAYS IN
CALIFORNIA'S CENTRAL VALLEY

Abstract

Understanding agriculturally co-located solar photovoltaic (PV) installation capacity, practices, and preferences is imperative to foster a future where solar power and agriculture co-exist with limited reduction in food production. Crops and solar panels are often co-located as they have similar ideal conditions for maximum yield. The recent boom in solar photovoltaics is thus replacing more cropland. Current literature on agriculturally co-located solar PV array installations lacks important spatiotemporal details that could help inform future array installations and improve associated policies and incentive programs. This study used the National Agriculture Imagery Program 0.6 meter imagery for object-based analysis (eCognition Developer), and Landsat 5 TM, Landsat 7 ETM+ and Landsat 8 OLI 30 meter imagery for temporal analysis (LandTrendr) to identify, classify, and characterize commercial-scale ground-mounted solar PV arrays in California's Central Valley installed between 2008 and 2018. This dataset provides spatiotemporal characterization of 210,368 individual panels grouped into 1006 PV arrays (69% of which are agriculturally co-located) by type of frame and year of installation. Fixed-axis arrays dominate the number of installed arrays and tend to be small (0.32 MW), while single-axis tracking arrays tend to make up less installations, but individual arrays have nearly four times the capacity (1.19 MW). These 1006 arrays account for 3.55 GW of capacity and have generated a cumulative of 36,531 GWh within the Central Valley. For the 694 agriculturally co-located arrays, significant sub-optimal installation practices were observed in the spacing and spatial field placement of the arrays. There was a dichotomy of crop conversion preferences with low value pastureland and high value orchards dominating the number of solar installations on

cropland. In addition, federal Solar Investment Tax Credit requirements and extensions were reflected in peak installation numbers in 2012 and 2016, suggesting another peak installation year in 2020 will be forthcoming. This study provides insights into dynamics of the commercial-scale ground-mounted solar PV array installation year, sub-optimal installation practices, crop preferences, and the electricity production over time for the installed arrays.

1. Introduction

Ground-mounted solar photovoltaic (PV) capacity in the Contiguous United States (CONUS) is projected to nearly triple from 32 GW (Energy Information Administration 2015) to 92 GW over the next decade (U.S. Energy Information Agency 2019) with current and future installations occupying less than 0.1% of contiguous land (Hartmann, H.M., Grippo, M.A., Heath, G., Macknick, J., Smith, K., Sullivan, R., Walston, L., Wescott 2016). In addition to the environmental benefits and economic incentives for California farmers, there are food, energy, and water benefits to co-locate medium sized PV arrays adjacent to cropland for both the farmers, and the asset owners (Barron-Gafford et al. 2019; Macknick 2019, 2020). Cropland is strategically located in regions of high solar irradiation for optimal crop yield, which is also the optimal location for PV arrays to attain peak generation (Adeh et al. 2019). Co-location has been shown to improve PV efficiencies due to cooler crop enhanced microclimates (9°C cooler) with 1-3% increase in generation (Barron-Gafford et al. 2019); a 5-15% increase in soil moisture retention (Barron-Gafford et al. 2019); and 200-300% yield increases for certain crops when co-located directly beneath panels (Barron-Gafford et al. 2019).

In addition to the many benefits, co-location creates local land use competition resulting in displacement of cropland by solar arrays. Innovative Site Preparations and Impact Reductions on the Environment, a coalition of federal institutions, universities, local governments and

groups, and industry partners, has provided the Low-Impact Solar Development Strategies Guidebook to promote best practices for low-impact co-location (NREL 2020). In addition, The University of Massachusetts Amherst Clean Energy Extension, which refers to co-location as “dual-use”, outlines several optimal co-location practices that allow local system owners to qualify for a financial incentive under the Solar Massachusetts Renewable Target program (Clean Energy Extension 2019). Although these programs outline optimal practices, they are missing information on how to tailor co-location practices regionally where placement optimization is not mandated.

Many existing planning and installation practices for commercial-scale ground-mounted arrays commonly do not fully consider the agricultural land use component of co-located efficiencies (Brooks and Dunlop 2013; Doyle et al. 2015). Unlike rooftop arrays, most ground-mounted arrays are not as space constrained. Therefore, typical ground-mounted array installations are optimized for cost of installation and electricity production by maximizing ground coverage and minimizing the cost of support structures, the impact of shading, and distance to access roads, and accounting for optimal orientation and wind loading (Brooks and Dunlop 2013; Doyle et al. 2015). Previous studies have noted the challenge of minimizing mutual shading by increasing interrow spacing, which also requires increased crop displacement (Awan et al. 2020).

Prior research in identifying solar PV arrays from satellite imagery has commonly focused on urban studies. Malof et al. (2019) and Malof et al. (2017) used a convolutional neural network to identify individual household PV installations in several cities across California. For training, these studies used a manually annotated dataset of over 19,000 individual rooftop systems collected in the cities of Fresno, Stockton, Modesto and Oxnard (Bradbury et al. 2016).

Their developed models detected urban rooftop PV arrays with a precision of 76% and a recall of 77% for the three cities. So et al. (2017) demonstrated a method to estimate solar PV capacity for these residential arrays using very high resolution color imagery (0.3 m) using a capacity-per-unit-area methodology. M. Wang et al. (2018) performed a panel detection analysis deploying template matching and object-based detection in the eCognition Developer software (Definiens 2000) to classify individual modules of a single commercial array with a 91% overall accuracy. Hernandez et al. (2014) developed a dataset of 200 PV and concentrating solar power, utility-scale solar energy installations in California by synthesizing county documents, Bureau of Land Management records, and environmental impact reports and statements. This was a pivotal study in terms of acquired characteristics (capacity, land footprint, technology type, location, and land ownership), and Hernandez et al. (2015) also assessed National Land Cover Database (NCLD) landcover types. However, these studies only looked at utility scale operations (20 – 1000 MW) which likely have differing landowner preferences and were still missing valuable information about installation practices.

Existing PV locations and characteristics for the Central Valley are available from a variety of academic, state, and industry sources (Barbose et al. 2020; Nyberg 2020; Solar Energy Industries Association 2015). However, this information is limited spatially (zip codes and counties), temporally (date of application approval, not completion of installation), and in completeness (e.g., missing permit applications, permit re-applications, and capacity thresholds).

The cropland and energy effects of co-locating PV arrays and agriculture depend on the year of installation and the area of converted land. In addition, electricity production from each array decreases over time due to module degradation (Jordan et al. 2016). Therefore, analyzing the effects of co-location on food and electricity production requires detection of the installation

years and the total converted area. This is a difficult process to automate across a large study area that has diverse land cover changes (such as the Central Valley). Quantifying PV array attributes and their changes through time requires frequent high-resolution data, with a long enough record to detect intra-annual installations back to the mid 2000's when PV installations became widespread.

The common paradigm of image classification has been centered around training machine learning algorithms that use strictly pixel based classification. However, previous studies have shown that at resolutions finer than the extent of the object of interest (i.e. many pixels making up a single PV panel), the statistical analysis of single pixels becomes less important than the spatial objects that they create (Baatz and Schape 2000; Blaschke and Strobl 2001). As resolution increases, the increase of within-class spectral variability decreases the potential accuracy of a purely pixel-based approach to classification (Blaschke et al. 2014) and favors using both spectral and object based features instead of simply spectral features. This is commonly referred to as 'The H-Resolution problem' (Hay, Niemann, and McLean 1996). One possible solution is an object-based analysis that includes morphological object features to improve spectral classification.

Due to the H-Resolution Problem, it becomes easier to differentiate more detailed land cover classes using both spectral and object based features as change becomes more heterogeneous. Detection capabilities at Landsat (includes 5, 7, and 8), Sentinel-2, and recent National Agriculture Imagery Program (NAIP) imagery scales, were impervious surfaces, rough PV arrays, and differentiated PV array panels/technologies respectively. With the evolution of higher resolution data, rulesets and assumptions about spectral indices and shape features must also evolve. eCognition can separately classify PV array technologies, panel area, and

orientations at multiple scales using a single developed ruleset.

Several previous studies have integrated temporal and object-based segmentation algorithms (Bueno et al. 2019; Cai, Lin, and Zhang 2019; Csillik et al. 2019; Hao et al. 2020; Nitze et al. 2017; Yu et al. 2020), and a few studies have integrated Landsat-based Detection of Trends in Disturbance and Recovery algorithms (LandTrendr) with eCognition (Bomber and Portelli 2020; Yin et al. 2018). Previously defined spectral impervious surface indices such as the normalized difference built-up index (NDBI), the modified normalized difference impervious surface index (MNDISI), the combinational biophysical composition index (CBCI), and the enhanced normalized difference index for impervious surface index (ENDISI), are usually complex and/or require a range of spectral wavelengths (often thermal infrared or short-wave infrared bands) that fall outside most high resolution (0.6-3 meter) aerial and space-borne remote sensing programs (Chen et al. 2019; Sun et al. 2017; Zha, Gao, and Ni 2003; S. Zhang et al. 2018) including NAIP. In this work, we develop new visible and NIR indices to assess PV land cover change.

We examined the geospatial coordinates, area (both panel and total), frame technology (orientation), and the year of completed installation. Characteristics derived from the identified panels were the packing factor, capacity, generation, foregone crop type and area removed, latitudinal and global horizontal irradiance (GHI) preferences, and the spatial relative land productivity of the area converted. Therefore, the detection framework demonstrated here will likely be useful for both spatial and temporal classification of land cover changes using temporal segmentation and object-based analysis in LandTrendr and eCognition respectively

Policy makers need to know the location and quantity of installed arrays, along with other array characteristics to understand and make informed decisions on energy, crops, water, and

economic policies. Research to date has not provided detailed estimates of commercial-scale ground-mounted PV arrays along with estimates of agricultural land use conversion to PV arrays. Such information is needed to better inform future installation practices based on efficiency of past practices. In addition, more studies are needed on proximally co-located arrays, where crops are grown around the arrays, as opposed to agrivoltaic co-located systems where crops are grown directly beneath the panels and frames.

Here, we provide an up to date (through 2018) novel dataset of regional PV array locations and unique attributes determined through a remote sensing algorithm framework that combines object-based and temporal segmentation. Solar co-location involves agricultural, livestock, or pollinator habitat land use directly underneath or adjacent to a ground-mounted solar array (Office of Energy Efficiency & Renewable Energy n.d.). We extend previous research by using this dataset to assess regional solar power implications and the agricultural implications of arrays adjacently co-located with active agriculture in California's Central Valley. Implications depend significantly on the size, technology, spatial placement and packing, type of land cover removed, and installation year, as implications pertaining to these factors vary temporally. The end goal was to develop information that can be used to inform array installation policies based on past practices to promote low-impact co-location of ground-mounted PV arrays with agriculture.

2. Methods

2.1 Study area

The massive increase in projected future installations is largely driven by the expected decreasing cost to manufacturer and install solar cells (Fu, Feldman, and Margolis 2018), increasing module efficiency (Figure A1.1, Barbose et al. 2020), and the continuation of federal

legislation supporting the U.S. solar industry. The federal Solar Investment Tax Credit (ITC) rebates 26% (though 2020, 30% prior to 2016) of the cost of residential and commercial solar systems installed in that tax year (Solar Energy Industries Association 2019, 2021; U.S. Department of Energy 2021). Since its conception in 2005 (Office 2005) and implementation in 2006, the U.S. solar industry has grown by more than 10,000% (Solar Energy Industries Association 2021). In addition to the Solar ITC, the Emergency Economic Stabilization Act of 2008 (Shah 2009) and the American Recovery and Reinvestment Act (Schoeffler 2009), along with more recent continued extensions, provided extensions on the ITCs also included a financial package to help encourage deployment of solar systems (Efficiency 2010). California's Central Valley (Figure 1.1) was chosen to be the study area because of these significant policy implementations for agriculturally co-located PV arrays, because its the state's most prolific agricultural region. The Central Valley domain was provided by Faunt (2012).

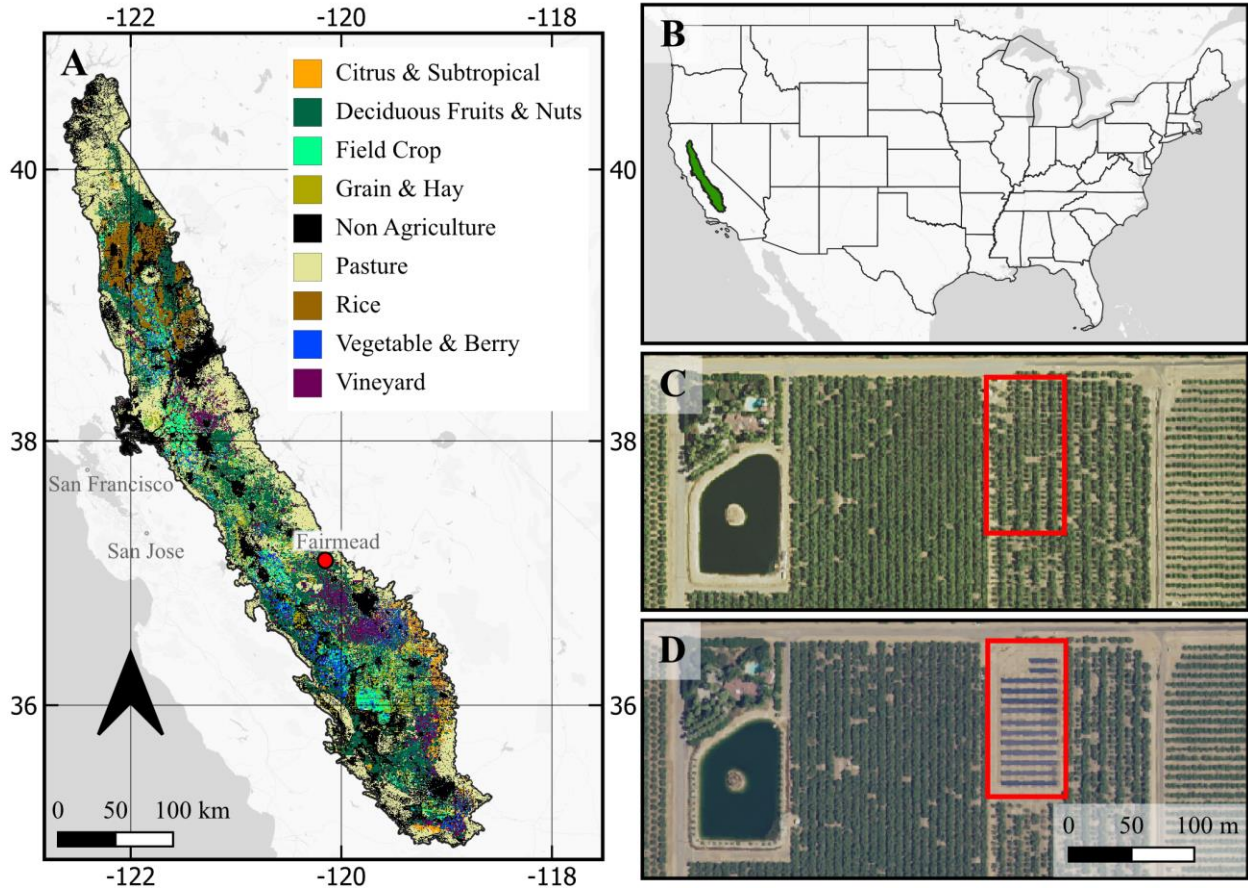


Figure 1.1. Agriculture in the Central Valley, California. 1.1A is the Central Valley alluvial boundary (modified from (Faunt 2012)) simplified and overlaid with the USDA 2018 Cropland Data Layer reclassified by the California Department of Water Resources (DWR) crop classes for simplicity (Kimmelshue 2021). The red point corresponds to the location of Figure 1.1C and 1.1D submaps, and the array described in Figure 1.4. 1.1C is a US scale map with state boundaries for spatial reference of the Central Valley California. Figure 1.1C shows 2014 NAIP imagery over an almond field near Fairmead, California with the red box corresponding to the same in 1.1D and outlining the foregone almond crop for the PV installation. Figure 1.1D shows 2016 NAIP imagery over the same almond field, now with the newly installed solar PV array converting some of the cropland outlined by the red box.

2.2 Data

To assess spatial attributes of PV arrays including packing factor, individual solar panels must be differentiated from each other and the surrounding landscape. To differentiate at this scale, imagery resolution of at least three meters was required as previous studies have predicted ground-mounted modules to have a width between 1 and 2.48 m (Awan et al. 2020; Jubayer,

Siddiqui, and Hangan 2016) respectively. Therefore, the freely available NAIP aerial imagery, which is collected roughly every two years at 0.6 meter resolution as of 2016 in many regions with red, blue, green, and near-infrared (NIR) wavelengths (USDA 2016). At the NAIP resolution (0.6 meter) it is possible to delineate individual module systems (panels), which was the basis to assess accuracy of this framework. NAIP imagery was accessed through the California Department of Fish and Wildlife ArcGIS portal (California Department of Fish and Wildlife 2020).

To assess the installation year, imagery with high temporal resolution and historical imagery back to 2007 (startYear of collection in Appendix Table A1.1) was required. Landsat 5 TM, Landsat 7 ETM+ and Landsat 8 OLI 30 meter imageries were optimal for this purpose and were already implemented in Google Earth Engine's (GEE) version of LandTrendr. Arrays without years of completed installation were manually interpreted and annotated using LandTrendr pixel time-series plots, Landsat 7 ETM+ and Sentinel-2 November-December imagery, NAIP imagery, and Google Earth Historical imagery for available years. Landsat 7 ETM+ imagery was also used to in creating growing season (June 1st – September 30th) NDVI maps needed for the relative land productivity (RLP) metric. Also required for this metric and for the crop analysis was the USDA's Cropland Data Layer (CDL), and the USDA's Farm and Ranch Survey (USDA 2013).

The to-date capacity analysis required the capacity equation and optimal packing factor constants from Martín-Chivelet (2016), along with efficiency data from Barbose et al. (2020). To determine electricity generation, the same efficiency data was required along with weather files from the National Solar Radiation Database (NREL 2015), hourly incident irradiance calculated from pvlib python modules developed by SANDIA National Laboratory (F. Holmgren, W.

Hansen, and A. Mikofski 2018), single-axis tracking daily rotation from Schneider (2012), PV efficiency degradation from Jordan et al. (2016), and soiling estimates from National Renewable Energy Laboratory (2017).

2.3 Integration of spatiotemporal segmentation to detect land cover change

Multiple PV technologies are being installed in California and elsewhere around the world. Technology differences include material (crystalline silicon, cadmium telluride, copper-indium-gallium-diselenide, silicon thin film, perovskite), structure (bifacial, concentrating solar power), frame technology (fixed, single-axis tracking, and 2-axis tracking), and orientation (N/S, E/W, or non-normal orientation) (Brooks and Dunlop 2013; Chu 2011). Optimal array orientation should correspond with frame technology due to the need to track the angle of direct solar irradiance in the E/W orientation, and the constant angle of direct solar irradiance in the N/W orientation depending on hemisphere. The application of the differing technologies can give information as to the intention of the array's electricity production, when peak power will be reached, the prominent technology of the installation period, cost effectiveness, and efficiency of installation practices (Chu 2011).

PV array panels are spectrally and geometrically distinct from most land covers and are therefore able to be identified using remote sensing. Crystalline silicon (C-Si) fixed axis and single-axis tracking arrays were the focus of this study because of their similar linear geometries and spectral signatures, and because they represent a majority of commercial scale PV modules (Brooks and Dunlop 2013; Chu 2011; Doyle et al. 2015). To develop this spatial dataset, we employed eCognition Developer.

Once the panels were identified, we assumed that spectrally, the year of greatest land use change within those panels was the year of completed installation. This year gives insight into

the removed crop type (accounting for crop rotation) that was forgone due to the installation, total electricity generation, efficiency, and installation practices of the period. To help fill this gap in understanding and analysis, we employ LandTrendr to estimate the year of each completed array. Our analysis produced a novel spatiotemporal dataset of regional PV array geospatial coordinates, along with information on array sizes, panel areas, orientations, and technologies, which can provide important information about regional solar power and its effects.

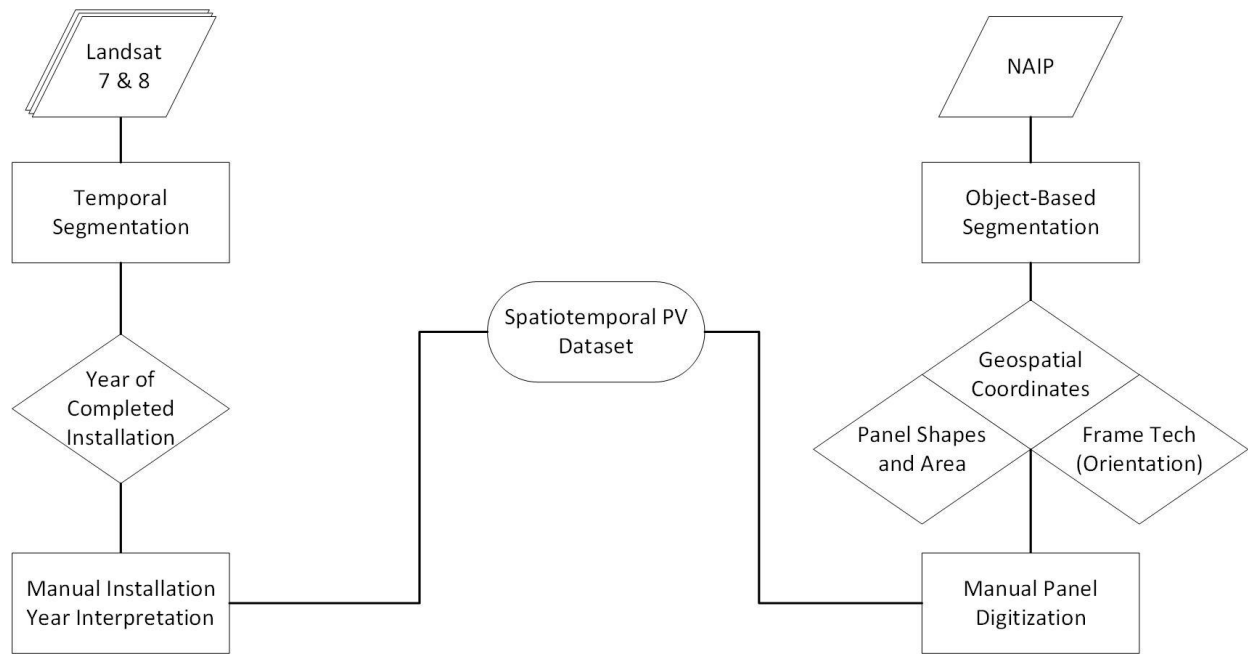


Figure 1.2. PV Identification Framework. The developed framework to integrate temporal and object-based segmentation for regional land cover change detection regarding PV array technologies. The parallelograms denote the input imagery, rectangles denote processes, and diamonds denote derived PV array attributes. The oval denotes the final dataset.

2.4 New indices: *NDPVI* and *NDB*

Silicon PV panels tend to have moderate to high blue reflectance largely due to their silicon composition and a low NIR reflectance due to the anti-reflective coating that improves spectral absorption and improves efficiency (Karin and Jain 2020). Thus, the normalized difference between the blue band and the NIR band seems a promising means of delineating PV

panels. We refer to this index as the Normalized Difference Photovoltaic Index (NDPVI) shown by equation 1.

$$NDPVI = \frac{\alpha * Blue - NIR}{\alpha * Blue + NIR} \quad (1)$$

Based on preliminary testing, other land covers with a similar spectral signature are impervious surfaces, water, shadows, and some bare soils. To reduce spectral overlap between these land covers and PV arrays, we added a weighting coefficient. Gitelson (2004) showed that the addition of a weighting coefficient (α) in the normalized difference vegetation index (NDVI) increased sensitivity at higher NDVI values due to the dampening the effect of variations in NIR reflectance and emphasizing the normalized difference. Inspired by this, a weighting coefficient was added to NDPVI to enhance the sensitivity to the difference between the blue and NIR and reduce sensitivity to the variation in the blue reflectance of PV panels, which varies drastically at the NAIP scale by scene. While many alpha coefficients were tested, an alpha of 0.5 was used in this analysis due to observed increase in NDPVI disturbance sensitivity and increased panel identification accuracy in test plots. More experimentation could improve the alpha and the index accuracy overall. Figure 1.4 portrays the usefulness of using NDPVI in the LandTrendr temporal breakpoint analysis.

In addition to NDPVI, we developed an index we refer to as the Normalized Blue Deviation (NBD). NBD was developed because even with the alpha weighting coefficient, NDPVI retained some shadows, water, and bare soil. The brightness threshold accounted for water, but also retained shadows, and some bare soil. NBD re-emphasizes the importance of C-Si blue reflectance, but in relation to the red and green bands instead of the NIR band. NBD was defined as shown in equation 2.

$$NBD = \frac{Blue - \frac{Red + Green}{2}}{Blue + \frac{Red + Green}{2}} \quad (2)$$

2.5 Identifying geometrically linear and parallel panel systems

eCognition developer is an image analysis software tool that provides a geographic object based image analysis platform (Definiens 2000). The application provides access to algorithms for segmentation and classification and the ability to create a systematic ruleset whose parameters are determined through expert knowledge along with machine learning. It was therefore important to know spatial PV panel attributes (shape, size, spectral signature, spacing, and technology preferences).

The workflow and thresholds shown in Figure 1.3 were developed through preliminary testing of 176 arrays identified across the Central Valley using preliminary methods described in Appendix Text A1.2.3. The newly derived spectral indices (NDPVI and NBD) and brightness were used in a multi-threshold segmentation. The goal of this segmentation was to differentiate panels from surrounding landscapes and minimize differences in scene values due to atmospheric effects (e.g., clouds), time of day, and other scene differencing effects. Segmented objects were filtered by multiple geometric thresholds including number of pixels, length to width ratio, and a border index (rectangular fit index) that resembles the object-based methodology that M. Wang et al. (2018) used to generate linear PV panel-like objects. Templates (30x30 meter) were then generated in eCognition pulling NDPVI textures from five arrays of differing panel width and packing shown in the third column of Figure 1.3. These templates were then processed in R to rotate templates in both the S oriented and E/W oriented directions, at multiple packing factors and panel widths. The template matching algorithm was applied to generate a raster of each pixel's surrounding fit to the template. If the linear panel-like objects were within 100 meters of a pixel with a 50% match to the template (based on template training in eCognition), then the object was considered a PV panel. The assumption was made that S-oriented panels were most

likely fixed angle mounted due to the fact that the optimal tilt angle for maximum solar irradiation is constant (fixed) for S-oriented arrays (Martín-Chivelet 2016). An additional assumption was made that any E/W panels were single axis mounted arrays for the similar reason that the optimal angle for maximum solar irradiation varies over the course of the day in the E/W direction (Martín-Chivelet 2016). Therefore, panels were further classified into orientations based on a derived orientation object feature and were separated into their final classes of C-Si single-axis tracking arrays and C-Si fixed axis arrays.

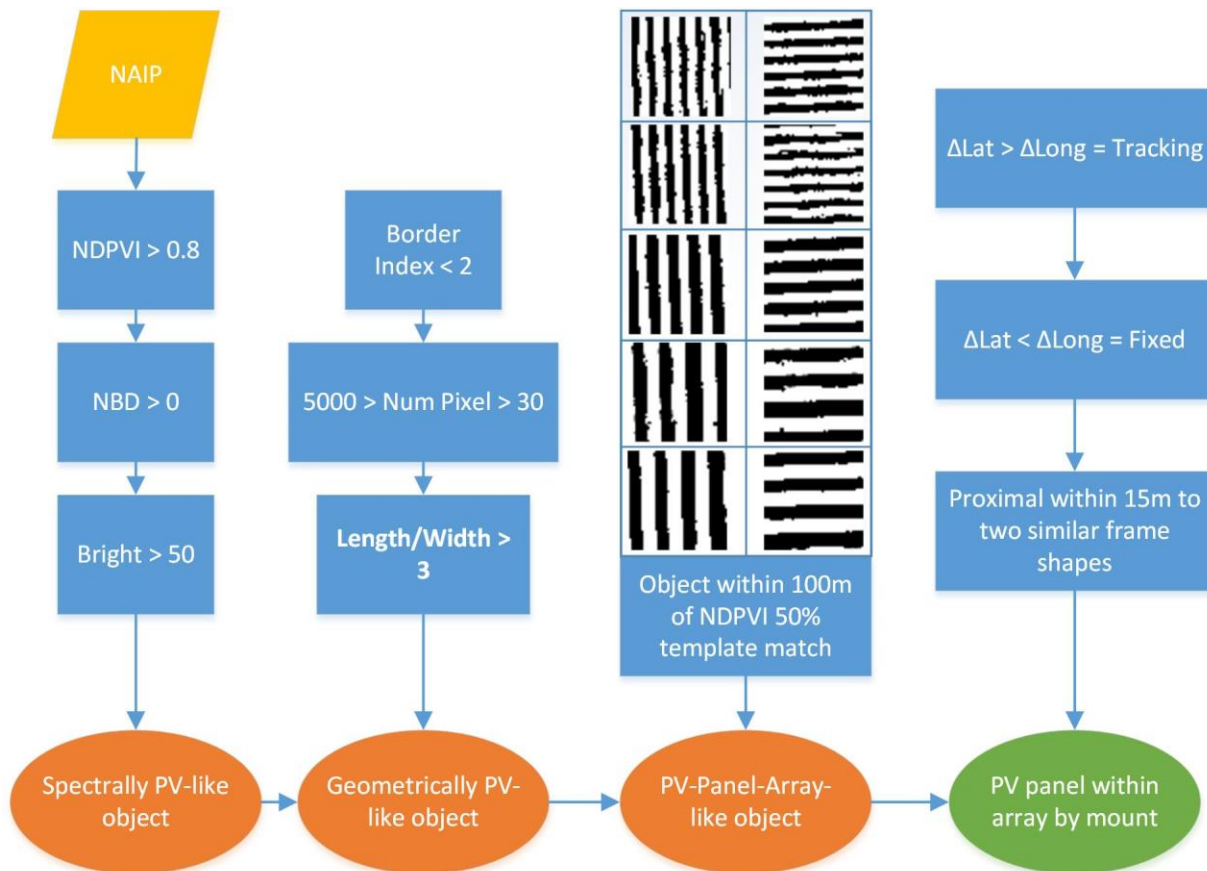


Figure 1.3. Object-Based Panel Identification Workflow. The spectral and object-based ruleset used to delineate solar PV panels from surrounding landscape and by frame mount across the Central Valley. Here, the parallelogram indicates input imagery, rectangles indicate thresholds, and ovals indicate preliminary (orange) and final (green) shapefile outputs. The images composed of black rectangles were the ten PV templates of varying panel width and packing used in the template matching process.

We developed a ruleset to classify panels using spectral segmentation and object

geometries. The full mosaiced 2018 NAIP image was parsed into eight segments which were each further tiled into 46,000 x 46,000 pixel images (maximum extent of eCognition, at NAIP resolution this is roughly 745 km²), and each of the 140 images was processed individually using the developed ruleset shown in Figure 1.3.

The eCognition segmentation and classification yielded a shapefile denoting individual PV panel locations, mounting technologies (orientation), and panel areas (number of pixels and NAIP resolution).

2.6 Identifying installation year

LandTrendr software is based on spectral-temporal segmentation algorithms that are useful for change detection in a time-series of moderate resolution satellite imagery (Landsat) and to generate trajectory-based spectral time-series data with minimal inter-annual signal noise (Kennedy, Yang, and Cohen 2010). LandTrendr takes the annual medoid composite pixel values, the band value closest to the median value of all corresponding pixels among each year considered (Kennedy et al. 2018), and uses user specified change and segmentation parameters to differentiate spectral epochs of a band of interest (in this case, NDPVI). The annual values were then fitted to a temporal vertex of the spectral segments as shown in Figure 1.4.

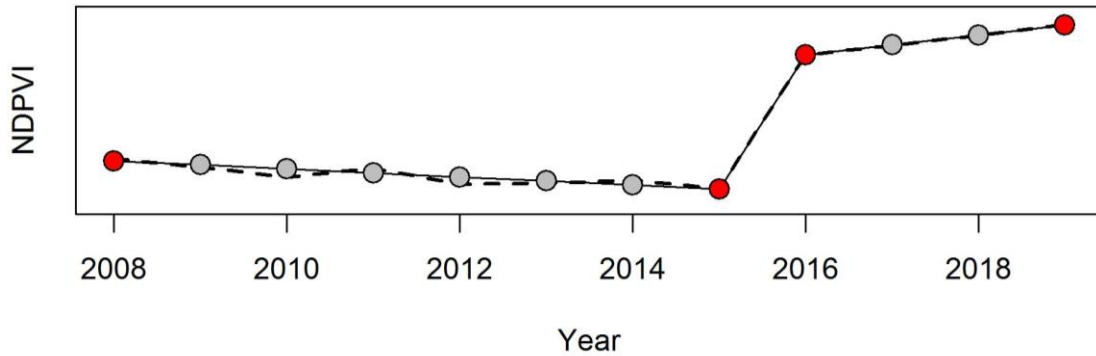


Figure 1.4. NDPVI Breakpoint Timeseries. The LandTrendr adjusted annual medoid NDPVI values (dotted line) with the Fit to Vertex (FTV) NDPVI time-series path (solid line and points) identified by LandTrendr of the array near Fairmead, California described in Figure 1.1. This figure shows the vertices (red) and segments after the FTV algorithms have been applied (adapted from (Kennedy et al. 2018)). This array was installed in 2016.

The geometry of these spectral segments and their vertices can be used to determine years of change, magnitude and duration of change, as well as magnitude and duration of recovery. Here, we used three spectral epochs, and because the arrays are permanent once completed, there was no recovery back to prior land cover. This helped reduce noise as other changes in NDPVI (such as removal of a crop for rotation) have recovery periods.

There are several pre-coded spectral indices that are implemented in LandTrendr for temporal change detection (Kennedy et al. 2018). Most prior studies that applied LandTrendr have examined large-scale forest disturbances, burn severity maps, cropland changes, and other coarse landscape changes (Cohen et al. 2018; FRAGAL, SILVA, and NOVO 2016; Reilly et al. 2017; Runge and Grosse 2020; Schneibel et al. 2017; Schwantes, Swenson, and Jackson 2016; Shen, Li, and Wei 2017; X. Wang et al. 2016; Yang et al. 2018). Some studies have used LandTrendr to quantify urban (impervious surface) development using indices and pixel based classification methods (Liu et al. 2019; B. Wang et al. 2019; Xu et al. 2019). However, few if any studies have used LandTrendr for high-resolution applications such as land cover changes due to installation of agriculturally influenced PV arrays.

LandTrendr has recently been implemented in GEE for use with its open source remote sensing repository (Kennedy et al. 2018). The GEE LandTrendr pre-processing and control scripts were downloaded from their public repository called eMapR by Oregon State University and the NDPVI was added to the list of change indices. The start year of installation detection were assigned as 2008 as this was the earliest year with a CDL product and was the culmination of major solar federal and technology incentives (Efficiency 2010; Schoeffler 2009; Shah 2009; Solar Energy Industries Association 2019); 2018 was selected as the end year as it was the most recent NAIP imagery available for the region at the time of the study. Therefore, only arrays installed by late summer 2018 (end of NAIP imaging period) were identified. Collection, running, and change parameters which dealt with specifics of the temporal segmentation regarding spectral recovery, number of segments, magnitude of change, duration of change, amongst others (Kennedy et al. 2018) are shown in Table A1.1. The characteristic time-series pattern that these parameters are looking to delineate is shown in Figure 1.4.

The red points in Figure 1.4 show the spectral epoch vertices identified by LandTrendr. The first vertex is the start year of detection, the second vertex is the year prior to change, the third vertex is the year of detection (YOD), and the fourth vertex is the end year of detection. The third vertex is the year of greatest spectral change (breakpoint) and was thus assumed to be the year of completed installation.

The result of the LandTrendr algorithm was a raster stack of variables pertaining to temporal change. One of the raster layers was the Year of Detection (YOD) layer. The eCognition shapefile, along with manually digitized omitted panels (Appendix Text A1.1.1 and A1.1.2) was used to clip the YOD image to acquire the assumed year of completed installation and remove other changes in impervious surfaces. All available imagery was analyzed and the

first year of apparent completed solar PV installation was recorded, regardless of when landcover was cleared, or what month the installation was completed.

One final detail in creating the dataset of remotely sensed ground-mounted solar PV arrays was the definition of an “array”. Here, we define arrays by a three-step process. First, identified panels were buffered by five meters and combined with nearby panels of the same orientation (class) to create a “sub-array”. The LandTrendr output was extracted from each sub-array resulting in an installation year. Finally, sub-arrays within 50 meters were combined with nearby sub-arrays of the same orientation (class) and year of installation to create an “array”.

To estimate year of installation accuracy, random samples were selected from 10% of the completed dataset, not including the 63 arrays where the year of installation was already manually interpreted, and the year of installation was manually interpreted using the same methodology described above. Therefore, 95 arrays were assessed in the validation.

2.7 Determining to-date capacity, generation, and installation practices

Once the dataset of PV locations and attributes was developed, the energy and crop implications of the array installation practices were assessed. Here we describe installed PV capacity, generation, and derived metrics of installation practices for each array.

Packing factor (PF) was defined as the ratio of the panel area to the total ground cover area encompassed by the array panels and the interrow space between panels (Ong et al, 2013). According to Martín-Chivelet (Martín-Chivelet 2016), an optimal packing factor based on latitude would minimize land use change and retain maximum irradiation given shading and orientation. PF_{opt} is calculated according to:

$$PF_{opt} = PF_0 - A\varphi^2 - B\varphi \quad (3)$$

where PF_0 is the packing factor at 0 degree latitude which is 91.5% for a single-axis tracking

E/W facing array, and 100% for a fixed axis S facing array, φ represents the latitude of each array centroid, and A and B are fit parameter coefficients (Martín-Chivelet 2016). This optimum packing factor minimizes the loss of electricity yield from the shadow effect while also minimizing land use change, and thus crop loss. If the installations are not following the optimum packing factor based on latitude, there was additional unneeded cropland transformation, and therefore crop loss from the system installation. To account for single-axis tracking array potential, tilt between 10 am and 2 pm, the NAIP imagery acquisition timing, panel areas were corrected for a maximum total panel area deviation where each panel was assumed to be tilted by 21.92 degrees given the NAIP best practices (Bunis and Mootz 2007), assumed maximum single-axis tracking tilt angles of 45 degrees in either direction (Schneider 2012), and the solar inclination timing for the Central Valley average latitude (NOAA 2016).

Martín-Chivelet (Martín-Chivelet 2016) also provides a methodology for calculating Technical PV Potential or *Capacity* (kW). The equation for calculating capacity is defined by:

$$Capacity = PF * \eta * G_{STC} * A_S \quad (4)$$

where PF is packing factor derived from the identified panels, η is the efficiency of the average commercial system at the year of installation from (Barbose et al. 2020), G_{STC} is the irradiance at standard test conditions and is assumed to be 1 kW/m² (Martín-Chivelet 2016), and A_S is the total area of the system. For simplicity, because this study focused on commercial-scale ground-mounted arrays, we assumed that the η of each array was the average efficiency of commercial systems during the same year.

The actual electricity generation (MWh) is dependent on weather, incident irradiance, tilt, efficiency, efficiency degradation, and soiling losses, and therefore must be modeled given these observations and assumptions. Each PV location's hourly global horizontal irradiance, direct

normal irradiance, direct horizontal irradiance, dry bulb temperature, and wind speed are taken from National Solar Radiation Database weather files (NREL 2015). The hourly incident irradiance on both fixed and tracker modules is calculated using the pvlib python modules developed by SANDIA National Laboratory (F. Holmgren, W. Hansen, and A. Mikofski 2018). The single-axis tracker panels are assumed to rotate up to 45° in east and west directions (Schneider 2012). As opposed to the technical PV potential, the actual hourly electricity generated from each panel is calculated using the simple efficiency model developed by National Renewable Energy Laboratory (Gilman 2015). The PV efficiency degradation is assumed to be 0.6%/year for pre-2010 installations and 0.3%/year for post-2010 installations based on Jordan et al. (Jordan et al. 2016). The soiling losses for PV electricity generation are taken as 3% for California (National Renewable Energy Laboratory 2017). Accounting for these factors, the annual timeseries of energy generation for each array was calculated.

Farmland contains gradients of crop productivity due to changes in geology, soil, and topography. Low yield land is often called marginal land, which can be in some cases resource expensive and low yielding that it gives farmers a negative cost margin on crops grown (Martinez-Feria and Basso 2020). Comparing productivity of the surrounding land of the same ownership, practices, and crop type as the cleared land gives insight into the level of informed placement decisions.

Metrics for determining the suitability of agricultural land to be converted to an array do not exist, so we developed a relative land productivity (*RLP*) metric, which is a calculation of the productivity of the land transformed relative to the productivity of the surrounding land of the same crop type and ownership. Here, NDVI is used as a proxy for crop productivity as it commonly has been used in the past (Benedetti and Rossini 1993; Bolton and Friedl 2013; Funk

and Budde 2009; Maselli et al. 1992; Mkhabela et al. 2011; Pettorelli et al. 2005; Rasmussen 1992; C. J. Tucker et al. 1985; Compton J. Tucker 1979). This metric provides insight about whether or not farmers and asset owners are installing PV arrays on plots of land that have been historically less productive compared to the rest of their fields. The framework for calculating relative land productivity is shown by:

$$RLP = \frac{\sum \frac{PV\ NDVI_1}{Qsec\ NDVI_1} + \frac{PV\ NDVI_2}{Qsec\ NDVI_2} + \dots + \frac{PV\ NDVI_n}{Qsec\ NDVI_n}}{n} \quad (6)$$

Where n is the number of years prior to the installation year to be considered, $PV\ NDVI_1$ is the growing season (June - September) mean normalized difference vegetation index (NDVI) of the cropland area and crop type cleared for the array one year prior to installation. This is repeated through n years prior for the same crop type as one year prior. This allows variations in NDVI due to crop rotations to be considered. Where $Qsec\ NDVI_1$ is the growing season mean NDVI of the cropland area and same crop type as that cleared for the array falling within the Public Land Survey System (PLSS) quarter (Q) section denomination through n years prior. The average farm size in California was 348 acres as of 2019 (Brown 2020) and the Q-section area is 160 acres, which was thus a good approximation of farmers locally owned fields as many large commercial farms drastically increased the mean farm size. The section delineation is 640 acres, and thus would encompass more than one farmer's field area on average and would not be representative of a single farmer's decisions. All arrays converting rice were removed from the relative land productivity analysis due to the difficulty in using NDVI as a proxy for crop productivity regarding multiple phenological phase crops and flood irrigated areas (Nguyen et al. 2012).

The eCognition panel shapefile was used to clip Landsat-derived growing season NDVI maps needed for the RLP metric. Because this is a relative metric, it is less important to determine what relationship NDVI has to each crop's quantitative productivity, and more

important to find regions of lower productivity compared to the surrounding field. Assuming fields contain these gradients of productivity, RLP values less than 1 indicate that the PV array was installed in an area of lower productivity cropland within a field (optimal placement decision), values equal to 1 indicate that the installed region of land was of equal productivity to the Q-section average (sub-optimal placement decision), and values of more than 1 indicate that the array was installed in a region of higher productivity (sub-optimal placement decision).

To evaluate t-test validity for both packing factor and relative land productivity, 1000 Monte-Carlo Kolmogorov-Smirnov (KS) normality tests were performed for each technology and each year of installation. If the KS test suggested a normal distribution, subsequent two-sided T-test were performed.

The eCognition shapefile was also used to clip the CDL yearly images to determine what type of crops are preferentially being converted to solar arrays. For the purpose of future work regarding historical irrigation data, CDL crop types were grouped into and reported as Farm and Ranch Survey (USDA 2013) crop types. Cumulative area was calculated by multiplying the area of converted cropland for each array by the difference in the installation year and the end year of the study (2018). The cumulative area converted also accounts for crop rotation by taking the crop distribution of the previous five years and projecting the proportion of each crop forward for the area of crop converted for each array. This metric emphasizes the importance of overall temporal tendencies in which crops and what area of crops are worth converting for the lifespan of typical solar arrays.

3. Results and Discussion

3.1 Performance of the NDPVI and NBD indices in classification

The NDPVI, NBD, and brightness spectral indices were able to spatially differentiate PV

arrays at NAIP scale, and NDPVI was able to temporally determine PV years of installation at Landsat scale as shown in Appendix Figure A1.3. C-Si PV panels tend to have high blue reflectance, high brightness compared to shadows, and a low to moderate NIR reflectance. Therefore, panels tend to have a NAIP derived NDPVI value > -0.25 , a Brightness value > 50 , and an NBD value > 0 (highly conservative values) at NAIP wavelengths. In addition, the change in this NDPVI was observed to be greater than the change in NDVI for converting agricultural land cover, and other land covers to a PV array. Remaining commissions were mostly removed via morphological and proximity features in eCognition, especially for tree row crops, and furrow irrigation which are both are spectrally similar to PV arrays and portray linear morphologies similar to PV panels. NDPVI was robust for differentiating the moderate-high blue reflectance and low NIR reflectance of PV arrays from surrounding land cover, and for detecting temporal disturbance in the LandTrendr algorithms.

3.2 Spatiotemporal identification of large-scale commercial PV arrays

Figure 1.5 shows the identified array centroid geospatial coordinates, year of completed installation, and the frame technology of the 1006 commercial scale ground-mounted solar PV arrays detected in the Central Valley. We identified 644 fixed axis arrays (64% of total) composing 15% of installed capacity and 362 single-axis tracking arrays (36% of total) composing 85% of installed capacity. Of the 1006 identified arrays, 694 were agriculturally co-located (active cropland the year prior to installation). The remaining 312 arrays co-located with fallow/idle cropland (189 arrays -- inactive agriculture), developed land (107 arrays), and other land cover classes (11 arrays). The definition of an array used in this study allowed for adjacent arrays installed in different years to be differentiated.

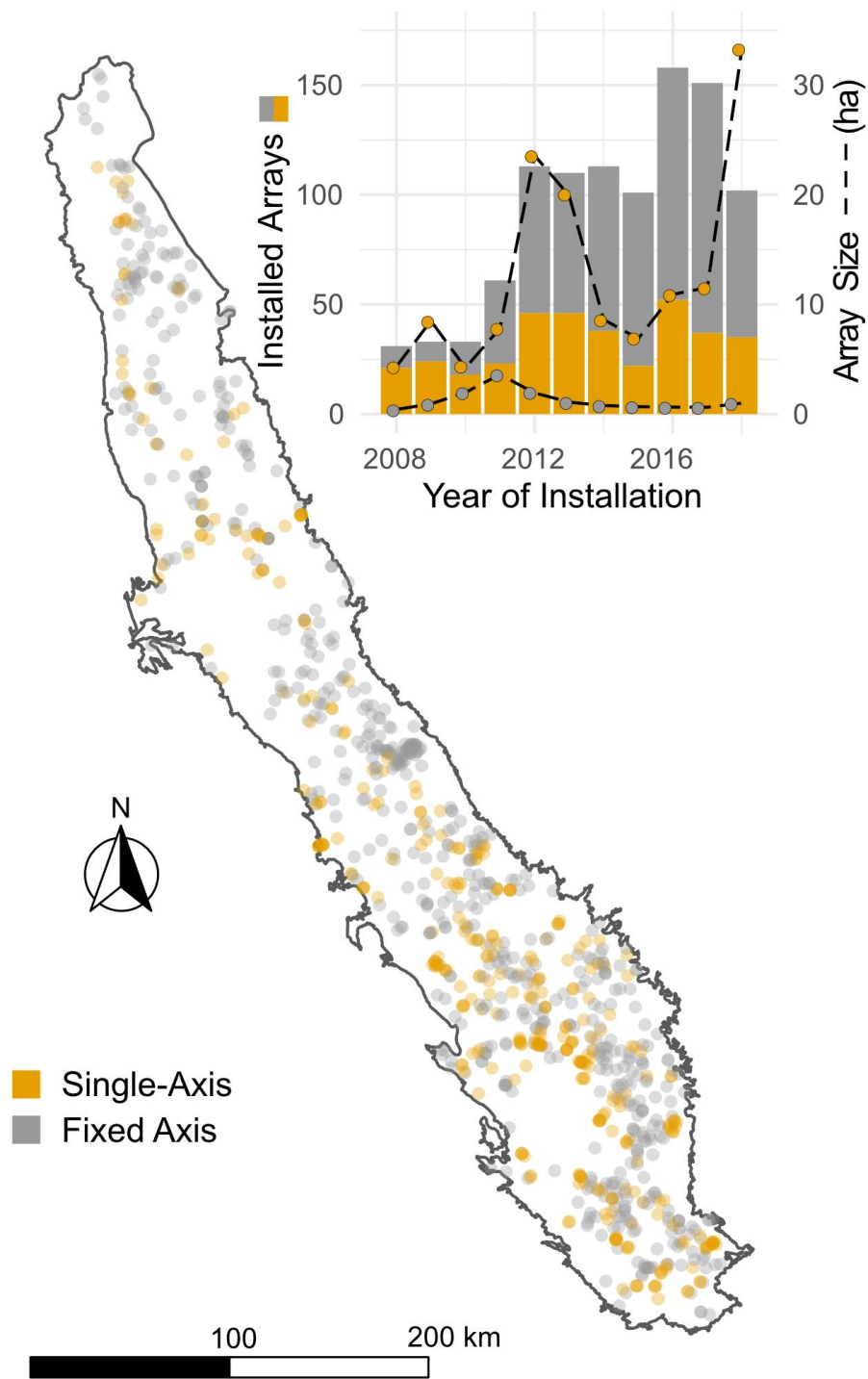


Figure 1.5. Solar PV Arrays in the Central Valley. Geospatial coordinates and year of installation for detected solar PV arrays in California’s Central Valley determined using the integrated object-based and temporal segmentation framework (LandTrendr + eCognition). Upper Right Inset) Annual distribution of array installations for each frame technology along with the average array size for each technology over time on the right axis. Note that single-axis tracking arrays (orange) and fixed axis arrays (grey) are delineated by color in both figures.

This dataset was derived using the integrated object-based and temporal segmentation framework through eCognition and LandTrendr respectively. The object-based ruleset developed in eCognition identified 181,593 unique panel shapes across the Central Valley. Of the identified unique panels, 5,502 panel shapes were manually removed using manual annotation of 2018 NAIP imagery resulting in 176,091 validated panel shapes (16,557,764 m² panel area) and a commission accuracy of 97.0% (commission error = 3.0%). Commissions were mostly of developed land, tree crop shadows, fallow or idle cropland, alfalfa, and other crop types. Manual digitization of omitted panels resulted in an additional 98,952 panel shapes, although 77,139 digitized panel shapes overlapped automated panel shapes in large part due to the use of template copying (see Appendix Text A1.1.1) and were merged with overlapped automated panels. In total, 210,368 individual panel shapes (22,227,832 m² panel area) were identified by merging the automated detection and the manual digitization. By area, the omission accuracy was 74.5% (omission error = 25.5%). Of the identified panel shapes, 6.9% were fixed axis (S oriented: 3,441,255 m² of panel area) and 93.1% of which were single axis (E/W oriented: 18,786,577 m² of panel area).

Of the 1006 arrays identified from those panel shapes, 63 (omission error = 6.26%) required manual interpretation of the year of completed installation (from 2008 to 2018) through interpretation of LandTrendr pixel time-series plots alongside historical imagery. Validation of installation year showed that 53 of 95 arrays (56%) had the same interpreted year of installation as the LandTrendr medoid prediction with an additional 22 arrays (23%) being within one year. Two arrays in the validation dataset were installed in 1998, which was outside of the timespan of LandTrendr, resulted in a year of installation of the final year of the study period, 2018. This should be noted as a limitation of LandTrendr, that any arrays installed prior to the beginning of

the study period will result in either a year of installation of the final year of the study period, or none at all. Including the two statistical outliers (20 year deviation, 2.86 standard deviations from the mean), the standard deviation of the year difference was 3.5 years. Further analysis is needed to determine how much impact this limitation had on boundary year installations (2008 and 2018). For many of the arrays where the LandTrendr year of installation was predicted one year later than the manually interpreted year of installation, the array was observed in the latter months of the manually interpreted year. So, although the “year of installation” was technically a year prior, the array likely generated very little electricity during the partial year (e.g., November-December 2013 vs 2014). Because LandTrendr by default returns a spectral annual medoid value, the year of installation will inherently be the year where the array was installed for a long enough portion of the year to drastically change the spectral trajectory of the annual medoid value and likely generate energy for a majority of the year.

3.3 Current commercial solar electricity production and observed policy responses

Figure 1.6 shows the installed capacity and generation of all arrays identified by this study. The cumulative capacity of the identified arrays was 3.55 GW. The cumulative generation of all identified arrays up to 2018 was 36,531 GWh, 7,798 GWh of which was generated in 2018 alone. The average annual electricity generation for single-axis tracking arrays in 2018 was 18.69 GWh and for fixed axis arrays was 1.60 GWh per array. Note annual installed capacity peaks at 2012, 2016, and 2018 for single-axis tracking arrays, and 2011 for fixed axis arrays.

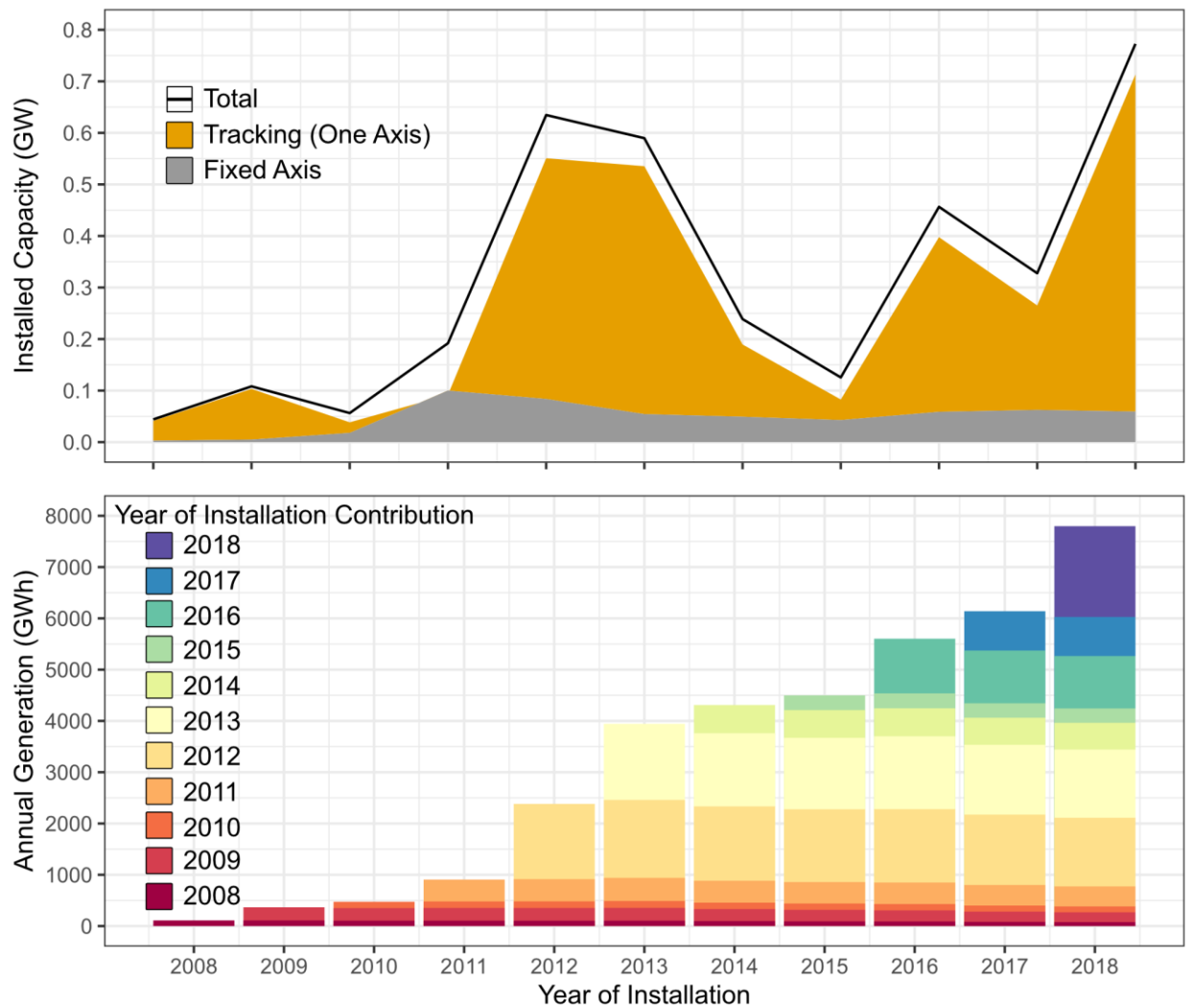


Figure 1.6. Installed Capacity and Annual Generation of Identified Arrays. The total installed capacity (top) and annual generation (bottom) for the identified arrays. Values are not cumulative, and only represent the contribution of arrays installed in the respective year of installation. Note that the colors in the installed generation plot delineate the relative contribution of arrays installed in respective years to total annual generation.

The California Energy Statistics and Data portal reports that as of 2018, 731 solar PV arrays were connected to the grid in all of California accounting for 10.64 GW of capacity and a generation of 24,981 GWh or 12.8% of California’s in-state generation in the same year (Nyberg 2020). Note that this excludes the solar thermal arrays (1.2 GW and 2,545 GWh reported in 2018) which were not the focus of this study because they are primarily located in the Mojave Desert outside of the Central Valley and thus are likely not co-located with agriculture.

Therefore, the 7,798 GWh and the 3.55 GW from the 1006 identified Central Valley arrays accounted for 31.2% of reported solar electricity generation and 33.36% of reported solar capacity respectively, and 3.99% of California's total in-state electricity production in 2018 (Nyberg 2020).

Module degradation was primarily responsible for the decreasing trend in electricity generation (Figure 1.6) in each year's respective contribution. Annual changes in local solar irradiance included in the generation model also impact the annual value, but did not show an annually decreasing trend. Note that 2013 and 2016 were years of high irradiance, which explains the installed generation increases of all arrays present in those years.

Notable peak years in the total number of installed arrays (Figure 1.5) were 2012 and 2016. The Emergency Economic Stabilization Act of 2008 (Shah 2009) included an eight year extension on the Solar ITC and eliminated the monetary cap of the credit (Solar Energy Industries Association 2019). However, a stipulation to be eligible for the ITC was that projects had to be in service no later than four calendar years after the calendar year in which construction began (U.S. Department of Energy 2021). It is likely that applications for the credit are concentrated at the end and beginning of each renewal in case the credit is not renewed. Therefore, if there was a surge in applications for the credit and "construction commencement" in the year of the original extension (2008), then the surge in the number of observed installations in 2012 and 2016 was likely indicative of this four year ITC eligibility requirement repeating itself, and the potential expiration of the extension in 2016. In addition, the ITC has been set to expire every four years since 2016 pending the Congressionally decided extension of the program (U.S. Department of Energy 2021). The ITC extension along with the end of the four year construction period requirement (since 2016) would suggest that another peak in the

number of solar installations would occur in 2020. Peak installations in also 2016 was perhaps also related to the California Public Utilities Commission (CPUC) adoption of the current Net Energy Metering (NEM) 2.0 program early in the 2016, which is available to customers in the major utility service providers in the Central Valley (PG&E, SCE, and SDG&E); this program provides full retail rate credit for overproduced energy exported to the grid (CAPUC 2016).

It must be noted, however, that the most recent ITC extension projects have decreasing tax incentives over the next four years. Projects starting construction between January 1st, 2020, and December 31st, 2022, will have a 26% tax credit, between January 1st, 2023 and December 31st, 2023 will have a 22% tax credit, between December 31st, 2023 and December 31st, 2025 will have a 10% tax credit (U.S. Department of Energy 2021). The decreasing credit incentives could drive up early installations over the next four years, with potentially fewer installations at the end of the extension period unless the program incentives change. However, this is also dependent on energy prices (typically increasing), other incentives, and general changes in the cost to install solar.

The distribution of frame technologies shows that fixed axis array installations vastly outnumber single-axis tracking installations over the last decade and tend to be smaller. Despite the lower proportion of installations compared to fixed axis, single-axis tracking arrays have contributed 84.86% of installed capacity over the study period. This was mostly due to the median size of single-axis tracking arrays (1.19 MW or 2.04 ha) which was more than ten times the median size of fixed arrays (0.32 MW or 0.39 ha). A possible reason is that fixed axis arrays are cheaper to install, and thus small scale farmers who are installing smaller capacity arrays are more likely to install fixed axis arrays. This may also suggests a difference in the purpose of the installation between the two frame technologies born out of cost.

Appendix Figure A1.2 shows the northward latitudinal deviation for fixed axis installations in 2008 and single-axis tracking installations in 2010 and the corresponding decrease in annual average Global Horizontal Irradiance (GHI). Note that only 31 arrays and 33 arrays were installed in 2008 and 2010 respectively, thus a few northward arrays draw the distribution towards lower GHI. However, a potential explanation for a northward trend in installations in both years is the Federal Depreciation Modified Accelerated Cost-Recovery System (MACRS) enacted in 2008, which was accelerated in 2010 by the Tax Relief, Unemployment Insurance Reauthorization, and Job Creation Act of 2010, where installers could claim a federal 50-100% (2008 vs. 2010) depreciation deduction on qualifying capital equipment purchased and placed in service by December 31, 2011 (N.C. Clean Energy Technology 2016).

3.4 Packing factor and relative land productivity

This study specifically looks at adjacent co-location where active cropland was replaced by solar arrays, and where surrounding cropland remains. Although, with the methods described here, there was no way to determine if some form of agricultural or pollinator habitat remained directly beneath the arrays.

Current optimal installation practices which emphasize the cost of installation and electricity production could lead to sub-optimal impacts falling on the agricultural stakeholder. Potential sub-optimal practices include a disregard for the productivity of farmers' fields and unnecessary spacing between parallel module arrays. Faults in placement and spacing of arrays might lead to significant and unintended losses in crop yield.

To assess co-location practices, the arrays that were both larger than one panel (non-array) and were within the CDL and Farm and Ranch Survey definition of cropland, were extracted from the 1006 identified arrays. Filtering by active cropland the year prior resulted in

694 arrays (69% of the dataset) for the agricultural co-location analysis.

Figure 1.7 shows the pacing factor (PF) deviation from optimum and the relative land productivity (RLP) distribution for the dominant frame technologies in the Central Valley. As evidence by the different distributions, fixed axis and tracking arrays have somewhat different installation practices. All distributions were sufficiently normal (minimum KS score of 0.51), thus a two-sided t-test was sufficient for further analysis.

Packing factor distributions for both technologies fell significantly below optimum in the Central Valley. Fixed axis packing factor was an average of 3.54% below optimum ($p < 2e-16$) while single-axis tracking packing factor was an average of 10.92% below optimum ($p < 2e-16$). When accounting for maximum potential panel tilt due to timing of NAIP imagery, single-axis tracking packing factor was an average of 8.58% below optimum ($p < 2e-16$). Relative Land Productivity distributions for fixed axis arrays fell significantly below an RLP of 1 ($p = 1e-12$), while single-axis tracking array distributions were not significantly different from 1 ($p = 0.66$).

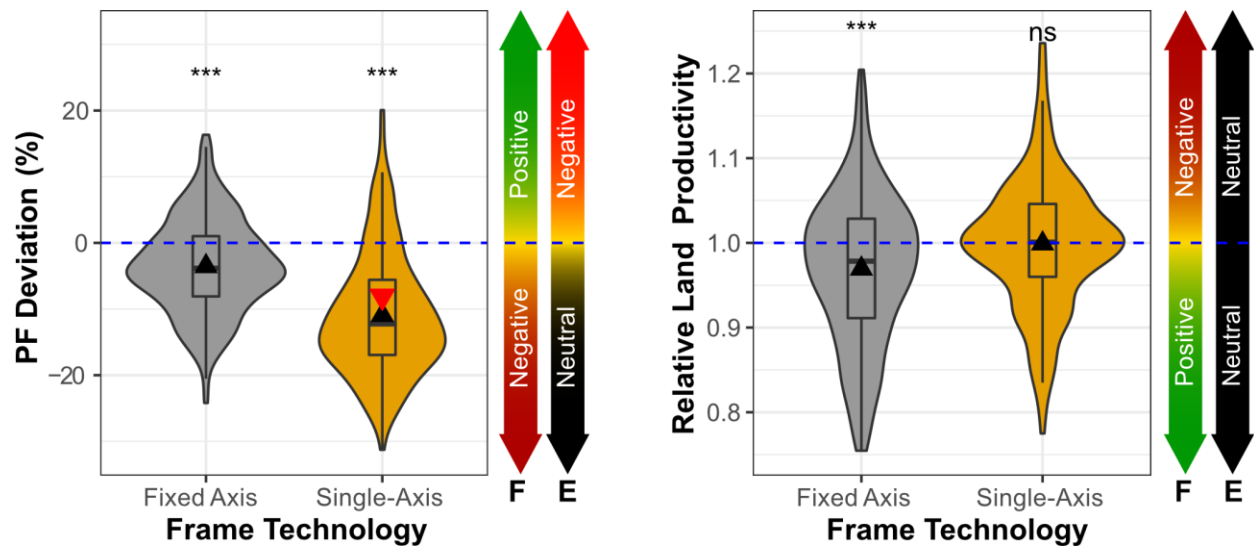


Figure 1.7. Packing Factor Deviation and Relative Land Productivity of frame technologies. (Left) Observed PF - Optimum PF of installations offsetting all crops across all years of installation for the two dominant technologies. The dotted blue line depicts the region where the actual packing factor is optimal. (Right) Relative Land Productivity across all crops for both dominant technologies. The blue line shows a RLP value of 1 indicating that the offset crop land perfectly represents the productivity of the surrounding cropland of the same crop type. Boxplots denote quartiles, and standard significance is denoted by the asterisks and the 'ns' for non-significant. The colored arrows to the right of each plot denote impact on cropland (C) and electricity production (E). Green, yellow, red, and black indicate positive, neutral, negative, and not effects respectively.

To assess temporal changes in packing factor and relative land productivity (Appendix Figure A1.4), these metrics were aggregated across arrays installed each year for each technology. For both packing factor and relative land productivity, all distributions were sufficiently normal (minimum KS score of 0.49 for both), thus a two-sided t-test was sufficient for further analysis.

Temporal packing factor distributions for both technologies fell significantly below optimum in the Central Valley. Packing factor p-values ranged from 0.0034 for 2010 to 7.1e-12 for 2015. Temporal relative land productivity p-values were non-significantly different from 1 until 2014. Relative land Productivity p-values ranged from 0.96 for 2011 to 7.2e-5 for 2017.

Figure 1.7 and Appendix Figure A1.4 show that packing factor deviations fell

significantly below optimal for both frame technologies, and in each year of the study period. This suggests that current practices place panels too far apart, resulting in unnecessary conversion of cropland, which has not improved through time. The main impact here was crop loss. Single-axis tracking arrays do need increased spacing compared to fixed axis arrays due to the shading factor of the angled modules (Martín-Chivelet 2016) which was accounted for in the PF_0 factor, however, this extra spacing was overcompensated. The large deviation in single-axis tracking array packing factor likely results from the perceived need for greater spacing to allow the passage of maintenance vehicles. In addition, single-axis tracking frames are more expensive to install, thus installers may preferentially forgo more cropland than was necessary to ensure that there is no shading. Single-axis tracking arrays were also ten times larger on average and often converted low value cropland (wheat and pastureland). For large and expensive arrays converting low value cropland which also require spacing for easy maintenance, there is no current incentive for the utility installer to minimize crop loss. This dataset suggests the need for a required standard for ground-mounted PV array packing distance which would reduce the unnecessary crop loss for both fixed axis and more so for single-axis tracking PV arrays while retaining maximum utility electricity generation.

Fixed axis arrays tended to be placed on marginal lands, while 1-axis tracking arrays showed no RLP preference. High RLP values suggests that a more effective placement decision could have been made to reduce loss agricultural production while low values suggest marginal land was used for the installation optimizing land use. For fixed axis arrays, RLP was significantly below field average while single-axis tracking arrays were not significantly different from the field average. Temporally, RLP was not significantly different from the field average until 2014 and 2016 when RLP was significantly lower and likely more effective spatial

placement began occurring. This suggests the field spatial productivity was not a consideration for either technology until 2014 where it became a consideration for fixed axis arrays. One factor that RLP does not account for is proximity to roads, which is a major factor in determining within field placement.

A potential economic explanation for single-axis tracking arrays not converting marginal land was that more expensive installations outcompete the opportunity cost for converting marginal land when converting larger arrays. Single-axis tracking arrays are more expensive than fixed arrays, therefore the opportunity cost of installing on lower productive land was too great in value to make marginal land decisions, especially when installing on larger proportions of a farmer's cropland. However, farmers installing single-axis arrays converted larger portions of their fields or entire fields (single-axis average total area: 35 acres, fixed axis average total area: 3 acres). Relative land productivity would not represent spatial field placement if an entire crop field was converted.

3.5 Trends in installation practices

Appendix Figure A1.2 the technology latitudinal and GHI poleward deviations in 2008 (fixed axis) and 2010 (single axis) where there was a significant shift poleward towards lower GHI values in these two years. The average latitude of all other study years was 37 degrees North with installations in all years of the study reaching into the northern Central Valley. Because GHI decreases with poleward installation, this tendency for installations to average in the mid-central valley, and the 2008 and 2010 northward tendency further indicate sub-optimal decisions for regional installation. Optimally, arrays would be installed toward the southern Central Valley for peak GHI and thus peak electricity generation (34-35 degrees north). Packing factor deviation, relative land productivity, and spatial GHI preference results demonstrate that

inefficiencies in installation practices have negatively impacted solar capacity in the Central Valley.

Overall, trends in installation practices were related to frame technology, and most likely resulted from differences in cost and purpose of the array. Fixed axis arrays tend to be cheaper to install, and smaller in size suggesting that these arrays are installed for local small scale farmer purposes (irrigation and farm operation) and therefore, more considerations are made in reference to crop loss (lower packing factor deviation than single-axis tracking arrays, and RLP that suggests the use of marginal land) to make solar PV a financially viable option for these smaller scale farmers and regular operation. Single-axis tracking arrays converted large plots of land for large solar electricity production. Therefore, there is little incentive to make decisions based on crop loss (large packing factor deviation, and RLP that suggests no consideration of spatial field productivity) when the value and cost of the solar installation is so high. However, despite the value and cost of single-axis tracking array installations, the observed deviation from best practices for installation have a negative impact on cropland.

3.6 Total estimated crop loss and crop preferences

Figure 1.8 shows the total area converted per crop and the array installation distribution per crop in the Central Valley from 2008 to 2018. In total, 33.8 km² of cropland was foregone for the installation of solar arrays in the Central Valley between 2008 and 2018. Three commodity crops, pastureland, wheat, and hay and haylage, accounted for 59% (20.0 km²) of total converted area. The opportunity cost of converting large plots of low value crops such as these to solar is lower than for specialty crops, and thus these crops are more cost effective to convert to solar. The other side of the dichotomy is that converted high value crops were mostly orchards. The total converted area was moderate to low in comparison to low value crops, however the total

number of arrays installed in almond, pistachio, and other orchard fields was second only to pastureland. This preference for co-locating smaller sized arrays (majority fixed axis) arrays with orchards and larger arrays with pastureland suggests that the high value crops such as orchards warrant small scale PV deployment (most likely for irrigation purposes) while pastureland warrants low opportunity cost to installing large PV arrays. Moderate value crops such as vegetables, corn, and many double crops, are high enough in value to not warrant installation, but low enough in value to not make the PV investment pay off in a reasonable amount of time.

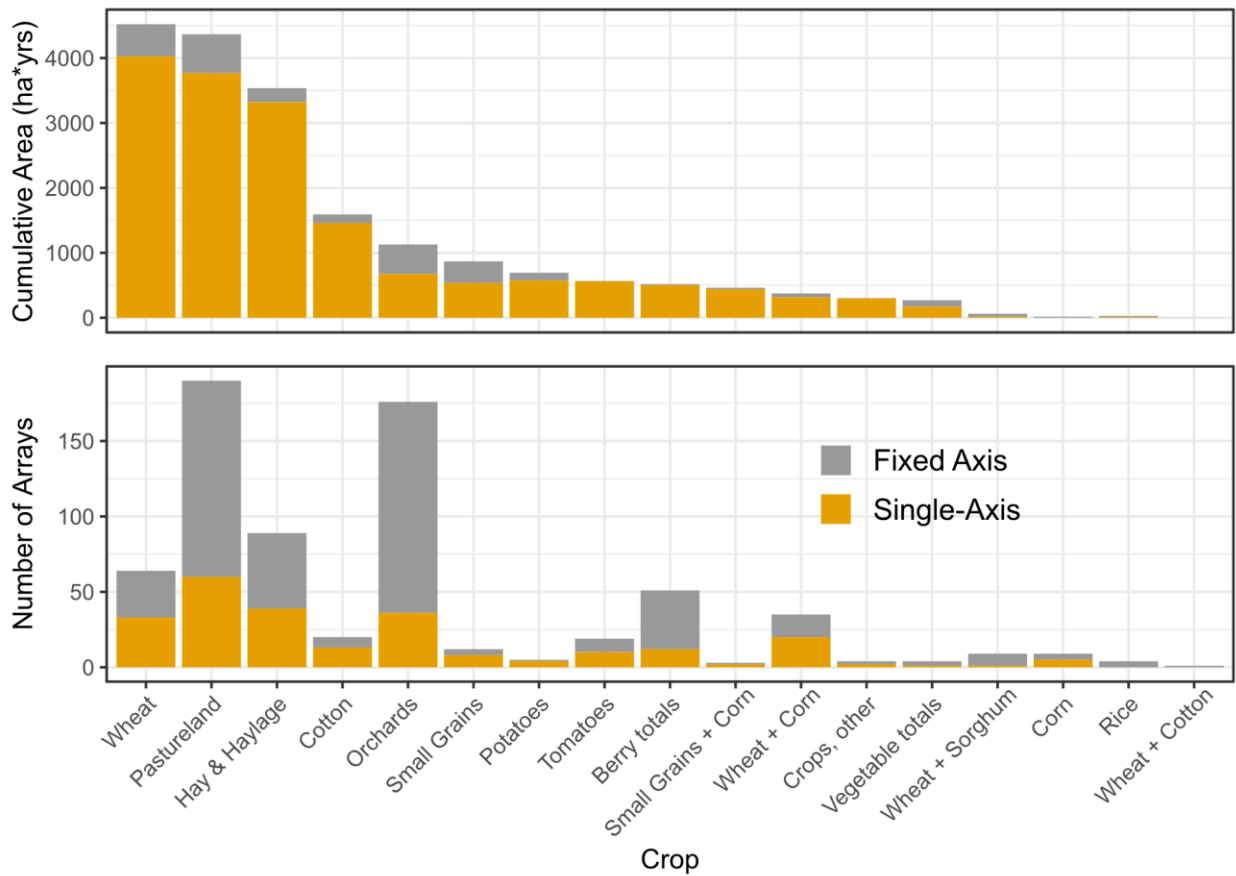


Figure 1.9. Installed Solar Crop Preferences. Farm and Ranch Survey crop groups (grouped from CDL crop type) involved in the co-location of 694 installed PV arrays in the Central Valley. Includes crops foregone in crop rotation of foregone cropland. (TOP) Cumulative crop loss area based on the total area of the array and the year of installation (cumulative up to 2018). (BOTTOM) Number of arrays installed by the most recent crop type and technology. Note that crops with “+” separating two crop types are double crops.

4. Conclusions

This new dataset provides information on individual installation practices as well as regional trends of solar array installation in space and time. The dataset provides a robust and unbiased prediction of actual installed capacity and generation of commercial scale solar electricity in the California's Central Valley. An overall assessment of to-date installation practices suggests that practices have been sub-optimal and have resulted in significantly more crop loss than was necessary and significantly less electricity production than what optimal practices would provide. The sub-optimal installation practices described here can influence future incentives for the agricultural switch to solar in California and ensure the utility and the farmer's interests are both considered. With the projected 60 GW increase in ground-mounted PV array capacity over the next ten years (Energy Information Administration 2015; U.S. Energy Information Agency 2019), is it imperative to institute policy to manage future installations and prevent unnecessary cropland losses while preserving energy and financial incentives for enhancing solar production.

Installing a PV array and removing a certain area of crops creates impacts across the food, energy, water nexus. Some aspect of the food and energy portion of the nexus were explored here, however, a full LCA of the foregone food production, foregone water consumption from both irrigation and prior energy source, foregone energy consumption, and associated carbon footprint would yield important data on the total effects of the large scale switch to solar. In addition to a FEW-LCA, this information has economic implications. At the FEW-LCA and economic level, efficiency of installation practices becomes a much more important factor in determining if PV array installation is at the moment beneficial with current practices. Therefore, future work will produce a FEW-LCA with an associated economic

cost/benefit analysis of the regional conversion to solar energy (Joshi et al. 2014).

As stated, C-Si linear arrays are the most common commercial installation of PV arrays. However, as more technologies are developed for cost and efficiency purposes, the classification ruleset described here will have to be expanded. Future work could include the application of this framework with additional technologies (Cadmium Telluride, diagonally oriented arrays, 2-axis arrays, concentrating solar power arrays, and bifacial arrays), which would simply require more installations and thus, more training locations as they become available to incorporate variability. In addition, NAIP 2020 imagery has recently been released for California, and will warrant evaluation using the new imagery. This new dataset also provides training data for machine learning algorithms such as a convolutional neural network to train and apply over all future imagery without the significant person-time investment described here. A streamlined workflow applying deep learning could be applied at the CONUS level to characterize solar electricity generation and installation practices. Other potential benefits of solar PV installation are enhanced recharge and reduced evaporation resulting in more positive hydrological budgets which would need to be modeled to quantify.

Acknowledgements

This chapter was coauthored by Siddarth Shulka, Annick Anctil, Anthony Kendall, and David Hyndman. We would like to thank Madison Witkowski for the initial literature review and project conceptualization. A thank you also to Raechel Portelli from the Department of Geography, Environment, and Spatial Sciences at Michigan State University for her help with the conceptualization and deployment of the eCognition methodology used here. The authors have no competing interests to declare. This work is supported by INFIEWS grant number 2018-67003-27406 (accession No. 1013707) from the USDA National Institute of Food and Agriculture. Any opinions, findings, and conclusions or recommendations expressed in this publication are those of the authors and do not necessarily reflect the views of the USDA.

APPENDIX

Text A1.1 Solar PV Detection and Characterization Methodologies

The following sections contain additional methodology for the detection and characterization of ground mounted solar PV arrays in the Central Valley.

Text A1.1.1 Manual Digitization of Omitted Panels and Systems

After the eCognition ruleset was executed across the entire study area, it was noted that many of the arrays contained omitted panels. It was conjectured that drawing results from incomplete arrays may result in misrepresentation of packing factor, capacity and generation, number of arrays, and year of detection, and also would not provide a sufficient dataset for future detection training frameworks. Therefore, the decision was made that to accurately depict current installation practices and create a usable dataset, all omitted panels must be manually digitized. Likely explanations for the omissions were as follows but not limited to: boundary panels omitted where eCognition texture threshold was not met because of few boundary panels in the training dataset, boundary panels of different lengths/shapes/sizes from rest of array, boundary panels where the minimum requirement of two proximal panels was not met, soiling (dusty) of panels where a portion of the array has been cleaned and a portion has not, vertically tilted panels that were conjectured to be out of commission, unfinished arrays where frames were installed but PV modules had not been installed yet, Poor contrast with underlying ground (usually, impervious surfaces), high variability of the underlying ground surface (grass, soil, impervious, etc.), arrays with panels overlapping NAIP exported scene boundaries, NAIP Stitching errors resulting in non (example near San Joaquin).

Text A1.1.2 Data and Digitization Workflow

Manual digitization occurred in ArcGIS Pro (Esri Inc. 2021). Prior to digitization, the panel, sub-array, and array grouping described in Methods 2.6. in the main paper was performed

to generate centroids for each potential array and simplify the search process. NAIP 2018 was imported into ArcGIS Pro from the California Department of Fish and Wildlife ArcGIS portal (California Department of Fish and Wildlife 2020). Identified panel shapes (grouped from each eCognition tile run) and potential array centroids were imported into ArcGIS Pro. Potential Array centroids were ordered by latitude (for progress record keeping purposes) and each was individually zoomed to and centered for analysis. For each centroid, eCognition identified panels were displayed and omitted panels were digitized using the “Draw Polygon” tool to best represent each linear module array within the larger array. For panels with partial identification, the panel was only completed if the new shape represents the orientation of the actual panel (ie: for south oriented panels, only complete portions of the panel which have an E/W length greater than the N/S length). Special care was taken to not include maintenance buildings (often similar size, but proximal and occasionally spectrally and qualitatively similar to panels). A general rule for digitization was to always keep the eCognition algorithm shape file and try to best represent the omitted panels with the identified shapes provided by the algorithm.

<u>Collection Param</u>	<u>NDPVI Setting</u>
startYear	2005
endYear	2019
startDay	1-Jan
endDay	31-Dec
index	NDPVI
maskThese	cloud, shadow, snow, water
<u>Run Param</u>	<u>NDPVI Setting</u>
maxSegments	6
spikeThreshold	0.5
vertexCountOvershoot	3
preventOneYearRecvoery	TRUE
recoveryThreshold	0.0909
pvalThreshold	0.05
bestModelProportion	0.75
minObservationsNeeded	6
<u>Change Param</u>	<u>NDPVI Setting</u>
delta	loss
sort	fastest
year	2008 - 2018
mag	> 50
mmu	3

Table A1.1. LandTrendr GEE Parameters. Parameters set within the LandTrendr GEE control scripts defining the NDPVI year of detection acquisition.

Text A1.2 Results and Discussion

The following sections contain results and discussion points of the methodology and sub-optimal practices.

Text A1.2.1 eCognition Computation Time

eCognition does have a server add on which can automatically tile and process large amounts of imagery, however that license was not obtained and eCognition runs had to be performed manually. eCognition ruleset runs were performed on two different computers. The primary computer contained an Intel 8 Core Xeon E5-2637 CPU at 3.50 GHz with 256 GB of RAM and secondary computer used an Intel Xeon E7-4860 at 2.27 GHz with 512 GB of RAM. Total eCognition computation time for the 137 NAIP tiles was 130 hours, 16 minutes, and 46 seconds with 81% (by number of images processed) of the processing occurring on the primary computer. The secondary computer was used mostly to run the smaller edge tile images of the dataset. However, this computation time does not account for tiling and NAIP imagery preparation which would add 80 – 120 hours to the processing.

Text A1.2.2 Net Energy Metering (NEM) Dataset

The numerically large number of permits in the Central Valley (compared to the 1006 identified arrays within this dataset) within the NEM dataset is most likely due to several common practices in PV permitting. A new permit must be filed every time a change is made, removal and replacement of panels requires a permit, and multiple permits can exist for a single array depending on how many connections the array has to the grid. Often, an approved PV system is not installed in the same year of application approval. Especially for larger arrays, this temporal gap in approval and completed installation can be up to several years. However, utility managers are required to use the panel models from the application approval year, and thus use

temporally inefficient panels for the actual installation. This study assumed that the average panel efficiency (derived from the NEM dataset itself) was the average efficiency for the year of installation. If optimal panel efficiency is not being deployed on an annual basis, potential electricity production has been hindered. Another source of error is the lack of completion of this dataset based on the absence of a requirement for the permitting companies themselves to acquire a permit to install PV arrays. The increase in capacity assuming complete monocrystalline solar modules for the created dataset accentuates the gap in capacity and demonstrates that inefficiencies in installation practices have negatively impacted solar capacity in the Central Valley.

Text A1.2.3 First Classification Attempts: Random Forest

The application of machine learning algorithms has seen an immense increase because of user interfaces such as Google Earth Engine expediting the learning curve (Kennedy et al. 2018). One of the more basic forms of machine learning regarding classification is the random forest classifier which is easily executable with GEE documentation. Following some methodology of Malof et al. (2016) the first attempt at creating this data set involved using a supervised classification random forest algorithm with both Landsat resolution (30m) and NAIP 2016 resolution (1m) with several thousand training data points and several indices including the newly developed NDPVI. An “agricultural” mask was applied to the entirety of the images using the CDL classification for “cultivated” to remove urban areas before classifying. The result of the mask and the random forest classifier incorporating NDPVI was impervious surfaces in agricultural areas. When applied over small regions (50km²) the random forest classifier for both image resolutions resulted in minimum omissions and inclusions and had overall accuracies in the 85-99 percentile.

If one assumes that NLCD is accurate, sub-setting changing impervious surfaces in agricultural settings yields the greatest potential for identifying the installation of PV arrays. This attempt was made and produced a preliminary dataset of 176 PV array locations and extents. However, after further analysis, it was noted that many arrays, specifically smaller array of less than around 0.8 hectares were simply missed by NLCD. This did, however, provide an initial training dataset of 176 PV array locations across the Central Valley that was pivotal in further classification.

A second attempt was made with multiresolution anomaly detection with random forest classifiers. This methodology was developed to emulate a single neuron of a neural network. A random forest classifier was run at Landsat 30m resolution with associated training data as an impervious surface “anomaly” detector. This detected large scale impervious surfaces for which higher resolution the NAIP 2016 1m image were subset to decrease computation time. The second random forest was run at NAIP scale only for locations associated with the Landsat scale anomaly. This did increase computational efficiency vs running a random forest at NAIP scale over the entire Central Valley, however, yielded too many omissions and inclusions to satisfy the needs of this study.

Inclusions for this technique numbered in the thousands, as well as many omissions. These misclassifications were most likely due to differences in spectral value of scenes due to different atmospheric weather conditions of the date of retrieval for each scene and low resolutions leading to more homogenous pixel values at the regional scale. Although this methodology was unsuccessful at the regional scale because of standard issues with remote sensing big data, this method of multiresolution anomaly detection using a series of random forests may be useful at finer scales to increase computational efficiency.

Text A1.2.4 Improvements in Remote Sensing Methods for Land Use Change Analysis

Standard pixel based classification algorithms work by taking in a user defined training dataset and developing threshold ranges and relationships to whatever input bands or data are given. When training these machine learning algorithms, the user inherently includes their own training selection bias. This bias is unavoidable. These trained algorithms then often only encompass the variability of the training dataset and potentially omit scenes with higher variability and different context (Blaschke et al. 2014; Blaschke and Strobl 2001; Hay, Niemann, and McLean 1996). This becomes even more of a problem when the scale of the desired classification is variable (Baatz and Schape 2000). However, by selecting conservative spectral and morphological thresholds as a trained user in as many dimensions as possible, the user encompasses the potentially higher variability of datasets than the training data, and thus creates a robust user-defined hyperspace for a land cover class to exist in. This is a different method for minimizing training bias as the conservative thresholds should allow for more variability than what is observed in the training dataset.

With enough research and experience, a user becomes an “expert” and is the best qualified “machine” for identifying the object-based attributes that make up a theoretical hyperspace that a solar panel object exists in. Therefore, these user set thresholds contain the intrinsic value of the user’s entire knowledge base. This is a common debate between OBIA and machine learning users. When training machine learning algorithms, the user inherently includes their own training selection bias. Using an expert knowledge base simplifies the algorithms and increases computational efficiency while retaining accuracy and potentially increasing it.

As the world population grows (and thus, urbanization), there grows a need to accurately classify this urbanization and quantify its effect on natural resources (Patela et al. 2015). Earlier

studies have looked to temporally classify urbanization (Liu et al. 2019; B. Wang et al. 2019; Xu et al. 2019) and this paper provides yet another method for quantification. The newly developed NDPVI is a simple two band index for identifying change in impervious surface (urban sprawl/development) over long already recorded time scales at high resolution. This new index could be used to validate previously made land use datasets with higher resolution images from the same time period that were previously unable to provide impervious surface information (Chen et al. 2019; Sun et al. 2017; Zha, Gao, and Ni 2003; S. Zhang et al. 2018). Other change indices like NDVI as values are extremely dependent on the crop type. NDVPI showed the greatest potential for identifying land use change to impervious surfaces across many crop types.

There are big data implications for the combining of this dataset and methodology with that being developed by Jordan Malof and those in the Duke Energy Initiative on urban PV installations (Bradbury et al. 2016; Malof et al. 2015). Filling the gaps in both datasets and methodologies would provide information on total energy grid implications of the move towards solar energy. The combined methodologies could then be applied across CONUS to observe a nationwide switch to solar and the associated implications both good and bad.

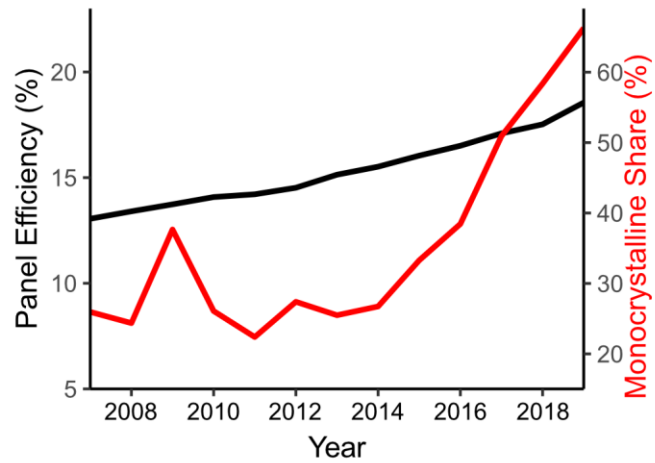


Figure A1.1 PV Module Efficiency and Monocrystalline Share Through Time. Reported solar PV module efficiency and monocrystalline share through time (Barbose et al. 2020). Figure A2.1 extrapolates mono and polycrystalline efficiency from a multiple linear regression using this data.

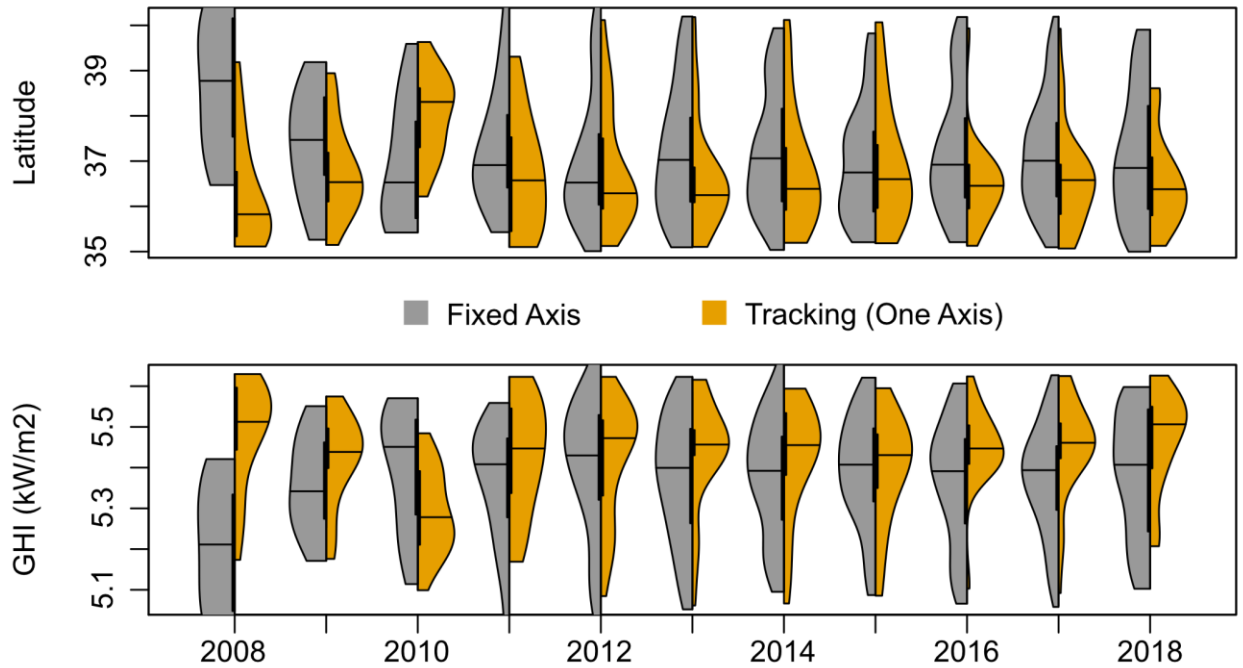


Figure A1.2 Identified PV Array Latitude and GHI Distributions. Latitude data was the centroid latitude of each array. Average GHI for each array was extracted from the array shape file. The GHI raster was downloaded from The World Bank (Alexandratos, Nikos & Bruinsma 2012) and are available at: solargis.com/maps-and-gis-data/download/world. Note that the plotting method used here uses as constant area plot method (non-normalized). Therefore, within year distributions are accurate, but can be misleading when comparing year to year distributions due to differing numbers of arrays in each distribution.

Text A1.2.5 Year of Detection Limitations

LandTrendr by nature searches the spectral history of a pixel for the single year of greatest spectral change for an index (NDPVI). Change in NDPVI from crops to PV arrays at Landsat resolution is significant enough to activate the LandTrendr breakpoint segmentation. However, the clearing of land from crops (usually low blue reflectance and high NIR reflectance, and therefore, low NDPVI) to bare soil, is often just a great change as the installation and even sometimes greater in magnitude. Therefore, it is likely that many of the years of detection are detecting the year of land use change and the completed installation may occur during the same year, or later. Ideally, the morpho-spectral segmentation rule set would be run on sub-meter resolution imagery every year over the entire Central Valley which would identify arrays installed in each year of the imagery. Therefore, only years of completed installation due to the spectral and morphological requirements of the segmentation ruleset. However, imagery of this resolution and return speed does not exist, and the computation to run such a dataset would be immense. Here we assumed that all YOD's were both the year of land use change and the year of completed installation.

Text A1.2.6 Detected Array and Technology Limitations

In addition, newer and less prevalent technologies like bifacial arrays and concentrating solar power arrays are not yet prevalent enough to produce a good dataset for differentiating characteristics at the regional scale. Crystalline Silicon linear arrays are the easiest to detect because although they do slightly vary in characteristics through time, in general their spectral and geometric information have remained constant. However, some crystalline silicon arrays did not fit the generated templates and were non-normally oriented, or panels with a width of more than 4-5 modules. Once these new technologies get a foothold in the PV industry and begin to

become more numerous, characteristics will homogenize, and regional detection will become possible.

Text A1.2.7 Limitations of Relative Land Productivity

RP is limited by the resolution (30m) and could be drastically improved with higher resolution data due to the fact that for certain crops, productivity might only be detectable at finer scales. However, for RP to make an estimate monthly imagery is required (minimum) over the entire study area and over a year range that is desired for comparison. Landsat is currently the best fit for those conditions. In addition, therein lies bias with using PLSS Q-sections as assumptions for a single farmer's proximally owned farmland. If the actual farm size falls below 160 acres, then we are biasing results by multiply owned farms and potentially different practices. If the actual farm size falls above 160 acres, then we are only analyzing a larger sample of a farmer's total field which may not represent the farmers total spatial productivity.

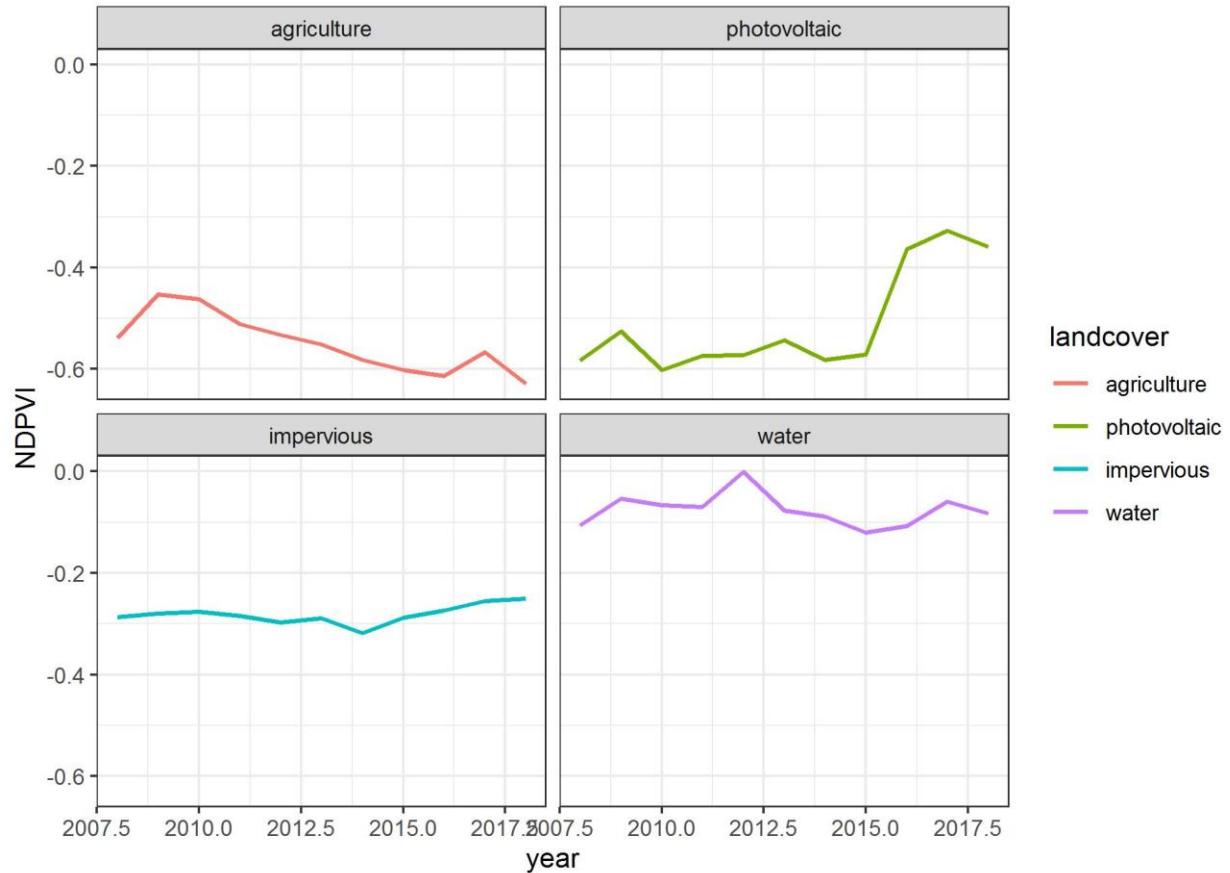


Figure A1.3 Landsat NDPVI Timeseries Across Differing Landcovers. Median annual NDPVI study period timeseries for four points near Fairmead, California. The photovoltaic timeseries is for the same array depicted in Figure 1.4. The agricultural example was a nearby almond field, the impervious surface example was a nearby parking lot, and the water example was a nearby agricultural pond. Note that LandTrendr was parameterized to look for a sudden increase in NDPVI which remains after the breakpoint as shown in the photovoltaic panel. Also note that the photovoltaic NDPVI values shown here differ from the NAIP reported values in Section 3.1 because these values were derived from Landsat Imagery which differs from NAIP in resolution and in spectral bandwidth.

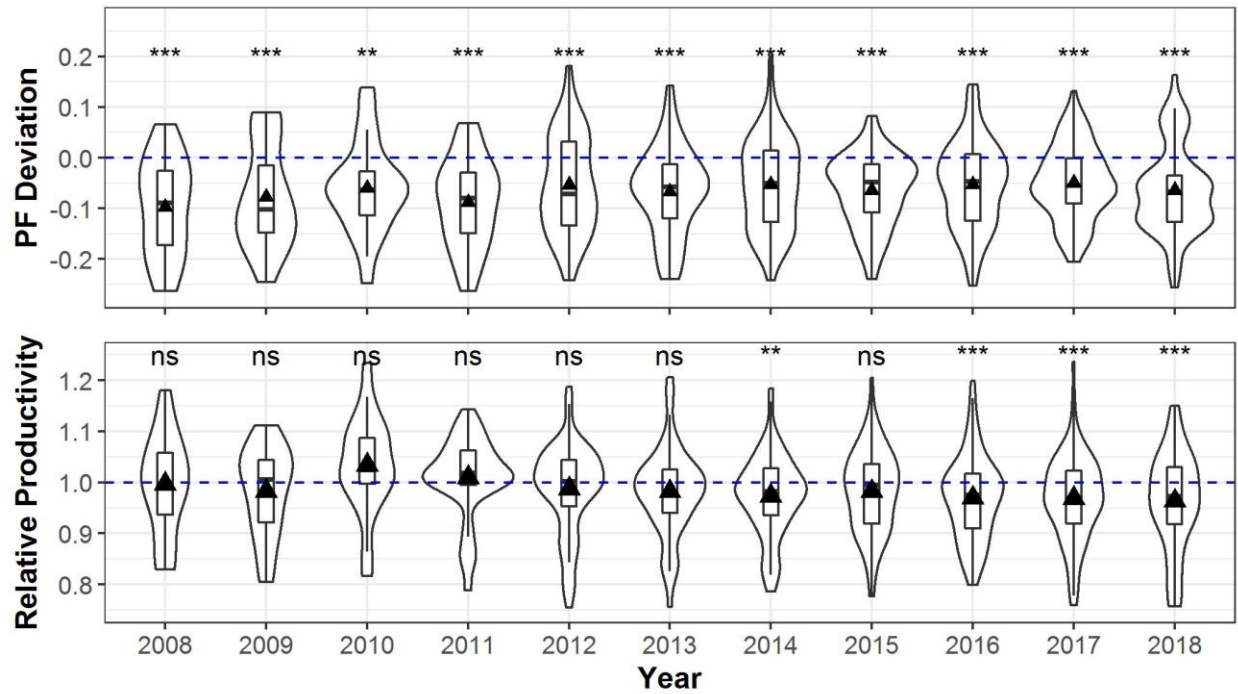


Figure A1.4. Temporal Trends in Packing Factor Deviation and Relative Land Productivity. (Top) Observed - Optimum PF for all installation years. The blue line represents the optimum packing factor. (Bottom) Relative Land Productivity across all crops for each installation year. The dotted blue line shows a RLP value of 1 where the offset crop land would perfectly represent the productivity of the surrounding cropland of the same crop type. Boxplots denote quartiles, and standard significance intervals are denoted by the asterisks and the ‘ns’ for non-significant.

CHAPTER 2: IMPLICATIONS OF CO-LOCATED SOLAR PV INSTALLATIONS ON THE FEW NEXUS IN THE CENTRAL VALLEY

Abstract

Crops and solar panels have recently had significant land use competition as they have similar ideal conditions for maximum yield. Understanding agriculturally co-located solar photovoltaic (PV) installation practices and preferences is important to foster a future where solar power and agriculture co-exist with limited impact on food production. The recent boom in solar photovoltaics is replacing cropland at an increasing rate, yet there is a gap in the literature with spatiotemporal details that would help inform and improve future array installations. To fill this gap, we investigated the impact of solar co-location through initial resource and economic values which promote best installation practices. We recently reported a novel dataset of commercial scale crystalline silicon fixed and single-axis tracking solar PV installations in the Central Valley which have been spatially and temporally delineated, 694 of which (2,052 MW) are adjacently co-located with active agriculture (Chapter 1). This study deployed that dataset to assess the broad food, energy, water (FEW) and carbon resource impacts and perform a simple economic budget of these co-located solar installations through the 25 year expected lifespan of each array. Major takeaways under our base case impact scenario (2008 – 2042) were the impact on food production (1.64×10^{12} forgone kcal), significantly higher forgone irrigation water use compared to lifetime O&M water use (factor of 5), and the significant reduction of CO₂ emissions when compared to natural gas for the study period (factor of 8). The lifespan (through 2042) simple economic budget analysis from the cropland owner's perspective yielded a net positive budget of \$13 billion, an economic payback year of 2023, and showed the budgetary gap between the final net positive budget, and cropland cultivation (16 times more valuable to install

solar than to cultivate cropland). This suggests the need for policy that balances cropland preservation when installing solar, to avoid a major negative impact on U.S. agricultural production as solar becomes more prevalent.

1. Introduction

The current climate change trajectory induces vulnerabilities to our finite food, energy, and water (FEW) resources. As we attempt to mitigate this challenge by transitioning from fossil fuels to renewable energy, it will be imperative to optimize new infrastructure for the entire FEW nexus. One mechanism to move towards sustainability and reduce carbon dioxide (CO₂) emissions is the broad-scale deployment of solar photovoltaic power which would drastically reduce future greenhouse gas emissions relative to typical fossil fuel consumption (Dolan et al. 2012; Hsu et al. 2012; Whitaker et al. 2012). While recent research identifies the spatial and temporal extent of solar PV (Barbose et al. 2020; Bradbury et al. 2016; Hernandez et al. 2014; Malof et al. 2019; Malof et al. 2017; M. Wang et al. 2018, Chapter 1), few studies have assessed current regional practices and long term FEW impacts of agriculturally adjacent solar co-location (Barron-Gafford et al. 2019). It is imperative to perform such research as ground-mounted solar photovoltaic (PV) capacity in the United States is projected to triple over the next decade (Energy Information Administration 2015; U.S. Energy Information Agency 2019).

Agricultural co-location has been proposed to have FEW benefits for both farmers, and the asset owners (Barron-Gafford et al. 2019; Macknick 2019, 2020), with some even proposing large scale dual-use deployment which is being called agletrics (Miskin et al. 2019). Solar electricity production and cropland share common optimal placement conditions in solar irradiation, topography, and climatic conditions (Adeh et al. 2019). These common conditions create local land use competition for cropland and electricity production. Specifically, the

Central Valley, California embodies some of the nation's most valuable land (25% of United States national crop output, 5% of United States utility-scale net electricity generation [entire state], 20% of the Nation's groundwater extraction, and 17% of the Nation's irrigated land, occurs on less than 1% of the nation's farmland (Faunt et al. 2009; US Energy Information Administration 2021). This highly valuable land is also where agricultural adjacent solar co-location has been widely incentivized and deployed resulting in California being the nation's top producer in electricity from solar (US Energy Information Administration 2021).

Therefore, the decision to convert Central Valley cropland to solar must be calculated. One consideration is that Central Valley irrigation has high energy requirements and is highly regulated due to the regions water scarcity and deep groundwater (California Department of Water Resources n.d.; Dickinson 2016; Pavley 2014, 2016). Therefore, irrigated cropland in the region brings risk which is accentuated in drought years. Converting this land to solar may reduce overall risks to the farmer, especially during drought years (He et al. 2019).

Additionally, the decision to convert land to solar could include solar financing incentives. With the aforementioned positive FEW and carbon impacts, these continued legislative efforts that improve the economic viability of co-location are The Solar Investment Tax Credit (ITC) from the Energy Policy Act (Office 2005; Solar Energy Industries Association 2021; U.S. Department of Energy 2021), The Emergency Economic Stabilization Act of 2008 (Shah 2009), The American Recovery and Reinvestment Act (Schoeffler 2009), the Sustainable Groundwater Management Act (SGMA) (California Department of Water Resources n.d.; Dickinson 2016; Pavley 2014, 2016) and The California Public Utilities Commission's (CPUC) Net Energy Metering (NEM) Tariff 2.0 (CAPUC 2016). These legislative efforts along with continuously decreasing costs to manufacture and install solar (Feldman et al. 2021; Fu,

Feldman, and Margolis 2018) make solar co-location an economically viable replacement for a large portion of fossil fuel electricity production by converting cropland.

Although there is evidence that PV systems could last as long as 30-40 years (Congress 2007; Dolan and Heath 2012; National Renewable Energy Laboratory et al. 2018) most current solar array system lifespans are assumed to be 25 years based on performance warranties, natural degradation (20% loss in efficiency after 25 years), and life cycle cost standards for electrical equipment (10 CFR 436 2017; Khan and Arsalan 2016; National Renewable Energy Laboratory et al. 2018). Once this period is met, asset owners have the options to: refurbish the system to extend its life; extend the term of the performance contract or power purchase agreement; sell the system at fair market value; or remove the system and return the site to the prior land use (National Renewable Energy Laboratory et al. 2018).

The recent boom in solar which began in 2008 because of the legislative efforts described above, decreasing costs to produce and install solar (Fu, Feldman, and Margolis 2018), and a more recent effort to combat climate change and finite fossil fuel sources with renewable energies (Abas et al. 2015), is still in its infancy (Walker et al. 2020). Walker et al. (2020) reports that roughly 90% of solar PV installations globally have begun operation in just the past 7 years (as of 2020). Solar arrays installed in 2008, approximately when the national surge in solar installations began (Chapter 1 of this Thesis), will not reach their 25 year PV warranty and lifetime assumption maturity until 2032. Thus, we've yet to see major decommission from solar back to agriculture or assess long term impacts of large land use competition between solar and agriculture.

Numerous studies have predicted the FEW nexus impacts of agrivoltaic solar installations, where field crops such as lettuce are grown directly beneath the shade of a solar

array installation (Amaducci et al. 2018; Aroca-Delgado et al. 2018; Barron-Gafford et al. 2019; Dinesh et al. 2016; Dupraz et al. 2011; Goetzberger et al. 1982; Macknick et al. 2014; Majumdar et al. 2018; Marrou et al. 2013; Ravi et al. 2016; Valle et al. 2017). In a recent study, Barron-Gafford et al. (2019) performed an empirical examination of the positive impact on food (200-300% increase in yield), water (5-15% increase in soil moisture retention), and energy (1-3% increase in generation) using a PV control, agricultural control, and agrivoltaic site in Biosphere 2. Many of these studies such as this consider small scale in-situ arrays and do not include regional adjacent co-located installation predictions. They are also often limited to annual growing season analysis rather than full solar life-cycle projections.

This study sought to assess the impact of co-located solar arrays in the Central Valley under the standard lifetime assumptions by forecasting food, energy, water, carbon, and economic implications through three “lifespan phases” of co-located solar arrays; the installation phase (2008-2018, given the dataset from Chapter 1) where arrays are being installed and operated, the operation phase (2019-2032) where there’s no new installations but all “current” installations are operating and maintained, and the decommission phase (2032-2042) where arrays which have been operating for 25 years are disconnected, deconstructed, recycled and disposed of, and follow the return to agriculture post-lifespan option the following year. We built our study scenario under the assumption that after 25 years of operation, land was returned to its prior use (in this case, agricultural production) to reduce assumptions regarding module replacement, resale, or continuation. Although, we acknowledge that actual practices will likely vary greatly across the available post-lifespan options, especially regarding specialty crops which can require multiple years of growth before viable yield. The three phases depicting the 25-year life cycle of an agriculturally adjacent solar co-located array are conceptually outlined in Figure

2.1. These three phases are similar to the upstream (installation), ongoing (operation), and downstream (decommission) life cycle stages used by Hsu et al. (2012).

We present a lifespan impact analysis (under the scenario assumptions described above, stopping at the field edge) of the newly developed spatiotemporal ground mounted co-located PV installation (2008-2018) dataset from Chapter 1, of broad FEW and carbon impacts and a simple economic budget of to-date agriculturally adjacent solar co-location installations in the Central Valley. We performed this analysis through the 25 year expected lifespan of each array.

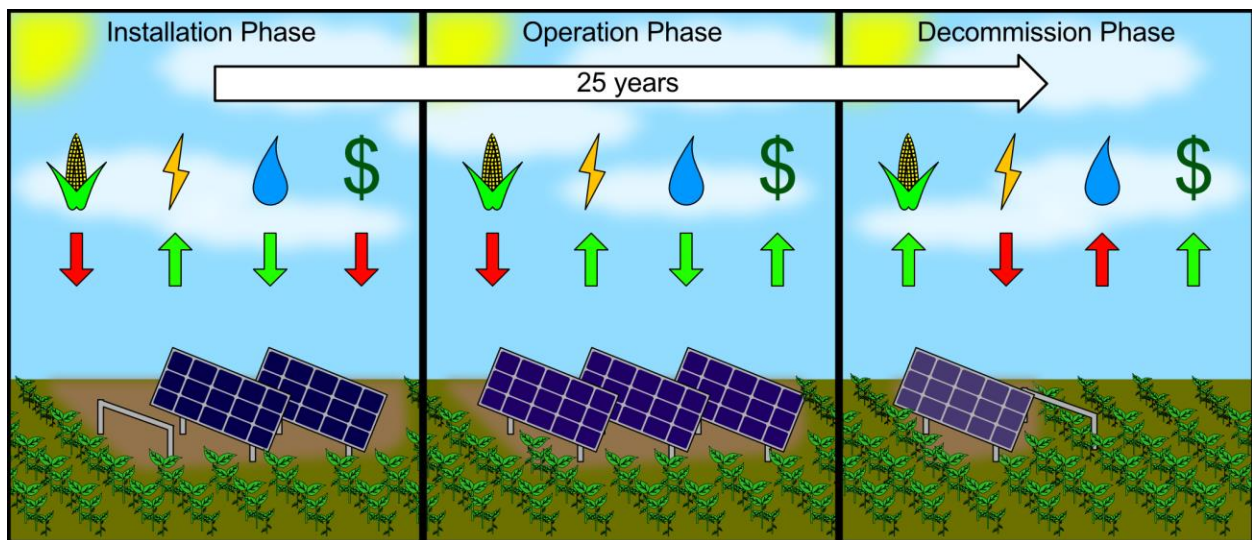


Figure 2.1. Solar PV Lifespan Conceptual Diagram. Graphical diagram of the 25-year life cycle of an agriculturally adjacent co-located solar array. For the purpose of this study, the Installation Phase was 2008 - 2018, the Operation Phase was 2019 - 2032, and the Decommission Phase was 2032 - 2042. The change in color of the solar panels depicts module degradation and therefore loss in efficiency over time. Note that the resources depicted in this figure are food production, electricity generation, water use, and economic budget from the perspective of the cropland owner. The direction of the arrows indicate whether a resource is increasing or decreasing during each phase, and its color indicates whether this change is a positive (green) or negative (red) impact.

2. Results

2.1 Resource and Economic Impact Result Description

The PV dataset provided by Chapter 1 contains 1006 solar PV arrays, 694 of which are co-located with agriculture. Both this study and Chapter 1 define co-location as solar PV installations which directly replace agricultural land and continue to have agricultural land adjacent to the array after placement. This study does not explicitly consider agrovoltaics, co-location with crops directly beneath arrays. Although we acknowledge that with the available information, we do not know what practices are occurring directly beneath the arrays. This study focused on the 694 agriculturally adjacent PV installations which account for 2,052 MW identified in Chapter 1. The phases of installation, operation, and decommission were applied to a base case scenario and an alternative high resource case scenario and low resource case scenario (uncertainty scenarios), described below. Assumptions described in the methods section are essential for the interpretation of these results. Measures of uncertainty for each resource and its economic dollar value differ between resources and are also described in the methods section with detailed descriptions in supplementary table 1. Final cumulative resource and economic values are displayed in Figure 2.2 and reported in Table 2.1.

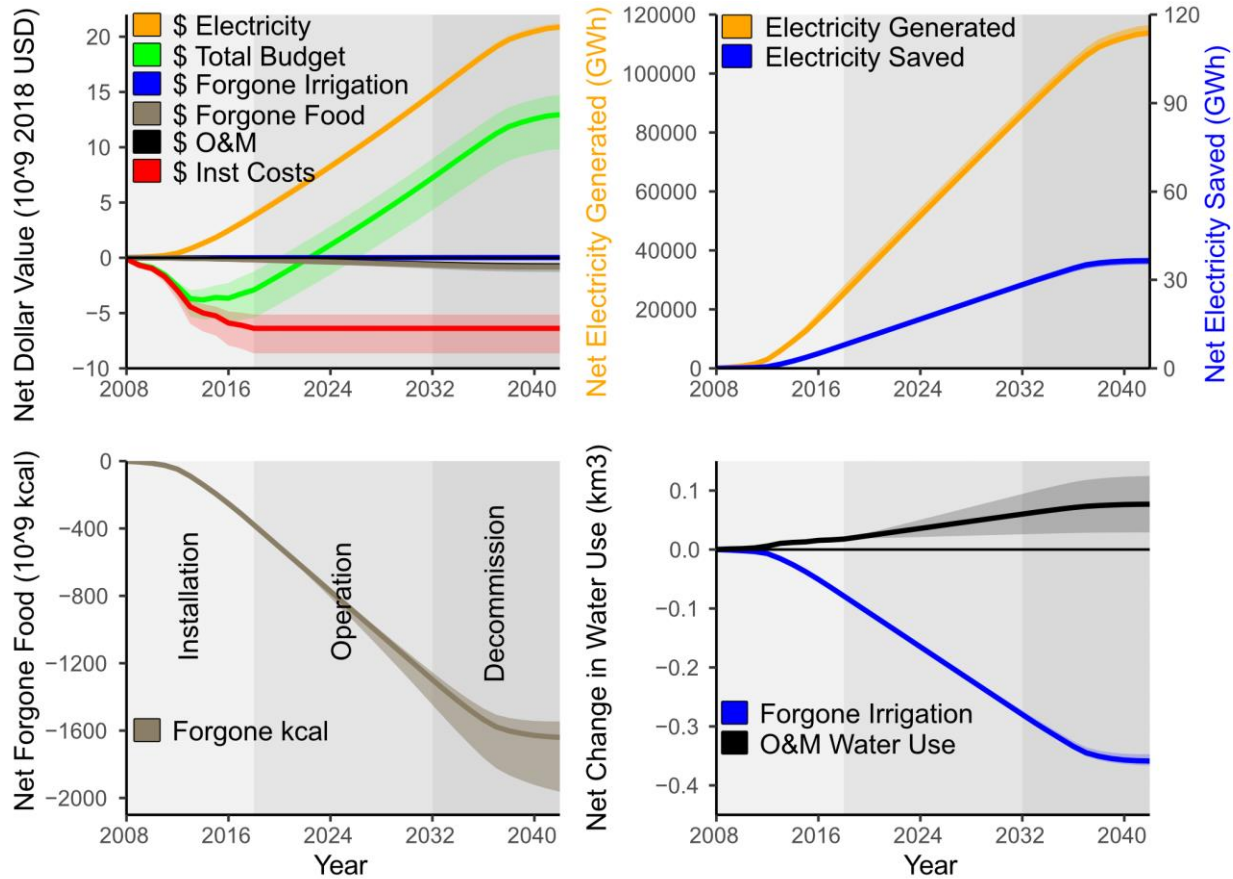


Figure 2.2. Cumulative Lifetime Food, Energy, Water, and Economic Impacts. 25-year lifespan impact analysis of solar co-location in the Central Valley, California for food (upper left), energy (upper right), water (lower left), with a simple economic budget from the cropland owner’s point of view (lower right). Note that the shaded regions for the installation, operation, and decommission phase shown in the upper left continue throughout the remainder of the figures. Shaded regions depict the uncertainty scenarios for each resource of the same color.

2.2 Predicted impact on food production

The dataset from Chapter 1 reports total area of the array which is assumed to be the total area of forgone cropland. The 694 agriculturally co-located arrays accounted for 33.8 km² of cropland, or roughly 0.034% of total state farmland (Brown 2020). Cumulatively through the 25 year lifespan of each array, the total area was 1,038.3 km² of forgone cropland. Results from Chapter 1 reports crop type derived from an extraction of the Cropland Data Layer (CDL) from each array shape which accounts for crop rotation five years prior to placement. Crop specific

kilocalorie (kcal) output forgone between 2008 and 2042 was 1.64×10^{12} kcal for the base case scenario. The yield based uncertainty scenarios for forgone crop production ranged from 1.55×10^{12} to 2.00×10^{12} kcal for the low and high case scenarios respectively.

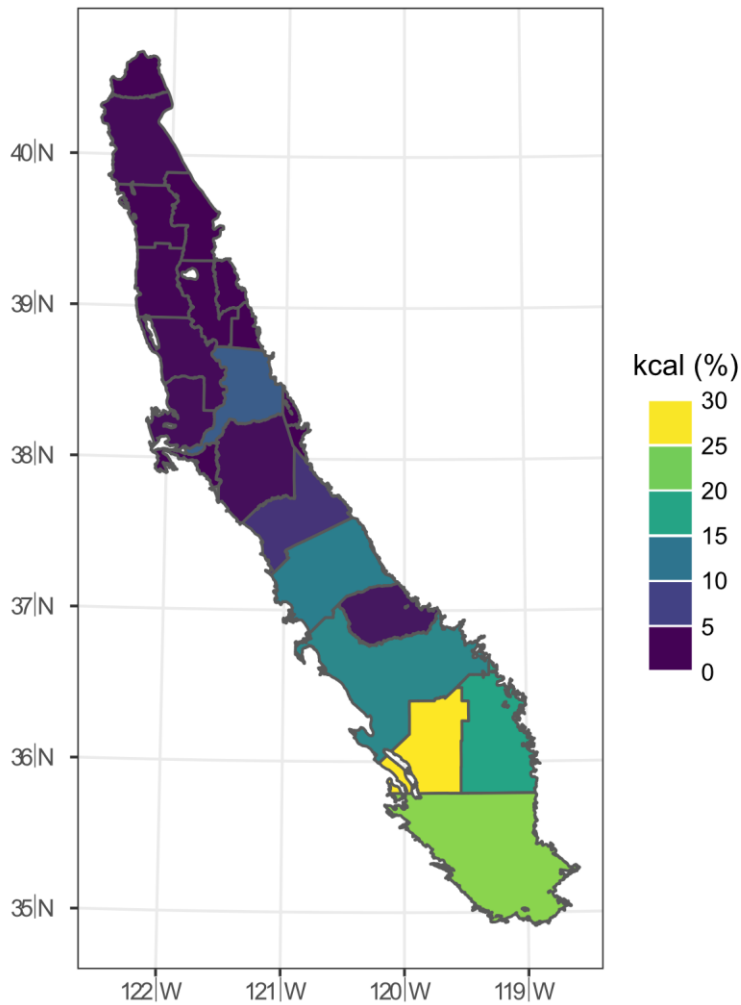


Figure 2.3. 2018 County Level Contribution to Forgone Kcal. Each counties contribution (%) to the total forgone kcal in 2018. Note that only counties which intersect the Central Valley Alluvial Boundary are shown.

Figure 2.3 gives spatial context to the forgone kcal. Note the increase in kcal contribution from Northern to Southern counties. Specifically, Kings, Kern, and Tulare counties account for 62% of total forgone kcal in 2018.

2.3 Predicted impact on electricity production and forgone carbon emissions

Total cumulative electricity generation of the 694 arrays by the year 2042 ranged from 113 TWh for the polycrystalline scenario to 116 TWh for the monocrystalline scenario with the actual reported mono-share (base) scenario resulting in 114 TWh generated. Assuming the average efficiency of each array type Barbose et al. (2020) represents the distribution of monocrystalline and polycrystalline installations in the identified dataset, a potential of 2 TWh was forgone due polycrystalline installations over monocrystalline installations. In the low case scenario, where all installations were polycrystalline, 3 TWh was forgone.

In terms of utility service districts, Pacific Gas & Electric (PG&E) dominated the solar co-located installations containing 62% of total installations totaling 847 MW of installed capacity. The nine other utility service providers contained identified solar co-located arrays are shown in Appendix Table A2.3.

Energy saved by not irrigating converted land ranged from 36.68 to 38.82 GWh (low and high scenarios respectively) with a base scenario of 38.01 GWh. Note that this is five orders of magnitude less than the total electricity generation.

Total cumulative forgone CO₂ emissions from switching to solar was 23.7 Mega-tonnes (Mt) and varied from 23.5 to 24.3 Mt given the monocrystalline vs. polycrystalline uncertainty scenarios. CO₂ emissions forgone by not irrigating converted land ranged from 0.128 to 0.136 Mt for the uncertainty scenarios, with a base scenario forgone emission of 0.133 Mt. CO₂ emissions due to the life cycle analysis (LCA) of C-Si solar PV installation, operation, and decommission ranged from 2.73 to 3.96 Mt for the uncertainty scenarios with a base scenario emission of 3.12 Mt. Temporal change in CO₂ emissions through 2042 are shown in Figure 2.4.

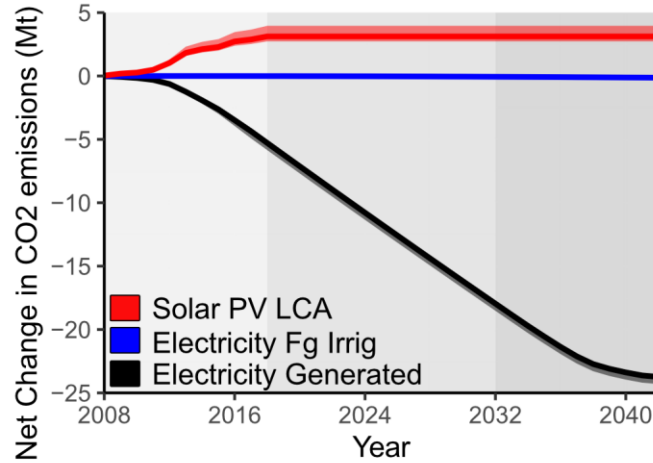


Figure 2.4. Cumulative Change in CO₂ Emissions from Installed Solar PV. Cumulative change in CO₂ emissions due to lifespan solar co-location installations in the Central Valley. In black is forgone CO₂ emissions from not using natural gas for energy generated, in blue is forgone CO₂ emissions from not using natural gas energy required for irrigating converted cropland, and in red is the CO₂ emissions from crystalline silicon ground mounted LCA through all three phases.

2.4 Predicted impact on water use

As of 2016 California Department of Water Resources irrigated maps, 63% (438) of the 694 arrays were on previously irrigated land. Cumulative forgone irrigation for the study period was 0.36 km³ or roughly 300,000 acre-feet. Under the differing precipitation uncertainty scenarios, this ranged from 0.35 to 0.37 km³. This is water that we assumed would have been used for irrigating the cropland that was converted to solar. For reference, the State of California uses roughly 25,800,000 acre-feet/yr for agricultural irrigation (Cody et al., 2015). Therefore, on a lifespan annual average basis (25-years), these solar installations forgo roughly 11,400 acre-feet/yr, or 0.044% of California's annual irrigation water use.

Operation and Maintenance (O&M) water use was cumulatively estimated to be between 0.029 to 0.130 km³ with a base case scenario water use of 0.077 km³ or roughly 62,000 acre-feet. This suggests an overall decrease in water use due to the removal of irrigated area which was 4.7 times the increase in water use due to operation and maintenance.

2.5 Predicted lifetime financial impact from the cropland owner's perspective

Our economic impact analysis was based on the discounted cash flow (DCF) model, predicting total future value of the array as compared to initial (and continuing) costs of installation, operation and maintenance, and now, crop loss. During the first several years of installation phase, the installation cost dominates the PV budget. However, by 2027 (high scenario), 2023 (base scenario) and 2020 (low scenario) the Economic Payback Time was reached, and the total PV budget became positive. Table 2.1 reports cumulative scenario values, and base scenario values per MW and per lifespan year (25-years). To inform future installations, this data suggests that a farmer stands to net \$254,000/MW/yr.

Resource	Base Scenario	High Scenario	Low Scenario	Per MW (2,052 MW)	Per Year (25 yr)	Units
Food	1.64	2.00	1.55	0.000799	0.0656	Trillion kcal
Energy	114	116	113	0.0556	4.56	TWh
Irrig Energy	0.037	0.037	0.035	0.000018	0.0015	TWh
Irrigation	0.36	0.37	0.35	0.00017	0.014	km ³
O&M Water Use	0.077	0.125	0.029	0.0000375	0.00308	km ³
Carbon	23.7	24.3	23.5	0.0116	0.949	Mt
Irrig Carbon	0.133	0.136	0.128	0.0000647	0.00531	Mt
Inst Carbon	3.12	3.96	2.73	0.00152	0.125	Mt
Food\$	\$830	\$990	\$780	\$0.404	\$33.2	2018 Mil USD
Energy\$	\$20,900	\$21,300	\$20,700	\$10.2	\$836	2018 Mil USD
Water\$	\$20.6	\$21.0	\$19.9	\$0.0100	\$0.823	2018 Mil USD
O&M\$	\$725	\$1,280	\$667	\$0.353	\$29.01	2018 Mil USD
InstCost\$	\$6,380	\$8,650	\$5,130	\$3.1	\$255	2018 Mil USD
Total Budget\$	\$13,000	\$14,700	\$9,800	\$6.34	\$520.00	2018 Mil USD

Table 2.1. Cumulative Resource and Economic Impact Values. End of lifespan cumulative resource and economic values for all analysis of this study. Results are shown for the base case scenario, high resource case scenario, low resource case scenario, and the base case scenario divided by total capacity (2,052 MW) and total system lifespan (25 years, not 36 years which is the length of the study period). Note that “Irrig Energy” is the energy that would have been required to irrigate the converted land, “Irrig Carbon” is the forgone CO₂ emissions from not using the energy required to irrigate converted land, and “Inst Carbon” is a prediction of CO₂ emissions based on Hsu et al., 2012, of harmonized CO₂ emissions due to the processes of production, transport, and installation.

3. Discussion

3.1 Food, energy, water, and carbon emission resource impacts

This study was a simple one way impact analysis (C. Zhang et al. 2018) because of its unilateral relationships and lack of feedback loops. However, because this data does not exist elsewhere, a simple impact analysis can help promote further investigation and new data collection.

Chapter 1 reports that 59% of cropland area forgone by arrays was composed of pastureland, wheat, and hay and haylage, which amongst other crops do not directly contribute to human diets. Thus, over 1.64×10^{12} kcal removed from cropland production is not equivalent to removing this amount directly from human diets. However, with expected food needs increasing between 60-110% by 2050 (Alexandratos, Nikos & Bruinsma 2012; Molotoks et al. 2018; Ray et al. 2013; Tilman et al. 2011), any negative impact on global crop production should be minimized through best installation practices. Especially considering 1.64×10^{12} kcal is enough kcal removed from production to feed roughly 90,000 people (2,000 Calorie diet) per year of the solar lifespan. Chapter 1 also reported that fixed axis arrays tended to be installed on marginal land (less productive land). This suggests that our predictions here are likely an over prediction, due to the use of average yields, when much of the converted land was therefore likely lower than average in yield. The preference for converting marginal should become common practice to minimize impact to crop production.

In 2019, the average U.S. residential utility customer consumed 10.6 MWh of electricity (EIA 2020). Using this assumption on a per year basis, the electricity generated from these 649 arrays (4.6 TWh) could account for roughly 428,000 U.S. households. In addition to the sub-optimal packing and spatial field placement (Relative Land Productivity and Global Horizontal Irradiance preferences) shown in Chapter 1, another source of sub-optimal installation practices shown here was the likely installation of polycrystalline modules rather than monocrystalline panels. Although monocrystalline modules are typically more efficient, they also have higher production costs (Luque and Hegedus 2011), and thus may be more attractive to the small-scale farmer. Under the low scenario, this resulted in a potential loss in cumulative electricity generation of 3 TWh, or enough electricity for 8,000 average U.S. homes for each year of the study period.

In regard to water, studies assessing the life-cycle of solar arrays often only look at O&M water use and report this as a potential negative of solar installations (Klise et al. 2013). Solar PV does not require active cooling like concentrating solar power (CSP) arrays, and thus only require water for washing and potable usage for monitoring the site (Klise et al. 2013). Klise et al. (2013) does acknowledge that the construction phase for solar PV arrays uses significantly higher O&M water use than any other portion of the lifespan of the array. This study found that co-located arrays forgo 4.7 times as much as would be used for O&M over the operational lifespan of the array. Despite the large uncertainty (drought year or wet year), by 2042 cumulative forgone irrigation was not highly variable under differing uncertainty scenarios. This suggests that forgone irrigation was largely driven by crop preferences, rather than year to year precipitation. Because the “value” of water is a difficult metric to measure and is not representative of the cropland owner's point of view (difference from the “cost” of water), we attempted to calculate a total cost for farmers to irrigate based on energy requirements and water right contracts. An assumption of this impact analysis was that water that would have been used for irrigation was truly forgone rather than redistributed. This is unlikely to be entirely the case due to an economics originating phenomenon known as Jevon's paradox in which improved access or efficiency of a resource does not necessarily result in the conservation of the resource, but instead results in increased consumption due to resource benefits (Alcott 2005; Jevons 1865). This is a question only solar-practicing farmers could answer and should be the focus of future surveys and policy to regulate water use.

Total forgone CO₂ emissions from forgone energy consumption by non-irrigating land was 0.133 Mt which was two orders of magnitude less than forgone emissions from energy generated. This quantification emphasizes the importance of sustainable practices reported in

McCarthy et al. (2020) in moving forward with sustainable irrigation practices and advances in energy technology. In addition, CO₂ emissions from the system LCA (3.12 Mt) were significantly less than forgone CO₂ from the switch away from natural gas consumption by a factor of 8.

Without focused sustainable management (e.g., conservation tillage rather than plow tillage) many agricultural lands are under a negative to neutral carbon budget (especially with tillage). Thus, carbon sequestration forgone due to the removal of crop was considered negligible and was left out of the quantified CO₂ emissions (Follett, 2001). This is an assumption that should be evaluated and tested in future work.

3.2 Economic analysis and the need for preserving cropland

The benefits of solar are far reaching in both the environmental and the economic realms. Even under the low scenario, CO₂ emissions are cut in half over the lifespan of solar arrays as compared to using a relatively “efficient” form of fossil fuel, natural gas. Economically for the farmer, the total net positive budget by 2042 was 16 times the value of crops forgone. The budget was largely dominated by energy generated from the solar installation. This suggests that from the farmers point of view, the most profitable practice by far is to convert cropland to solar. With no incentive to continue or return to cropland production, there will likely be a large-scale conversion of cropland to solar, challenging both national and global food security, and potential increasing prices of food. Unless the value of food increases ten-fold to the point where this gap in land value is closed, financially, a farmer should install solar. We should evaluate policies that prioritize cropland, despite this difference in value.

Under the return to agriculture scenario, there was significant financial gain for the farmer, and crop loss was reduced as compared to a non-return to agriculture. In Chapter 1, we

found a dichotomy of crop conversion preferences with commodity crops (pastureland) dominating area converted and high value specialty crops (orchards) having a large number of solar installations on cropland with less area converted. Specialty perennial crops such as many orchards tend to be climatically constrained and can take years to go from planting to production (Lobell et al. 2006). Unregulated conversion of high value land could have impacts on future crop prices and availability. However, converting irrigated orchards rather than non-irrigated pastureland could reduce overall water consumption. Overall, solar co-location was shown to be highly profitable, and thus likely to continue to expand without regulation, this could have significant impacts on food production and water availability. Thus, our research suggests the need to account for location-specific food and water resources when co-locating solar PV to reduce impacts on U.S. agricultural production and water as solar becomes more prevalent. In addition, localized social resistance is a primary opposition for broad scale implementation of solar (Pascaris et al. 2021), and regulation prioritizing cropland and local hydrology would likely improve social acceptance, and large implementation of solar. Regulation such as this would switch the solar co-location conversation from land use competition to complementary land use (Pascaris et al. 2021).

3.3 Limitations

This one way impact analysis was intended to provide a starting point for more detailed research on FEW, carbon, and economic feedbacks of solar co-location. This study therefore has several areas that could be expanded in future work. In terms of assessing CO₂ emissions, this study does not look at changes in carbon cycling from ground cover change under different ground cover conditions (bare soil, cover or pollinator crop, agrivoltaic cover crop, and gravel covered), changes in microbial respiration, or CO₂ emissions from production of solar array. In addition, CO₂ emission values are constant and based on life cycle averages.

This study also does not attempt to incorporate changes in property value, price of food,

or the water and energy consumed for the material acquisition, production, transport, installation, or recycling of the arrays. In general, there was minimal to no feedback between resources, and thus a complex multiple way impact analysis would better be able to assess scenario impacts on all the others.

4. Methods

4.1 Site description

The legislative incentives and changes in decision making were the motivation for the Central Valley study area. The area used to delineate the Central Valley was the alluvial boundary derived by Faunt 2012 (Faunt 2012). Chapter 1 reports the necessary spatiotemporal data of solar PV installations in the Central Valley for this analysis. The entirety of data required for this analysis are rarely included in other solar PV datasets, making it difficult to perform a similar regional analysis elsewhere.

4.2 Projected Resource Assumptions

For the base scenario of each resource, annual values were calculated for the installation phase based on reported total cropland area (food, water), energy generated (energy, carbon), growing season precipitation and USGS water use (water), historical installation costs (budget), and historical averages for O&M water use and cost. The value of the resource forgone or generated in 2018 was forecast forward through the operation and decommission phase assuming that the crop rotation pattern persists, resource impacts end after the 25th year of operation, other than forgone which returns one year post termination. More detailed descriptions of resource values used and scenarios can be found Appendix Table A2.1.

4.3 Forgone food

Heller et al., 2013 suggests that one possible functional unit for assessing food related LCA questions in the production perspective is a single nutritional aspect such as energy (kcal) or protein (g) (Heller, Keoleian, and Willett 2013). For the purpose of this study, we chose kcal as our functional LCA unit. To estimate forgone kcal given a total forgone area for each crop type, we first calculated the Caloric density per square meter of 45 crop types (including double crops) forgone due to solar co-location. Kcal and historic yield data was gathered for each crop. Kilocalorie and yield food data sources were the USDA FoodData portal, Independent California Department Reports, nutritional food dietary websites, and assumptions based on similarity to other crop types depending on the availability of the data. Double crop forgone kcal were also assumed to simply be the kcal sum of the two comprising crop types. A table of sources can be found in Appendix Table A2.2, and is being actively updated to improve sources. The calculation of forgone kcal was calculated by:

$$Food_{Forgone}(kcal) = Caloric\ Density \left(\frac{kcal}{kg} \right) * Yield \left(\frac{kg}{m^2} \right) * Area (m^2) \quad (7)$$

The dollar value of food was calculated using the 2013 USDA Farm and Ranch Irrigation Survey (FRIS) and 2018 Irrigation and Water Management Survey (IWMS) (USDA 2013, 2018). Missing crop types (including double crops) were assumed based on perceived similarity to other crop types which were present in the data. Again, double crop dollar value was assumed to be the sum of the two crop type dollar values. Depending on crop type, yield data was collected using differing mass units and thus unit conversions were performed to normalize crop masses to kilograms from pounds, tons, hundredweights, boxes, and bushels. Yield data was from the USDA's National Agriculture Statistics Service Crop releases from 2018 through 2021. The dollar value of forgone food was calculated by:

$$Food_{Forgone}(\$) = \$Value \left(\frac{\$}{kg} \right) * Yield \left(\frac{kg}{m^2} \right) * Area (m^2) \quad (8)$$

Yield forecasts are difficult and often highlight differing future trends depending largely on assumptions. A study from Ray et al., (Ray et al. 2013) found that although not enough to account for the predicted doubling in food needs by 2050, some of the world's key crops (maize, rice, wheat, soybean) will likely increase in yield over the next 30 years, while Lee et al (Lee, Gryze, and Six 2011) found overall decreases in yield for wheat over the same study period, but acknowledged potential increases with CO₂ fertilization. Unlike annual crops, perennial crops are less adaptable and thus more susceptible to climate change and are more agreed upon to decrease in yield by 2050, especially with decreases in water availability in California (Lobell et al. 2006; Pathak et al. 2018).

Because the primary crops forgone were both low value annual crops such as wheat and high value perennial crops such as almonds, we used a combination of scenarios (overall increase and decrease in yield, and consistent yield at 2018 predictions. The base case scenario for forgone food in kcal and the dollar value of forgone food was thus a continuation of 2018 predicted yield. The uncertainty scenarios used were an overall (high) 0.82%/year increase in yield (United States mean wheat yield increase by 2050 from (Ray et al. 2013) supporting information Data S1.), and a (low) 0.24%/year decrease in yield (median decrease in almond yield of 12% from 2000 to 2050 assumed from Figure 3 of (Lobell et al. 2006)).

4.4 Electricity production and carbon emissions

Major assumptions regarding electricity production included: all arrays were connected to the grid during the time of operation, no arrays were installed before 2008 or after 2018, thus efficiencies for all three scenarios are based on 2008 - 2018 data, arrays are disconnected from the grid after 25 years of service (post installation year) meaning modules are not replaced or

connected for longer than their warranty, and after 25 years, the arrays no longer require maintenance and do not generate any energy.

Electricity generation for the installation phase was taken from Chapter 1 where weather, incident irradiance, tilt, efficiency, efficiency degradation, and soiling losses were accounted for in a simple efficiency model developed by National Renewable Energy Laboratory (Gilman 2015). Generation was projected during the operation phase with all arrays operating at 2018 conditions including an annual 0.6% (pre-2010 installations) and 0.3% (post-2010 installations) efficiency degradation as described by Jordan et al. (Jordan et al. 2016). As stated, during the decommission phase, arrays that reach their 25 year limit for each respective year were removed from operation and thus did not generate energy post termination. This trend continued until 2042, the final year of operation for arrays installed in 2018.

Not only is there energy generated by the solar arrays, but also forgone energy consumption from not irrigating the array area. This assumes that irrigation was truly forgone and not redistributed, an assumption we discuss in the next methods section. County level energy requirements to irrigate were calculated from total energy use and total groundwater and surface water irrigated water use reported in (McCarthy et al. 2021). Resulting county level rates for irrigative energy use were given in GWh/m³. This was multiplied by the predicted change in water use (forgone irrigation - O&M water use) for the base, high, and low change in water use scenarios. Although this study did not consider energy requirements for the material acquisition, production, transportation, and installation of the solar arrays due to missing data sources, we do account for CO₂ emissions from these processes.

For the Installation Phase historical energy prices, utility service districts which contained co-located solar arrays were either directly contacted (Modesto Irrigation District, Sacramento

Municipal Utility District), or their data was gathered via their utility websites (Power and Water Resource Pooling Authority, PG&E, Eastside Power Authority, Southern California Edison), or via openEI database (Lodi Electric Utility, Merced Irrigation District, Redding Electric Utility, Turlock Irrigation District).

To determine the utility provider region for each array, array centroids were intersected with the California Electric Utility Service Areas shape file from California Energy Commission, 2019. Historical utility service provider specific energy cost data was used for the dollar value of energy generated and forgone energy consumption from not irrigating during the installation phase. This data was therefore sensitive to which utility provider the array was connected during operation.

The EIA definition, agricultural production falls within the industrial sector (U.S. Energy Information Administration 2021). According to the EIA, nominal electricity prices will increase by 1.8% per year (compound annual growth rate) from 2020 to 2050 (U.S. Energy Information Administration 2015) for the industrial sector. This assumption was used to estimate the increase in the price of electricity during the operation and decommission phases (2019 - 2042).

Uncertainty scenarios for energy generated were based on two end member technologies: 100% monocrystalline installations (high scenario) or 100% polycrystalline installations (low scenario). Lawrence Berkeley National Lab's (LBNL) Tracking the Sun report database (Barbose et al. 2020) reports temporal average efficiency and % monocrystalline share of modules installed nationally. We performed a multiple linear regression explaining large non-residential (>100 kW & ≤ 5000 kW) efficiency by monocrystalline share and installation year. We then set the monocrystalline share variable to 0 (100% polycrystalline) and to 1 (100% monocrystalline) to predict average temporal efficiencies of the two module compositions.

Figure A2.1 in the supplementary material shows the reported average efficiency and predicted monocrystalline and polycrystalline efficiencies through time.

Three sources of change in CO₂ emission were assessed for this study; CO₂ forgone from natural gas consumption by energy generated, CO₂ emissions forgone from natural gas consumption by energy that would have been used for irrigation, and CO₂ emissions generated from the PV system LCA (Leccisi et al. 2016). The PV system LCA from Leccisi et al. (2016) includes monocrystalline and polycrystalline CO₂ emissions from ground mounted solar array material acquisition, manufacturing, transport, and installation (installation phase) for the three major PV producing regions (European Union, The United States, and China). To calculate predicted emissions for our arrays, the high scenario assumed monocrystalline, the low scenario assumed polycrystalline, and the base scenario accounted for temporal monocrystalline share from Barbose et al. (2020). This does not include CO₂ emission from the forgone need to irrigate which is why it was included separately in this study.

4.5 Change in water use

The presence of irrigation for an array area was inferred from the Chapter 1 PV array dataset and the most recent (2016) irrigated area raster from the California Department of Water Resources. If any part of the array shape was considered irrigated in the nearest year prior to installation, then the cropland area and all respective crops within the rotation were assumed to be irrigated. A major assumption here regarding irrigation was that irrigation was truly forgone and not redistributed to surrounding cropland. We acknowledge that this is likely not the case for many arrays but yields a potential benefit to solar in water scarce areas if redistribution is prohibited.

Crop specific irrigated depths were taken from the 2013 USDA FRIS and 2018 IWMS

(USDA 2013, 2018). As was the case with forgone food, irrigated depths for double crops were assumed to be the sum of irrigated depths for each crop. Total irrigation needs are highly dependent on many factors, one of the most important being growing season precipitation (Hane, Pumphrey, and Station 1984; Narasimhan and Srinivasan 2005). 2013 was the driest year of the study, and 2018 was roughly average. Thus, reported irrigated depth varies greatly between these two surveys and would likely vary more during wet years. To extrapolate changes in irrigation dependent on growing season precipitation, we started by performing a county level linear regression between five-year USGS Water Use (USGS 2015) and respective gridMET growing season average precipitation (Abatzoglou 2013). This linear regression along with annual gridMET precipitation was used to predict water use during each installation phase year relative to water use in 2013 and in 2018 respectively, resulting in a scalar coefficient for each FRIS and IWMS year. Each crop specific irrigated depth was multiplied by these two scalar coefficients, the result of which was averaged to predict a crop specific irrigated depth in a given year dependent upon precipitation. The major assumption here was that changes in irrigation directly scale with changes in county level water use.

The scenario delineation was based on potential future precipitation scenarios. The base case scenario assumed 2018 (average) precipitation and thus 2018 irrigative depth, while the high resource scenario assumed 2013 (lowest precipitation of installation phase, highest irrigation water use) precipitation and irrigation, and the low scenario assumed 2017 (wettest year of installation phase, lowest irrigation water use) precipitation and irrigation, all projected forward to 2042.

To determine the “cost” of irrigation water to the farmer, we applied the same price estimation as total energy generated (utility specific), with the amount of forgone energy from

not irrigating as the assumed electricity generation. Therefore, the total dollar cost of the change in water use was the sum of the cost of energy required to irrigate converted land, A Central Valley wide average water right contract rate (\$40 per acre-foot from Baldocchi 2018) and a subtraction of O&M predicted water use.

Klise et al. (2013) reports O&M water use predictions on a capacity basis rather than generation basis of 7 acre-feet/MW for the installation phase of PV plants, and between 0.23 and 2.16 acre-feet/MW/yr for dry cooled systems post-installation operational water use including cleaning and potable use. Thus, for the installation phase, 7 acre-feet/MW were distributed over the 11 years of the phase, and the dry cooled value range of 0.23 acre-feet/MW/yr (low scenario) and 2.16 acre-feet/MW/yr (high scenario) with a mean of 1.20 acre-feet/MW/yr (base scenario) were used for the three differing scenarios.

4.6 Simple economic budget from the cropland owner’s perspective

One purpose of this study was to assess the economic effects of co-locating solar with agriculture from the standpoint of the stakeholder who owns the cropland. This point of view gives insight into future regional trends in co-location preferences. The economic dollar value of each resource was calculated individually given predicted increases or decreases and was adjusted for inflation relative to 2018 dollars using the U.S. Bureau of Labor Statistics Consumer Price Index (CPI) for All Urban Consumers (U.S. Bureau of Labor Statistics 2021). The total budget from the point of view of the cropland owner was calculated according to:

$$Budget (\$) = Energy_{\$} + Water_{\$} - Food_{\$} - O\&M_{\$} - InstCost_{\$} \quad (9)$$

Where, Energy\$ is the dollar value of energy, Water\$ is the dollar value of the cost of the change in water use and predicted water contract rates, Food\$ is the dollar value of forgone food, O&M\$ is dollar value of operations and maintenance, and InstCost\$ is the total cost of installation

(which ceases in 2018 under our scenario).

The method for deducing the dollar value of Food\$, Energy\$, and Water\$, is described above, and the uncertainty dollar value for each was based on the uncertainties of each respective resource. A temporal average of O&M costs does a good job estimating costs through time (Walker et al. 2020) and thus a temporally constant base case dollar value of O&M\$ was taken from Walker et al, 2020 annualized unit O&M costs at \$14.14/kW/yr (a similar value to the EIA, 2021 reported fixed O&M cost of \$15.33/kW/yr). This value was modeled for a 10 MW ground mounted tracking array with 10 inverters. Factors included in the O&M cost were vegetation management, snow removal, and cleaning requirements in reference to dirt and pollen. The uncertainty in O&M cost was based on Wisner et al. (Ryan H Wisner, Mark Bolinger 2020) which suggested that across 13 sources, the range in O&M expense was \$13/kW/yr (high scenario) to \$25/kW/yr (low scenario). Walker et al., 2020 suggests that uncertainty in O&M costs is due to system scale, configuration, climate, and site , which this study does not attempt to address. Note also that these values were assumed to include the O&M water requirements also assessed in this study.

Installation costs were taken from the 2020 NREL Solar Cost Benchmark (Feldman et al. 2021). This installed price included in this report accounts for permitting, inspection, interconnection (PII), land acquisition, transmission line, sales tax, overhead, profit, install labor, hardware balance of system (BOS), inverter, and module costs. The base scenario was the NREL installation cost benchmark for “Commercial Rooftop Arrays (200kW)” due to the similar median sizes of identified co-located arrays (fixed axis: 341 kW, single-axis tracking: 1,207 kW). The high scenario was the NREL installation cost benchmark for “Residential PV (22 Panel System)” and the low scenario was the average NREL installation cost benchmark for

“Utility Scale PV, Fixed-Tilt (100 MW)” and “Utility Scale PV, One-Axis Tracker (100 MW)”.
Reported values calculated using NREL’s bottom-up cost model and are national averages using average values across all states.

Acknowledgments

This chapter was coauthored by Siddarth Shulka, Annick Anctil, Anthony Kendall, and David Hyndman. The authors have no competing interests to declare. This work is supported by INFEWS grant number 2018-67003-27406 (accession No. 1013707) from the USDA National Institute of Food and Agriculture. Any opinions, findings, and conclusions or recommendations expressed in this publication are those of the authors and do not necessarily reflect the views of the USDA.

APPENDIX

Resource	Base Description	High Description	Low Description
Food	2018 annual resource continuation	0.82%/year increase in yield (Deepak et al. 2013)	0.24%/year decrease in yield (Lobell et al. 2011)
Energy	Reported efficiency generation (Barbose et al. 2020)	Monocrystalline derived efficiency generation (Barbose et al. 2020)	Multicrystalline derived efficiency generation (Barbose et al. 2020)
Irrig Energy	GWh/m ³ derived from Mccarthy et al. (2021) for total forgone irrigation	GWh/m ³ derived from Mccarthy et al. (2021) for total forgone irrigation	GWh/m ³ derived from Mccarthy et al. (2021) for total forgone irrigation
Irrigation	2018 FRIS and IWMS irrigation continuation	2013 Irrigation projected forward (low precip = high irrig)	2017 Irrigation projected forward (high precip = low irrig)
O&M Water Use	Installation phase: 7 af/MW, 1.20 af/MW/yr continuation (average of high and low scenarios)	Installation phase: 7 af/MW, 2.16 af/MW/yr (Klise et al. 2013)	Installation phase: 7 af/MW, 0.23 af/MW/yr (Klise et al. 2013)
Carbon	PG&E natural gas emission rate (13.446 lbs/therm) with 2018 base scenario energy generation continuation	PG&E natural gas emission rate (13.446 lbs/therm) with 2018 high energy generation continuation	PG&E natural gas emission rate (13.446 lbs/therm) with 2018 low scenario energy generation continuation
Irrig Carbon	PG&E natural gas emission rate (13.446 lbs/therm) with 2018 base scenario forgone irrig energy continuation	PG&E natural gas emission rate (13.446 lbs/therm) with 2018 high scenario forgone irrig energy continuation	PG&E natural gas emission rate (13.446 lbs/therm) with 2018 low scenario forgone irrig energy continuation
Inst Carbon	Mono/Polycrystalline share emissions derived from Barbose et al. (2020) & Leccisi et al. (2016)	Monocrystalline LCA emissions from Leccisi et al. (2016)	Polycrystalline LCA emissions from Leccisi et al. (2017)

Table A2.1. Base, Low, and High Scenario Assumptions and Sources. Source and value descriptions for each of the three scenarios for every resource and economic value assessed in this study.

Table A2.1. (cont'd)

Resource	Base Description	High Description	Low Description
Food\$	USDA Crop Survey Yield data from 2018-2021 with USDA FRIS and IWMS crop value data from 2005 to 2018 for the base forgone food yield (2018 yield continuation) scenario	USDA Crop Survey Yield data from 2018-2021 with USDA FRIS and IWMS crop value data from 2005 to 2018 for the high forgone food yield (0.82%/yr increase) scenario	USDA Crop Survey Yield data from 2018-2021 with USDA FRIS and IWMS crop value data from 2005 to 2018 for the high forgone food yield (0.23%/yr decrease) scenario
Energy\$	Reported efficiency generation value + annual 1.8% compound increase (Barbose et al. 2020)	Multiple linear regression derived monocrystalline efficiency generation value + annual 1.8% compound increase, (Barbose et al. 2020)	Multiple linear regression derived multicrystalline efficiency generation value + annual 1.8% compound increase, (Barbose et al. 2020)
Water\$	Same as base Energy\$ for forgone irrigation energy + \$40 average water right (Baldocci 2018) - O&M water use energy	\$25/kW/yr (Wiser et al. 2020)	\$13/kW/yr (Wiser et al. 2020)
O&M\$	\$14.14/kW/yr (Walker et al. 2020)	\$25/kW/yr (Wiser et al. 2020)	\$13/kW/yr (Wiser et al. 2020)
InstCost\$	Mono/Polycrystalline share emissions derived from Barbose et al. 2020 & Leccisi et al. 2016	Monocrystalline LCA emissions from Leccisi et al. 2016	Polycrystalline LCA emissions from Leccisi et al. 2017
Total Budget\$	Eq 9 for all base scenario values	Eq 9 for all high (unless inverse in equation 9) scenario values	Eq 9 for all low (unless inverse in equation 9) scenario values

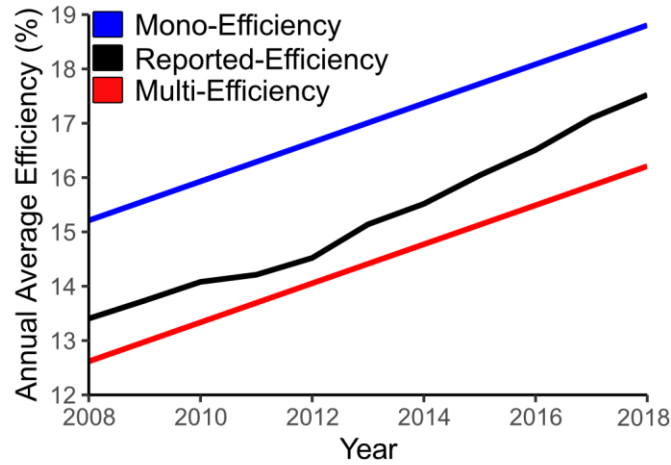


Figure A2.1 Reported Temporal Module Efficiency and Extrapolated Monocrystalline and Polycrystalline Module Efficiencies. The multiple linear model (Efficiency \sim Year + Monocrystalline Share) resulted in an $R^2 = 0.9903$. Data used was from Barbose et al. (2020). To extrapolate differing crystalline efficiencies, the monocrystalline share coefficient was set to 0 (entirely polycrystalline) and 1 (entirely monocrystalline). These efficiencies as shown were used as the three scenarios (high, base, and low respectively) for electricity generation. Figure A1.1 shows the temporal trend in monocrystalline share as well.

<u>Crop</u>	<u>FRIS Crop</u>	<u>Kcal/m²/yr</u>	<u>Caloric Density Source</u>	<u>Yield Source</u>
corn	Corn	1847	www.gardeningplaces.com/articles/nutrition-per-hectare1.htm	www.gardeningplaces.com/articles/nutrition-per-hectare1.htm
cotton	Cotton	570.3	www.fsa.usda.gov/Assets/USDA-FSA-Public/usdfiles/FactSheets/2018/seed_cotton_base_acre_allocation_fact_sheet_august_2018.pdf	www.calories.info/food/nuts-seeds
rice	Rice	1482	www.gardeningplaces.com/articles/nutrition-per-hectare1.htm	www.gardeningplaces.com/articles/nutrition-per-hectare1.htm
sorghum	Sorghum	529	www.gardeningplaces.com/articles/nutrition-per-hectare1.htm	www.gardeningplaces.com/articles/nutrition-per-hectare1.htm
sunflower	Crops, other	868	www.gardeningplaces.com/articles/nutrition-per-hectare1.htm	www.gardeningplaces.com/articles/nutrition-per-hectare1.htm
barley	Hay & Haylage	982	www.gardeningplaces.com/articles/nutrition-per-hectare1.htm	www.gardeningplaces.com/articles/nutrition-per-hectare1.htm
durum wheat	Wheat	1083	www.gardeningplaces.com/articles/nutrition-per-hectare1.htm	www.gardeningplaces.com/articles/nutrition-per-hectare1.htm
winter wheat	Wheat	1083	www.gardeningplaces.com/articles/nutrition-per-hectare1.htm	www.gardeningplaces.com/articles/nutrition-per-hectare1.htm
oats	Small Grains	871	www.gardeningplaces.com/articles/nutrition-per-hectare1.htm	www.gardeningplaces.com/articles/nutrition-per-hectare1.htm
safflower	Crops, other	475	www.gardeningplaces.com/articles/nutrition-per-hectare1.htm	www.gardeningplaces.com/articles/nutrition-per-hectare1.htm
alfalfa	Hay & Haylage	4828.4	www.dekalbasgrowdeltapine.com/en-us/agronomy/alfalfa-yield-quality-management.html	www.dayvillesupply.com/hay-and-horse-feed/calorie-needs.html
other hay/non alfalfa	Hay & Haylage	4828.4	www.dekalbasgrowdeltapine.com/en-us/agronomy/alfalfa-yield-quality-management.html	www.dayvillesupply.com/hay-and-horse-feed/calorie-needs.html

Table A2.2. Food Kcal Sources and Assumptions. Table of caloric density (kcal/kg) sources, historic yield (kg/m²) sources, and resulting spatial caloric density (kcal/m²) for use in the forgone food impact analysis. Note the “compare” values means that values were duplicated from other crops with reported caloric density and yield values. Also note that double crop values were the sum of the two crops making up the double crop.

Table A2.2. (cont'd)

<u>Crop</u>	<u>FRIS Crop</u>	<u>Kcal/m²/yr</u>	<u>Caloric Density Source</u>	<u>Yield Source</u>
dry beans	Beans	229	www.gardeningplaces.com/articles/nutrition-per-hectare1.htm	www.gardeningplaces.com/articles/nutrition-per-hectare1.htm
potatoes	Potatoes	1318	www.gardeningplaces.com/articles/nutrition-per-hectare1.htm	www.gardeningplaces.com/articles/nutrition-per-hectare1.htm
sweet potatoes	Potatoes	1140	www.gardeningplaces.com/articles/nutrition-per-hectare1.htm	www.gardeningplaces.com/articles/nutrition-per-hectare1.htm
watermelons	Crops, other	1068.2	www.agmrc.org/commodities-products/vegetables/watermelon	www.myfitnesspal.com/food/calories/fruit-by-pound-watermelon-515333007
onions	Vegetable totals	1993.2	farm.bot/pages/yield	farm.bot/pages/yield
peas	Vegetable totals	510.5	www.gardeningplaces.com/articles/nutrition-per-hectare1.htm	www.gardeningplaces.com/articles/nutrition-per-hectare1.htm
tomatoes	Tomatoes	255.85	farm.bot/pages/yield	farm.bot/pages/yield
clover/wildflowers	Pastureland	2138.6	enlightenedequine.com/2020/11/29/calories-101-part-3-the-brown-brown-grass-of-home/	www.nrcs.usda.gov/Internet/FSE_DOCUMENTS/stelprdb1167344.pdf
cherries	Orchards	763.31	USDA FoodData	coststudyfiles.ucdavis.edu/uploads/cs_public/6f/9b/6f9b0a93-163b-4060-ba94-8a3fc689e97d/cherryvn2011.pdf
peaches	Orchards	1884.72	USDA FoodData	anrcatalog.ucanr.edu/pdf/8276.pdf
apples	Orchards	1171.22	USDA FoodData	ucanr.edu/datastoreFiles/391-69.pdf
grapes	Berry totals	588.8	srealproperty.com/ever-wonder-how-many-bottles-of-wine-are-made-from-1-acre-of-vineyard/	www.weightlossresources.co.uk/calories-in-food/grapes-red-green-black-seedless-seeded.htm
citrus	Orchards	1252.8	Compare to Orchard Average	Compare to Orchard Average
almonds	Orchards	1490.88	USDA FoodData	californiaagnet.com/2021/05/12/larger-ca-almond-crop-forecasted-this-year/

Table A2.2. (cont'd)

<u>Crop</u>	<u>FRIS Crop</u>	<u>Kcal/m²/yr</u>	<u>Caloric Density Source</u>	<u>Yield Source</u>
walnuts	Orchards	3961.95	USDA FoodData	coststudyfiles.ucdavis.edu/uploads/cs_public/de/5b/de5b047e-efb5-4145-b618-1c643240abe9/walnutsv2012.pdf
grassland/ pasture	Pastureland	2138.6	enlightenedequine.com/2020/11/29/calories-101-part-3-the-brown-brown-grass-of-home/	www.nrcs.usda.gov/Internet/FSE_DOCUMENTS/stelprdb1167344.pdf
pistachios	Orchards	1759.07	USDA FoodData	www.farmfundr.com/blog/pistachio-development-in-california
triticale	Small Grains	871	Compare to Oat Crop	Compare to Oat Crop
carrots	Vegetable totals	1591	farm.bot/pages/yield	farm.bot/pages/yield
garlic	Vegetable totals	828	farm.bot/pages/yield	farm.bot/pages/yield
cantaloupes	Crops, other	621	farm.bot/pages/yield	farm.bot/pages/yield
prunes	Orchards	134.62	USDA FoodData	www.nass.usda.gov/Statistics_by_State/California/Publications/Specialty_and_Other_Releases/Dried_Plums/Forecast/201906prunf.pdf
olives	Orchards	1760	www.gardeningplaces.com/articles/nutrition-per-hectare1.htm	www.gardeningplaces.com/articles/nutrition-per-hectare1.htm
oranges	Orchards	1252.8	USDA FoodData	coststudyfiles.ucdavis.edu/uploads/cs_public/19/d4/19d4f1bb-408a-443e-a759-36fd53a2948f/oranges_vs_2015.pdf
honeydew melons	Crops, other	621	farm.bot/pages/yield	farm.bot/pages/yield
broccoli	Vegetable totals	675	www.gardeningplaces.com/articles/nutrition-per-hectare1.htm	www.gardeningplaces.com/articles/nutrition-per-hectare1.htm

Table A2.2. (cont'd)

<u>Crop</u>	<u>FRIS Crop</u>	<u>Kcal/m²/ yr</u>	<u>Caloric Density Source</u>	<u>Yield Source</u>
pomegranates	Orchards	1252.8	Compare to Orchard Average	Compare to Orchard Average
nectarines	Orchards	1252.8	Compare to Orchard Average	Compare to Orchard Average
plums	Orchards	134.62	Compare to Orchard Average	Compare to Orchard Average
dbl crop winwht/corn	Wheat & Corn	1465	Compare to Sum of Wheat and Corn Crop	Compare to Sum of Wheat and Corn Crop
dbl crop oats/corn	Small Grains & Corn	1359	Compare to Sum of Small Grain and Corn Crop	Compare to Sum of Small Grain and Corn Crop
dbl crop winwht/ sorghum	Wheat & Sorghum	1188	Compare to Sum of Wheat and Sorghum Crop	Compare to Sum of Wheat and Sorghum Crop
dbl crop winwht/cotton	Wheat & Cotton	826.65	Compare to Sum of Wheat and Cotton Crop	Compare to Sum of Wheat and Cotton Crop

<u>Utility</u>	<u>Num Install</u>	<u>Capacity (MW)</u>
Power and Water Resource Pooling Authority	82	669
Pacific Gas & Electric Company	429	847
Modesto Irrigation District	30	31
Eastside Power Authority	49	129
Southern California Edison	46	243
Turlock Irrigation District	29	31
Lodi Electric Utility	1	1
Sacramento Municipal Utility District	15	91
Merced Irrigation District	11	9
Redding Electric Utility	2	1

Table A2.3. Utility Service Provider Contribution to Co-Location. The ten utility service providers with identified co-located solar arrays in their districts.

REFERENCES

REFERENCES

- 10 CFR 436. 2017. *Federal Energy Management Program*.
<https://www.govinfo.gov/content/pkg/CFR-2017-title10-vol3/pdf/CFR-2017-title10-vol3-part436.pdf>. <https://www.govinfo.gov/content/pkg/CFR-2017-title10-vol3/pdf/CFR-2017-title10-vol3-part436.pdf> (July 20, 2021).
- Abas, N., A. Kalair, and N. Khan. 2015. "Review of Fossil Fuels and Future Energy Technologies." *Futures* 69: 31–49.
- Abatzoglou, John T. 2013. "Development of Gridded Surface Meteorological Data for Ecological Applications and Modelling." *International Journal of Climatology*.
- Adeh, Elnaz H., Stephen P. Good, M. Calaf, and Chad W. Higgins. 2019. "Solar PV Power Potential Is Greatest Over Croplands." *Scientific Reports*.
- Alcott, Blake. 2005. "Jevons' Paradox." *Ecological Economics* 54(1): 9–21.
- Alexandratos, Nikos & Bruinsma, Jelle. 2012. "WORLD AGRICULTURE TOWARDS 2030 / 2050 The 2012 Revision PROOF COPY." *ESA Working paper* 12(12): 146.
<https://ageconsearch.umn.edu/record/288998> (July 22, 2021).
- Amaducci, Stefano, Xinyou Yin, and Michele Colauzzi. 2018. "Agrivoltaic Systems to Optimise Land Use for Electric Energy Production." *Applied Energy* 220: 545–61.
- Aroca-Delgado, Raúl, José Pérez-Alonso, Ángel Jesús Callejón-Ferre, and Borja Velázquez-Martí. 2018. "Compatibility between Crops and Solar Panels: An Overview from Shading Systems." *Sustainability (Switzerland)* 10(3).
- Awan, Ahmed Bilal et al. 2020. "Comparative Analysis of Ground-Mounted vs. Rooftop Photovoltaic Systems Optimized for Interrow Distance between Parallel Arrays." *Energies*.
- Baatz, Martin, and A Schape. 2000. "Multiresolution Segmentation - An Optimization Approach for High Quality Multi-Scale Image Segmentation Angewandte Geographische Informationsverarbeitung XII." *Proceedings of Angewandte Geographische Informationsverarbeitung XII*.
- Baldocchi, Dennis D. 2018. "The Cost of Irrigation Water and Urban Farming." *Berkeley News*.
https://news.berkeley.edu/berkeley_blog/the-cost-of-irrigation-water-and-urban-farming/ (August 11, 2021).
- Barbose, Galen, Na'im Darghouth, Eric O'shaughnessy, and Sydney Forrester. 2020. *Distributed Solar 2020 Data Update**.
https://emp.lbl.gov/sites/default/files/distributed_solar_2020_data_update.pdf (June 16, 2021).

- Barron-Gafford, Greg A. et al. 2019. “Agrivoltaics Provide Mutual Benefits across the Food–Energy–Water Nexus in Drylands.” *Nature Sustainability*.
- Benedetti, Roberto, and Paolo Rossini. 1993. “On the Use of NDVI Profiles as a Tool for Agricultural Statistics: The Case Study of Wheat Yield Estimate and Forecast in Emilia Romagna.” *Remote Sensing of Environment*.
- Blaschke, Thomas et al. 2014. “Geographic Object-Based Image Analysis - Towards a New Paradigm.” *ISPRS Journal of Photogrammetry and Remote Sensing*.
- Blaschke, Thomas, and Josef Strobl. 2001. “What’s Wrong with Pixels? Some Recent Developments Interfacing Remote Sensing and GIS.” *Geo-Information-Systeme*.
- Bolton, Douglas K., and Mark A. Friedl. 2013. “Forecasting Crop Yield Using Remotely Sensed Vegetation Indices and Crop Phenology Metrics.” *Agricultural and Forest Meteorology*.
- Bomber, M., and R. Portelli. 2020. “Multi-Scale Analysis of Jack Pine Saplings after Fire across Burn Severities.” *International Archives of the Photogrammetry, Remote Sensing and Spatial Information Sciences - ISPRS Archives* 43(B3): 671–75.
- Bradbury, Kyle et al. 2016. “Distributed Solar Photovoltaic Array Location and Extent Dataset for Remote Sensing Object Identification.” *Scientific Data*.
- Brooks, William, and James Dunlop. 2013. “NABCEP PV Installation Professional Resource Guide.” *Nabcep* 6: 1–160. www.nabcep.org (June 16, 2021).
- Brown, Edmund G. 2020. California Agricultural Statistics Review *California Agricultural Statistics Review 2019-2020*. www.cdfa.ca.gov/statistics (June 16, 2021).
- Bueno, Inacio T. et al. 2019. “Object-Based Change Detection in the Cerrado Biome Using Landsat Time Series.” *Remote Sensing*.
- Bunis, Linda, and John Mootz. 2007. *Aerial Photography Field Office-National Agriculture Imagery Program (NAIP) Suggested Best Practices-Final Report*.
- Cai, Yaotong, Hui Lin, and Meng Zhang. 2019. “Mapping Paddy Rice by the Object-Based Random Forest Method Using Time Series Sentinel-1/Sentinel-2 Data.” *Advances in Space Research*.
- California Department of Fish and Wildlife. 2020. “Base_Remote_Sensing/NAIP_2018_4Band (ImageServer).” https://map.dfg.ca.gov/arcgis/rest/services/Base_Remote_Sensing/NAIP_2018_4Band/ImageServer (June 16, 2021).
- California Department of Water Resources. “Sustainable Groundwater Management Act (SGMA).” <https://water.ca.gov/programs/groundwater-management/sgma-groundwater-management> (July 20, 2021).

- CAPUC. 2016. “Decision Adopting Successor to Net Energy Metering Tariff.” <https://docs.cpuc.ca.gov/PublishedDocs/Published/G000/M158/K285/158285436.pdf> (July 20, 2021).
- Chen, Junyi et al. 2019. “Enhanced Normalized Difference Index for Impervious Surface Area Estimation at the Plateau Basin Scale.” *Journal of Applied Remote Sensing*.
- Chu, Yinghao. 2011. “Review and Comparison of Different Solar Energy Technologies.” *Global Energy Network Institute*.
- Clean Energy Extension. 2019. *What Does Dual-Use Mean?* <http://s3.us-east-2.amazonaws.com/bluewave-shade/jan23-1002/index.html> (June 16, 2021).
- Cohen, Warren B. et al. 2018. “A LandTrendr Multispectral Ensemble for Forest Disturbance Detection.” *Remote Sensing of Environment*.
- Congress, US. 2007. “U.S. Energy Independence and Security Act of 2007.” *Public Law: 110–40*.
- Csillik, Ovidiu, Mariana Belgiu, Gregory P. Asner, and Maggi Kelly. 2019. “Object-Based Time-Constrained Dynamic Time Warping Classification of Crops Using Sentinel-2.” *Remote Sensing*.
- Definiens. 2000. *4 ECognition Professional User Guide*.
- Dickinson. 2016. *AB 1739*.
- Dinesh, Harshavardhan, and Joshua M. Pearce. 2016. “The Potential of Agrivoltaic Systems.” *Renewable and Sustainable Energy Reviews* 54: 299–308.
- Dolan, Stacey L., and Garvin A. Heath. 2012. “Life Cycle Greenhouse Gas Emissions of Utility-Scale Wind Power: Systematic Review and Harmonization.” *Journal of Industrial Ecology* 16(SUPPL.1): S136–54. <https://onlinelibrary.wiley.com/doi/full/10.1111/j.1530-9290.2012.00464.x> (July 21, 2021).
- Doyle, C et al. 2015. “SAPC Best Practices in PV System Installation - Version 1.0, March 2015.” *NREL* (March): 36. www.nrel.gov/publications. (June 16, 2021).
- Dupraz, C. et al. 2011. “Combining Solar Photovoltaic Panels and Food Crops for Optimising Land Use: Towards New Agrivoltaic Schemes.” *Renewable Energy* 36(10): 2725–32.
- Efficiency, Energy. 2010. “2008 Solar Technologies Market Report.” *US Department of Energy Energy Efficiency Renewable Energy* (January): 131. <http://escholarship.org/uc/item/5f24h660.pdf> (June 16, 2021).
- EIA. 2020. “Frequently Asked Questions (FAQs) - U.S. Energy Information Administration (EIA).” *EIA*. <https://www.eia.gov/tools/faqs/faq.php?id=97> (July 25, 2021).

- Energy Information Administration. 2015. “Electric Power Monthly: With Data for January 2020.” *U.S. Energy Information Administration* (August).
- Esri Inc. 2021. “ArcGIS Pro (Version 2.7.3).” *Esri Inc.*
- F. Holmgren, William, Clifford W. Hansen, and Mark A. Mikofski. 2018. “Pvlib Python: A Python Package for Modeling Solar Energy Systems.” *Journal of Open Source Software*.
- Faunt, Claudia C. 2012. “Alluvial Boundary of California’s Central Valley.”
https://pubs.usgs.gov/pp/1766/PP_1766.pdf.
https://water.usgs.gov/lookup/getspatial?pp1766_Alluvial_Bnd (June 16, 2021).
- Faunt, Claudia C., and Ed. 2009. *Program Groundwater Availability of the Central Valley Aquifer, California: U.S. Geological Survey Professional Paper 1766*.
- Feldman, David et al. 2021. National Renewable Energy Laboratory *U.S. Solar Photovoltaic System and Energy Storage Cost Benchmark: Q1 2020*. Golden, CO.
<https://www.nrel.gov/docs/fy21osti/77324.pdf> (June 16, 2021).
- FRAGAL, Everton Hafemann, Thiago Sanna Freire SILVA, and Evlyn Márcia Leão de Moraes NOVO. 2016. “Reconstructing Historical Forest Cover Change in the Lower Amazon Floodplains Using the LandTrendr Algorithm.” *Acta Amazonica*.
- Fu, Ran, David Feldman, and Robert Margolis. 2018. “U.S. Solar Photovoltaic System Cost Benchmark: Q1 2018.” *Nrel* (November): 1–47.
<https://www.nrel.gov/docs/fy19osti/72399.pdf> (June 16, 2021).
- Funk, Chris, and Michael E. Budde. 2009. “Phenologically-Tuned MODIS NDVI-Based Production Anomaly Estimates for Zimbabwe.” *Remote Sensing of Environment*.
- Gilman, Paul. 2015. “SAM Photovoltaic Model Technical Reference SAM Photovoltaic Model Technical Reference.” *Solar Energy* 63(May): 323–333. www.nrel.gov/publications. (June 16, 2021).
- Gitelson, Anatoly A. 2004. “Wide Dynamic Range Vegetation Index for Remote Quantification of Biophysical Characteristics of Vegetation.” *Journal of Plant Physiology*.
- Goetzberger, A., and A. Zastrow. 1982. “On the Coexistence of Solar-Energy Conversion and Plant Cultivation.” *International Journal of Solar Energy* 1(1): 55–69.
<https://www.tandfonline.com/doi/abs/10.1080/01425918208909875> (August 15, 2021).
- Hane, Dan C., F. V. (Floyd Vance) Pumphrey, and Oregon State University. Agricultural Experiment Station. 1984. “Crop Water Use Curves for Irrigation Scheduling.” (March).
<http://ir.library.oregonstate.edu/xmlui/handle/1957/4991>.
- Hao, Yuzhu et al. 2020. “Bidirectional Segmented Detection of Land Use Change Based on Object-Level Multivariate Time Series.” *Remote Sensing*.

- Hartmann, H.M., Grippo, M.A., Heath, G., Macknick, J., Smith, K., Sullivan, R., Walston, L., Wescott, K. 2016. “Understanding Emerging Impacts and Requirements Related to Utility-Scale Solar Development.” *Environmental Science Division, Argonne National Laboratory ANL/EVS-16*. <https://publications.anl.gov/anlpubs/2016/10/130700.pdf> (June 16, 2021).
- Hay, G. J., K. O. Niemann, and G. F. McLean. 1996. “An Object-Specific Image-Texture Analysis of H-Resolution Forest Imagery.” *Remote Sensing of Environment*.
- He, Xiaogang et al. 2019. “Solar and Wind Energy Enhances Drought Resilience and Groundwater Sustainability.” *Nature Communications* 10(1): 1–8. <https://www.nature.com/articles/s41467-019-12810-5> (August 16, 2021).
- Heller, Martin C., Gregory A. Keoleian, and Walter C. Willett. 2013. “Toward a Life Cycle-Based, Diet-Level Framework for Food Environmental Impact and Nutritional Quality Assessment: A Critical Review.” *Environmental Science and Technology*.
- Hernandez, Rebecca R. et al. 2015. “Solar Energy Development Impacts on Land Cover Change and Protected Areas.” *Proceedings of the National Academy of Sciences of the United States of America* 112(44): 13579–84. <https://www.pnas.org/content/112/44/13579> (July 30, 2021).
- Hernandez, Rebecca R, Madison K Hoffacker, and Christopher B Field. 2014. “Land-Use Efficiency of Big Solar.” *Environmental Science and Technology* 48(2): 1315–23. <https://pubs.acs.org/sharingguidelines> (July 30, 2021).
- Hsu, David D. et al. 2012. “Life Cycle Greenhouse Gas Emissions of Crystalline Silicon Photovoltaic Electricity Generation: Systematic Review and Harmonization.” *Journal of Industrial Ecology* 16(SUPPL.1): S122–35. <https://onlinelibrary.wiley.com/doi/full/10.1111/j.1530-9290.2011.00439.x> (July 21, 2021).
- Jevons, William Stanley. 1865. “The Coal Question: Can Britain Survive.” *First published in*.
- Jordan, Dirk C., Sarah R. Kurtz, Kaitlyn VanSant, and Jeff Newmiller. 2016. “Compendium of Photovoltaic Degradation Rates.” *Progress in Photovoltaics: Research and Applications*.
- Joshi, Bikash, Baluyan Hayk, Amer Al-Hinai, and Wei Lee Woon. 2014. “Rooftop Detection for Planning of Solar PV Deployment: A Case Study in Abu Dhabi.” *Lecture Notes in Computer Science (including subseries Lecture Notes in Artificial Intelligence and Lecture Notes in Bioinformatics)*.
- Jubayer, Chowdhury Mohammad, Kamran Siddiqui, and Horia Hangan. 2016. “CFD Analysis of Convective Heat Transfer from Ground Mounted Solar Panels.” *Solar Energy*.
- Karin, Todd, and Anubhav Jain. 2020. “Visual Characterization of Anti-Reflective Coating on Solar Module Glass.” In *Conference Record of the IEEE Photovoltaic Specialists Conference*,.
- Kennedy, Robert E. et al. 2018. “Implementation of the LandTrendr Algorithm on Google Earth

- Engine.” *Remote Sensing*.
- Kennedy, Robert E., Zhiqiang Yang, and Warren B. Cohen. 2010. “Detecting Trends in Forest Disturbance and Recovery Using Yearly Landsat Time Series: 1. LandTrendr - Temporal Segmentation Algorithms.” *Remote Sensing of Environment*.
- Khan, Jibrán, and Mudassar H. Arsalan. 2016. “Solar Power Technologies for Sustainable Electricity Generation - A Review.” *Renewable and Sustainable Energy Reviews* 55: 414–25.
- Kimmelshue, Joel. 2021. “I15_Crop_Mapping_2018.”
- Klise, Geoffrey T et al. 2013. *Water Use and Supply Concerns for Utility-Scale Solar Projects in the Southwestern United States*. <http://www.ntis.gov/help/ordermethods.asp?loc=7-4-0#online> (July 25, 2021).
- Leccisi, Enrica, Marco Raugei, and Vasilis Fthenakis. 2016. “The Energy and Environmental Performance of Ground-Mounted Photovoltaic Systems - A Timely Update.” *Energies* 9(8): 622. <https://www.mdpi.com/1996-1073/9/8/622/htm> (August 16, 2021).
- Lee, Juhwan, Steven De Gryze, and Johan Six. 2011. “Effect of Climate Change on Field Crop Production in California’s Central Valley.” *Climatic Change* 2011 109:1 109(1): 335–53. <https://link.springer.com/article/10.1007/s10584-011-0305-4> (July 24, 2021).
- Liu, Chong et al. 2019. “An Efficient Approach to Capture Continuous Impervious Surface Dynamics Using Spatial-Temporal Rules and Dense Landsat Time Series Stacks.” *Remote Sensing of Environment*.
- Lobell, David B., Christopher B. Field, Kimberly Nicholas Cahill, and Celine Bonfils. 2006. “Impacts of Future Climate Change on California Perennial Crop Yields: Model Projections with Climate and Crop Uncertainties.” *Agricultural and Forest Meteorology* 141(2–4): 208–18.
- Luque, Antonio, and Steven Hegedus. 2011. *Handbook of Photovoltaic Science and Engineering Handbook of Photovoltaic Science and Engineering*.
- Macknick, Jordan. 2019. “Co-Location of Agriculture and Solar : Opportunities to Improve Energy , Food , and Water Resources.”
- . 2020. *26 Co-Location of Agriculture & Solar*. <http://energy21symposium.org/wp-content/uploads/2020/10/Macknick-InSPIRE-Energy21st.pdf> (June 16, 2021).
- Macknick, Jordan, Brenda Beatty, and Graham Hill. 2014. “Overview of Opportunities for Co-Location of Solar Energy Technologies and Vegetation.” In *Solar Energy Sites: Considerations for Areas of Vegetation or Contaminated and Disturbed Lands*, , 1–21. www.nrel.gov/publications. (August 15, 2021).
- Majumdar, Debaleena, and Martin J. Pasqualetti. 2018. “Dual Use of Agricultural Land:

- Introducing ‘Agrivoltaics’ in Phoenix Metropolitan Statistical Area, USA.” *Landscape and Urban Planning* 170: 150–68.
- Malof, Jordan M. et al. 2015. “Automatic Solar Photovoltaic Panel Detection in Satellite Imagery.” In *2015 International Conference on Renewable Energy Research and Applications, ICRERA 2015*,.
- . 2019. “Mapping Solar Array Location, Size, and Capacity Using Deep Learning and Overhead Imagery.” *arXiv*. <http://arxiv.org/abs/1902.10895> (June 16, 2021).
- Malof, Jordan M., Leslie M. Collins, and Kyle Bradbury. 2017. “A Deep Convolutional Neural Network, with Pre-Training, for Solar Photovoltaic Array Detection in Aerial Imagery.” In *International Geoscience and Remote Sensing Symposium (IGARSS)*,.
- Malof, Jordan M., Leslie M. Collins, Kyle Bradbury, and Richard G. Newell. 2016. “A Deep Convolutional Neural Network and a Random Forest Classifier for Solar Photovoltaic Array Detection in Aerial Imagery.” In *2016 IEEE International Conference on Renewable Energy Research and Applications, ICRERA 2016*,.
- Marrou, H., J. Wery, L. Dufour, and C. Dupraz. 2013. “Productivity and Radiation Use Efficiency of Lettuces Grown in the Partial Shade of Photovoltaic Panels.” *European Journal of Agronomy* 44: 54–66.
- Martín-Chivelet, Nuria. 2016. “Photovoltaic Potential and Land-Use Estimation Methodology.” *Energy*.
- Martinez-Feria, Rafael, and Bruno Basso. 2020. “Predicting Soil Carbon Changes in Switchgrass Grown on Marginal Lands under Climate Change and Adaptation Strategies.” *GCB Bioenergy*.
- Maselli, F., C. Conese, L. Petkov, and M. A. Gilabert. 1992. “Use of NOAA-AVHRR NDVI Data for Environmental Monitoring and Crop Forecasting in the Sahel. Preliminary Results.” *International Journal of Remote Sensing*.
- McCarthy, Benjamin et al. 2020. “Trends in Water Use, Energy Consumption, and Carbon Emissions from Irrigation: Role of Shifting Technologies and Energy Sources.” *Environmental Science and Technology*.
- . 2021. “Water Use, Energy Consumption, and Carbon Emissions from Irrigation.”
- Miskin, Caleb K. et al. 2019. “Sustainable Co-Production of Food and Solar Power to Relax Land-Use Constraints.” *Nature Sustainability* 2(10): 972–80. <https://www.nature.com/articles/s41893-019-0388-x> (July 22, 2021).
- Mkhabela, M. S. et al. 2011. “Crop Yield Forecasting on the Canadian Prairies Using MODIS NDVI Data.” *Agricultural and Forest Meteorology*.
- Molotoks, Amy et al. 2018. “Global Projections of Future Cropland Expansion to 2050 and

- Direct Impacts on Biodiversity and Carbon Storage.” *Global Change Biology* 24(12): 5895–5908. <https://onlinelibrary.wiley.com/doi/full/10.1111/gcb.14459> (July 22, 2021).
- N.C. Clean Energy Technology. 2016. “Database of State Incentives for Renewables and Efficiency (DSIRE).” <https://www.dsireusa.org/> (June 16, 2021).
- Narasimhan, B., and R. Srinivasan. 2005. “Development and Evaluation of Soil Moisture Deficit Index (SMDI) and Evapotranspiration Deficit Index (ETDI) for Agricultural Drought Monitoring.” In *Agricultural and Forest Meteorology*.
- National Renewable Energy Laboratory. 2017. *Photovoltaic Module Soiling Map*. <https://www.nrel.gov/pv/soiling.html>.
- National Renewable Energy Laboratory, SunSpec Alliance Sandia National Laboratory, and the SunShot National Laboratory Multiyear Partnership, and (SuNLaMP) PV O&M Best Practices Working Group. 2018. *NREL Best Practices for Operation and Maintenance of Photovoltaic and Energy Storage Systems ; 3rd Edition*. www.nrel.gov/publications. (July 20, 2021).
- Nguyen, Thi Thu Ha et al. 2012. “Mapping the Irrigated Rice Cropping Patterns of the Mekong Delta, Vietnam, through Hyper-Temporal Spot NDVI Image Analysis.” *International Journal of Remote Sensing*.
- Nitze, Ingmar et al. 2017. “Landsat-Based Trend Analysis of Lake Dynamics across Northern Permafrost Regions.” *Remote Sensing*.
- NOAA. 2016. “NOAA Solar Calculator.” *National Oceanic & Atmospheric Administration. Earth System Research Laboratory. Global Monitoring Division. Global Radiation Group.*: 1–4. <https://gml.noaa.gov/grad/solcalc/index.html> (June 16, 2021).
- NREL. 2015. “NSRDB Data Viewer.” *National Renewable Energy Laboratory*. <https://maps.nrel.gov/nsrdb-viewer/> (June 16, 2021).
- . 2020. “Low-Impact Solar Development Strategies Guidebook.” <https://openei.org/wiki/InSPIRE/Guidebook> (June 16, 2021).
- Nyberg, Michael. 2020. “California Solar Energy Statistics and Data.” *California Energy Commission*. https://ww2.energy.ca.gov/almanac/renewables_data/solar/index cms.php#pvThermal (June 16, 2021).
- Office, Congressional Budget. 2005. *Energy Policy Act of 2005*. Washington: House of Representatives. <https://www.govinfo.gov/content/pkg/BILLS-109hr6enr/pdf/BILLS-109hr6enr.pdf> (June 16, 2021).
- Office of Energy Efficiency & Renewable Energy. “Solar and Agriculture Co-Location | Department of Energy.” <https://www.energy.gov/eere/solar/solar-and-agriculture-co-location> (June 16, 2021).

- Pascaris, Alexis S., Chelsea Schelly, Laurie Burnham, and Joshua M. Pearce. 2021. "Integrating Solar Energy with Agriculture: Industry Perspectives on the Market, Community, and Socio-Political Dimensions of Agrivoltaics." *Energy Research and Social Science* 75: 102023.
- Patela, Nirav N. et al. 2015. "Multitemporal Settlement and Population Mapping from Landsat using Google Earth Engine." *International Journal of Applied Earth Observation and Geoinformation*.
- Pathak, Tapan B. et al. 2018. "Climate Change Trends and Impacts on California Agriculture: A Detailed Review." *Agronomy* 8(3): 25. <https://www.mdpi.com/2073-4395/8/3/25/htm> (July 24, 2021).
- Pavley. 2014. *SB 1319*.
- . 2016. *74 SB 1168*.
- Pettorelli, Nathalie et al. 2005. "Using the Satellite-Derived NDVI to Assess Ecological Responses to Environmental Change." *Trends in Ecology and Evolution*.
- Rasmussen, M. S. 1992. "Assessment of Millet Yields and Production in Northern Burkina Faso Using Integrated NDVI from the AVHRR." *International Journal of Remote Sensing*.
- Ravi, Sujith et al. 2016. "Colocation Opportunities for Large Solar Infrastructures and Agriculture in Drylands." *Applied Energy* 165: 383–92.
- Ray, Deepak K., Nathaniel D. Mueller, Paul C. West, and Jonathan A. Foley. 2013. "Yield Trends Are Insufficient to Double Global Crop Production by 2050." *PLoS ONE* 8(6): e66428. <https://journals.plos.org/plosone/article?id=10.1371/journal.pone.0066428> (July 24, 2021).
- Reilly, Matthew J. et al. 2017. "Contemporary Patterns of Fire Extent and Severity in Forests of the Pacific Northwest, USA (1985-2010)." *Ecosphere*.
- Runge, Alexandra, and Guido Grosse. 2020. "Mosaicking Landsat and Sentinel-2 Data to Enhance LandTrendr Time Series Analysis in Northern High Latitude Permafrost Regions." *Remote Sensing*.
- Ryan H Wisner, Mark Bolinger, Joachim Seel. 2020. *Benchmarking Utility-Scale PV Operational Expenses and Project Lifetimes: Results from a Survey of U.S. Solar Industry Professionals*. <https://escholarship.org/uc/item/2pd8608q> (July 20, 2021).
- Schneibel, Anne et al. 2017. "Assessment of Spatio-Temporal Changes of Smallholder Cultivation Patterns in the Angolan Miombo Belt Using Segmentation of Landsat Time Series." *Remote Sensing of Environment*.
- Schneider, Dorian. 2012. "Control Algorithms for Large-Scale Single-Axis Photovoltaic Trackers." *Acta Polytechnica*.

- Schoeffler, Lee E. 2009. “The American Recovery and Reinvestment Act of 2009.” *The Journal of the Oklahoma State Medical Association* 102(3): 80–81.
<https://www.congress.gov/111/plaws/publ5/PLAW-111publ5.pdf> (June 16, 2021).
- Schwantes, Amanda M., Jennifer J. Swenson, and Robert B. Jackson. 2016. “Quantifying Drought-Induced Tree Mortality in the Open Canopy Woodlands of Central Texas.” *Remote Sensing of Environment*.
- Shah, Archit. 2009. “Emergency Economic Stabilization Act of 2008.” *Harvard Journal on Legislation*.
- Shen, Wenjuan, Mingshi Li, and Anshi Wei. 2017. “Spatio-Temporal Variations in Plantation Forests’ Disturbance and Recovery of Northern Guangdong Province Using Yearly Landsat Time Series Observations (1986–2015).” *Chinese Geographical Science*.
- So, Brenda et al. 2017. “Estimating the Electricity Generation Capacity of Solar Photovoltaic Arrays Using Only Color Aerial Imagery.” In *International Geoscience and Remote Sensing Symposium (IGARSS)*.
- Solar Energy Industries Association. 2015. “Major Solar Projects Map.”
<https://www.seia.org/research-resources/major-solar-projects-list> (June 16, 2021).
- . 2019. “Solar Investment Tax Credit (ITC).” https://www.edf-re.com/wp-content/uploads/SEIA-ITC-Basics-Factsheet-2019-March_1.pdf (June 16, 2021).
- . 2021. “Solar Investment Tax Credit (ITC).”
<https://www.seia.org/sites/default/files/2021-01/SEIA-ITC-Factsheet-2021-Jan.pdf> (June 16, 2021).
- Sun, Zhongchang, Cuizhen Wang, Huadong Guo, and Ranran Shang. 2017. “A Modified Normalized Difference Impervious Surface Index (MNDISI) for Automatic Urban Mapping from Landsat Imagery.” *Remote Sensing*.
- Tilman, David, Christian Balzer, Jason Hill, and Belinda L. Befort. 2011. “Global Food Demand and the Sustainable Intensification of Agriculture.” *Proceedings of the National Academy of Sciences of the United States of America* 108(50): 20260–64.
<https://www.pnas.org/content/108/50/20260> (July 22, 2021).
- Tucker, C. J., C. L. Vanpraet, M. J. Sharman, and G. Van Ittersum. 1985. “Satellite Remote Sensing of Total Herbaceous Biomass Production in the Senegalese Sahel: 1980-1984.” *Remote Sensing of Environment*.
- Tucker, Compton J. 1979. “Red and Photographic Infrared Linear Combinations for Monitoring Vegetation.” *Remote Sensing of Environment*.
- U.S. Bureau of Labor Statistics. 2021. “Consumer Price Index (CPI) Databases.”
<https://www.bls.gov/cpi/data.htm> (July 29, 2021).

- U.S. Department of Energy. 2021. *Guide to the Federal Investment Tax Credit for Commercial Solar Photovoltaics*. [https://www.energy.gov/sites/default/files/2021/02/f82/Guide to the Federal Investment Tax Credit for Commercial Solar PV - 2021.pdf](https://www.energy.gov/sites/default/files/2021/02/f82/Guide%20to%20the%20Federal%20Investment%20Tax%20Credit%20for%20Commercial%20Solar%20PV%20-%202021.pdf) (June 16, 2021).
- U.S. Energy Information Administration. 2015. “Table A3 . Energy Prices by Sector and Source.” In *Annual Energy Outlook 2015*, <https://www.eia.gov/outlooks/aeo/data/browser/#/?id=3-AEO2021&cases=ref2021~aeo2020ref&sourcekey=0> (July 23, 2021).
- . 2021. “EIA Glossary - Industrial Sector.” [https://www.eia.gov/tools/glossary/index.php?id=Industrial sector](https://www.eia.gov/tools/glossary/index.php?id=Industrial%20sector) (July 23, 2021).
- U.S. Energy Information Agency. 2019. “Annual Energy Outlook 2020 with Projections to 2050.” *Annual Energy Outlook 2019 with projections to 2050* 44(8): 1–64. www.eia.gov/aeo (June 16, 2021).
- US Energy Information Administration. 2021. “California - State Energy Profile Analysis - U.S. Energy Information Administration (EIA).” *California State Profile and Energy Estimates*. <https://www.eia.gov/state/analysis.php?sid=CA> (July 20, 2021).
- USDA. 2013. “Farm and Ranch Irrigation Survey (2013).” *2012 Census of Agriculture*. https://www.nass.usda.gov/Surveys/Guide_to_NASS_Surveys/Farm_and_Ranch_Irrigation/
- . 2016. “NAIP Imagery.” *Aerial Imagery*. <https://www.fsa.usda.gov/programs-and-services/aerial-photography/imagery-programs/naip-imagery/> (June 16, 2021).
- . 2018. “Irrigation and Water Management Results from the 2018 Irrigation and Water Management Survey.” *USDA NASS 2018 Irrigation and Water Management Survey (2017 Census of Agriculture)*.
- USGS. 2015. “USGS Water Use Data for California.” <https://waterdata.usgs.gov/ca/nwis/wu> (July 20, 2021).
- Valle, B. et al. 2017. “Increasing the Total Productivity of a Land by Combining Mobile Photovoltaic Panels and Food Crops.” *Applied Energy* 206: 1495–1507.
- Walker, Andy et al. 2020. “Model of Operation-and-Maintenance Costs for Photovoltaic Systems, Technical Report NREL/TP-5C00-74840.” *NREL* (June). <https://www.nrel.gov/docs/fy20osti/74840.pdf>. (July 20, 2021).
- Wang, Beibei et al. 2019. “Multi-Level Classification Based on Trajectory Features of Time Series for Monitoring Impervious Surface Expansions.” *Remote Sensing*.
- Wang, Min, Qi Cui, Yujie Sun, and Qiao Wang. 2018. “Photovoltaic Panel Extraction from Very High-Resolution Aerial Imagery Using Region–Line Primitive Association Analysis and Template Matching.” *ISPRS Journal of Photogrammetry and Remote Sensing*.

- Wang, Xiaoyi et al. 2016. “Quantifying Multi-Decadal Change of Planted Forest Cover Using Airborne LiDAR and Landsat Imagery.” *Remote Sensing*.
- Whitaker, Michael, Garvin A. Heath, Patrick O’Donoughue, and Martin Vorum. 2012. “Life Cycle Greenhouse Gas Emissions of Coal-Fired Electricity Generation: Systematic Review and Harmonization.” *Journal of Industrial Ecology* 16(SUPPL.1): S53–72.
<https://onlinelibrary.wiley.com/doi/full/10.1111/j.1530-9290.2012.00465.x> (July 21, 2021).
- Xu, Hanzeyu et al. 2019. “A Scheme for the Long-Term Monitoring of Impervious-Relevant Land Disturbances Using High Frequency Landsat Archives and the Google Earth Engine.” *Remote Sensing*.
- Yang, Yongjun et al. 2018. “Detecting the Dynamics of Vegetation Disturbance and Recovery in Surface Mining Area via Landsat Imagery and LandTrendr Algorithm.” *Journal of Cleaner Production*.
- Yin, He et al. 2018. “Mapping Agricultural Land Abandonment from Spatial and Temporal Segmentation of Landsat Time Series.” *Remote Sensing of Environment*.
- Yu, Wenjuan et al. 2020. “Quantifying Highly Dynamic Urban Landscapes: Integrating Object-Based Image Analysis with Landsat Time Series Data.” *Landscape Ecology*.
- Zha, Y., J. Gao, and S. Ni. 2003. “Use of Normalized Difference Built-up Index in Automatically Mapping Urban Areas from TM Imagery.” *International Journal of Remote Sensing*.
- Zhang, Chi et al. 2018. “Water-Energy-Food Nexus: Concepts, Questions and Methodologies.” *Journal of Cleaner Production* 195: 625–39.
- Zhang, Shaohua et al. 2018. “Combinational Biophysical Composition Index (CBCI) for Effective Mapping Biophysical Composition in Urban Areas.” *IEEE Access*.